LAWRENCE
LIVERMORE
NATIONAL
LABORATORY

LLNL-TR-408276

Development of a Composite Non-Electrostatic Surface Complexation Model Describing Plutonium Sorption to Aluminosilicates

Brian A. Powell, Annie Kersting, Mavrik Zavarin, PIhong Zhao

January 06, 2011

Disclaimer

This work performed under the auspices of the U.S. Department of Energy by Lawrence Livermore National Laboratory under Contract DE-AC52-07NA27344.

Development of a Composite Non-Electrostatic Surface Complexation Model Describing Plutonium Sorption to Aluminosilicates

by

[1]Brian A. Powell, [2]Annie Kersting, [2,3]Mavrik Zavarin, [2,3]Pihong Zhao

[1]Environmental Engineering and Earth Sciences, Clemson University

[2]The Glenn T. Seaborg Institute, Physical and Life Sciences Directorate, Lawrence Livermore National Laboratory

[3]Environmental Radiochemistry Group, Physical and Life Sciences Directorate, Lawrence Livermore National Laboratory

January, 2011

TABLE OF CONTENTS

ABSTRACT

Due to their ubiquity in nature and chemical reactivity, aluminosilicate minerals play an important role in retarding actinide subsurface migration. However, very few studies have examined Pu interaction with clay minerals in sufficient detail to produce a credible mechanistic model of its behavior. In this work, Pu(IV) and Pu(V) interactions with silica, gibbsite (Al-oxide), and Na-montmorillonite (smectite clay) were examined as a function of time and pH. Sorption of Pu(IV) and Pu(V) to gibbsite and silica increased with pH (4 to 10). The Pu(V) sorption edge shifted to lower pH values over time and approached that of Pu(IV). This behavior is apparently due to surface mediated reduction of Pu(V) to Pu(IV). Surface complexation constants describing Pu(IV)/Pu(V) sorption to aluminol and silanol groups were developed from the silica and gibbsite sorption experiments and applied to the montmorillonite dataset. The model provided an acceptable fit to the montmorillonite sorption data for Pu(V). In order to accurately predict Pu(IV) sorption to montmorillonite, the model required inclusion of ion exchange.

1 INTRODUCTION

1.1 Motivation

The objective of this work is to measure the sorption of Pu(IV) and Pu(V) to silica, gibbsite, and smectite (montmorillonite). Aluminosilicate minerals are ubiquitous at the Nevada National Security Site and improving our understanding of Pu sorption to aluminosilicates (smectite clays in particular) is essential to the accurate prediction of Pu transport rates. These data will improve the mechanistic approach for modeling the hydrologic source term (HST) and provide sorption Kd parameters for use in CAU models. In both alluvium and tuff, aluminosilicates have been found to play a dominant role in the radionuclide retardation because their abundance is typically more than an order of magnitude greater than other potential sorbing minerals such as iron and manganese oxides (e.g. Vaniman et al., 1996).

The sorption database used in recent HST models (Carle et al., 2006) and upscaled for use in CAU models (Stoller-Navarro, 2008) includes surface complexation constants for U, Am, Eu, Np and Pu (Zavarin and Bruton, 2004). Generally, between 15 to 30 datasets were used to develop the constants for each radionuclide. However, the constants that describe Pu sorption to aluminosilicates were developed using only 10 datasets, most of which did not specify the oxidation state of Pu in the experiment. Without knowledge or control of the Pu oxidation state, a high degree of uncertainty is introduced into the model. The existing Pu surface complexation model (e.g. Zavarin and Bruton, 2004) drastically underestimates Pu sorption and, thus, will overestimate Pu migration rates (Turner, 1995). Recent HST simulations at Cambric (Carle et al., 2006) suggest that the existing surface complexation model may underpredict Pu K_ds by as much as 3 orders of magnitude.[1] In order to improve HST and CAU-scale transport models (and, as a result, reduce the conservative nature Pu migration estimates), sorption experiments were performed over a range of solution conditions that brackets the groundwater chemistry of the Nevada National Security Site. The aluminosilicates examined were gibbsite, silica, and montmorillonite.

1.2 Pu Geochemistry Relevant to UGTA Project

Under environmental conditions, plutonium can exist in four possible oxidation states, possibly simultaneously. The coexistence of plutonium at several oxidation states is due to the proximity of electrochemical potentials among each redox couple (Table 1.1). In neutral pH oxic solutions, the predominant oxidation states are Pu(IV), Pu(V), and Pu(VI). Due to the negative formal electrochemical potential of the Pu(IV)/Pu(III) couple, Pu(III) can be oxidized by water at neutral pH values. Neither highly reducing nor highly oxidizing conditions were maintained in the present work. Therefore, the predominant oxidation states are expected to be Pu(IV) and Pu(V). These oxidation states represent the Pu species with the highest (Pu(V)) and lowest (Pu(IV)) subsurface mobilities and, therefore, "bound" the range of potential Pu mobility.

[1] The difference between measured and predicted cavity k_ds at Cambric are likely the result of a combination of effects which includes uncertainty in radionuclide partitioning, sorption/desorption reversibility, as well as sorption affinity.

Table 1.1 Formal electrochemical potentials for Pu redox couples (versus SHE). Table modified from Clark et al. (2006).

Couple	Acidic[a]	Neutral[b]	Basic[c]
Pu(IV)/Pu(III)	0.982	-0.39	-0.96
Pu(V)/Pu(IV)	1.170	0.70	-0.67, 0.52[d]
Pu(VI)/Pu(V)	0.913	0.60	0.12
Pu(VI)/Pu(IV)	1.043	0.65	0.34

[a]In 1M $HClO_4$ (Lemire et al., 2001)
[b]pH 8 (Allard et al., 1980)
[c]In 1 M NaOH (Peretrukhin and Spitsyn, 1982)
[d]Formal oxidation potential (Allard et al., 1980)

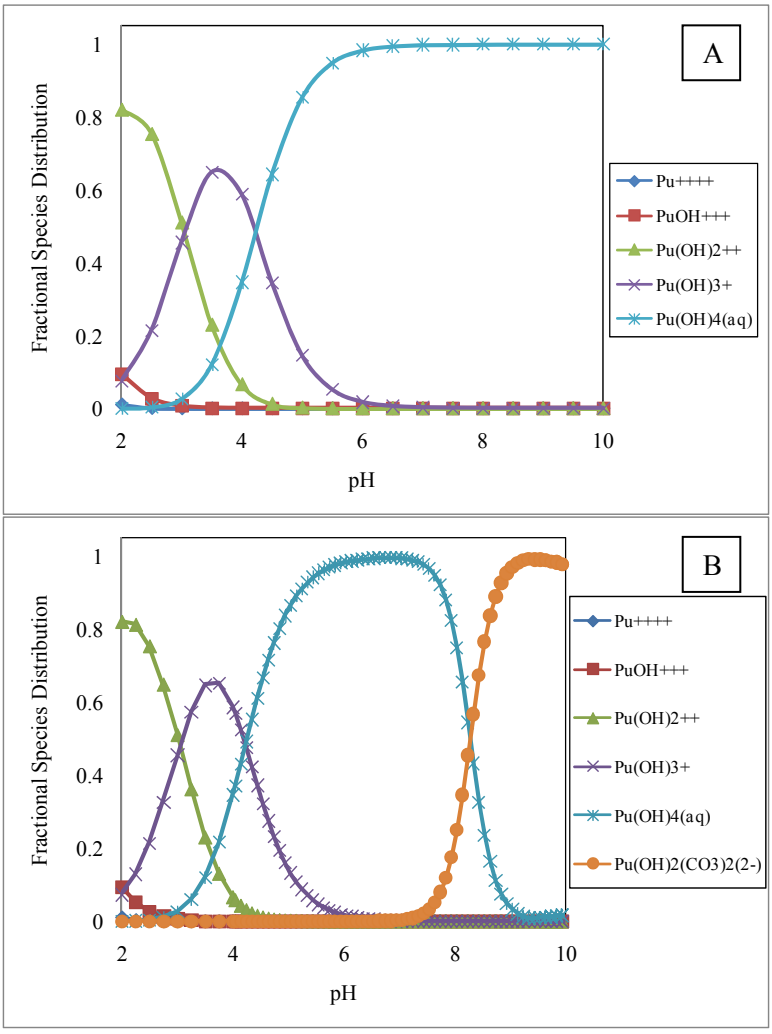

Figure 1.1: Speciation of Pu(IV) in(A) CO_2(g)-free and (B) atmospheric CO_2(g)-equilibrated systems, respectively. Calculations performed using thermodynamic constants from the existing UGTA database.

Tetravalent Pu undergoes extensive hydrolysis to form $Pu(OH)_x^{4-x}$ species (Figure 1.1a).[2] Even in acidic solutions, Pu(IV) is not present as a free ion. Rather hydrolysis begins near pH 1 and progresses in a stepwise manner until the $Pu(OH)_4(aq)$ species is dominant at pH > 4. In addition, hydrolysis products can polymerize and form colloidal or macroscopic precipitates. The aqueous phase concentration of Pu(IV) is limited by the formation of these insoluble precipitates. Rai et al. (2001) reported solubility product values for amorphous $Pu(OH)_4(s)$ of 10^{-56}. Using only this constant, the maximum aqueous Pu concentration at neutral pH values would be in the 10^{-13} to 10^{-15} M range. However, during Pu solubility studies in oxic solutions, 10^{-6} M aqueous Pu concentrations are routinely measured. The higher Pu concentrations are due to oxidation of Pu(IV) to more soluble Pu(V/VI) species and formation of colloidal Pu(IV) (Neck et al., 2007; Rai et al., 2001). Neck et al. (2007) recently determined an equilibrium constant of log K = -8.3 +/- 1.0 for $Pu(IV)_{colloid}$. Soderholm et al. (2008) determined that aggregated Pu colloids are comprised of ~2 nm crystalline Pu colloids. Oxidation state measurements by Rai et al. (1999) and Neck et al. (2007) have verified aqueous Pu(V) and Pu(VI) in Pu solubility experiments. From these data, a solubility model based on equilibrium with PuO_{2+x} was reported. Trace levels of dissolved oxygen were observed to affect the data indicating oxidation of Pu(IV) by dissolved oxygen in these systems (Neck et al., 2007).

The highly charged nucleus of Pu(V) is stabilized by axial oxygen bonds such that the predominant Pu(V) solution species is PuO_2^+. The axial oxygen bonds lower the effective charge of Pu to approximately +2.2. This lowered effective charge limits the affinity of Pu(V) for solid phases. Therefore, Pu(V) readily partitions to the aqueous phase and remains relatively mobile in the subsurface. At high Pu concentrations, Pu(V) has a tendency to disproportionate. As a result, there are very few studies of $Pu(V)O_2^+$ hydrolysis. The thermodynamic constants used in the current UGTA database were taken primarily from DATACOM.V8.r6 of the GEMBOCHS thermodynamic database (Turner et al., 1998). These constants (discussed and listed in Chapter 4) were used to calculate the aqueous Pu(V) speciation shown in Figure 1.2. Due to its low complexation affinity, PuO_2^+ remains a free oxycation up to pH 8.

The hydrolysis behavior of Pu(IV) and Pu(V) is related to sorption behavior. At low pH, Pu(IV) undergoes strong hydrolysis (Figure 1.1). Under these same conditions, Pu(IV) tends to sorb strongly to mineral surfaces, presumably through formation of inner sphere surface complexes with surface hydroxyl groups. Pu(V) does not undergo hydrolysis until pH ~8 (Figure 1.2) and significant sorption is not typically observed until pH > 7. At low pH, Pu(V) sorption is weak due to electrostatic repulsion of the positive mineral surface and the dioxycation PuO_2^+. The correlation between hydrolysis and sorption behavior was the basis for the proposal by Bradbury and Baeyens (2005) that linear free energy relationships between sorption constants and hydrolysis constants can be used to predict sorption behavior.

In systems with carbonate present, both Pu(IV) and Pu(V) are expected to form carbonate species above pH 8 (Figures 1.1b and 1.2b). The effects of these carbonate species on Pu sorption has not been rigorously examined. However, it is expected that formation of soluble, anionic carbonate species will prevent Pu sorption. The importance of soluble Pu(IV) carbonates

[2] The hydrolysis constants used to calculate the speciation diagrams in Figure 1.1 are those currently employed in the UGTA thermochemical database. The constants and this database will be discussed in greater detail below.

was demonstrated in a study by Rai et al. (1999) where formation fo Pu(IV) hydroxycarbonates was found to increase the solubility of Pu(IV) in PuO_2(am) saturated systems.

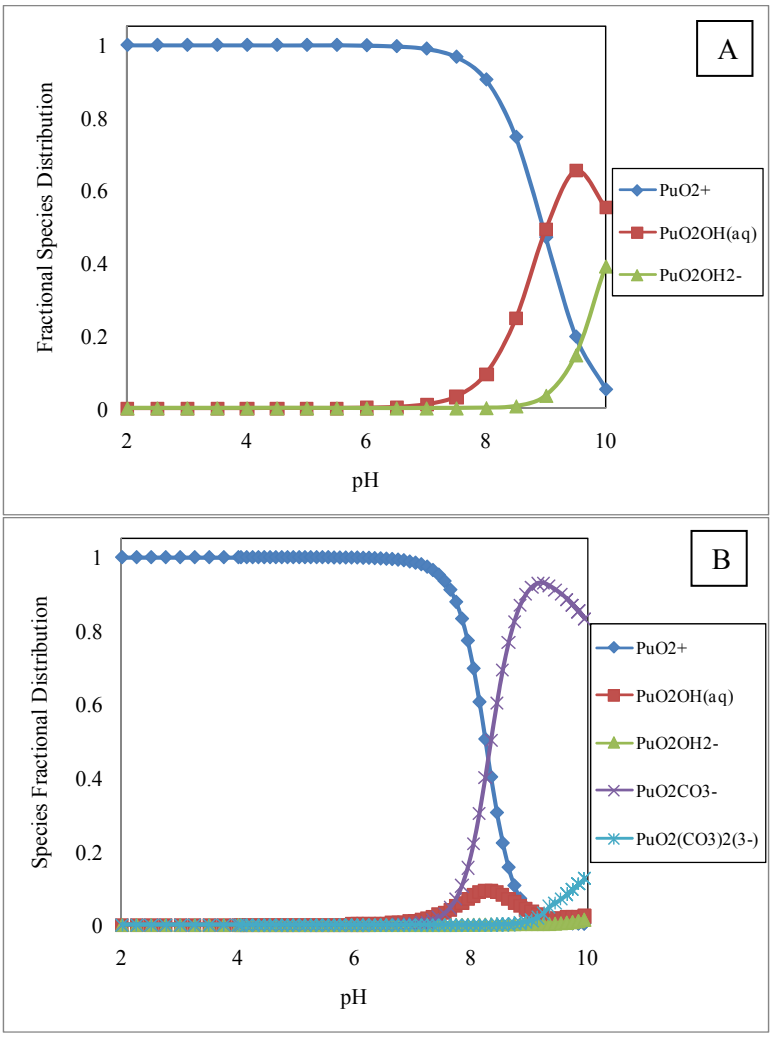

Figure 1.2: Speciation of Pu(V) in (A) CO_2(g)-free and (B) atmospheric CO_2(g)-equilibrated systems, respectively. Calculations performed using thermodynamic constants from the existing UGTA database.

1.3 Composite Surface Complexation Modeling Approach

In the present work, a composite surface complexation model (SCM) was developed by first generating surface complexation constants describing Pu(IV) and Pu(V) sorption to gibbsite and silica. Those constants were then used to predict Pu sorption to montmorillonite. The major assumption in this model is that the clay edge sites on montmorillonite that contain tetrahedral silica sites and octahedral alumina sites (Figure 1.3) will behave as aluminol (AlOH) and silanol (SiOH) sites in gibbsite and silica, respectively. A similar modeling approach was used by Turner et al. (1998) and McKinley et al. (1995) to model Np(V) and U(VI) sorption to montmorillonite, respectively. In the case of Pu, this modeling approach is complicated by the

redox cycling between Pu(IV) and Pu(V). As discussed above, the various Pu oxidation states exhibit drastically different sorption behavior. Therefore, a model capable of predicting not only partitioning of Pu but the oxidation state speciation would provide a more robust, mechanistic description of Pu geochemical behavior. To date, such a model has not been developed and incorporated into reactive transport modeling efforts. To allow for integration with the existing UGTA database and to compare the effects of the Pu(IV)/Pu(V) couple on model output, two modeling exercises are presented in this work. In the first, a non-electrostatic surface complexation model was developed without coupling Pu(IV) and Pu(V) (Chapter 4). In the second exercise, the Pu(IV)/Pu(V) redox couple was based upon the following reaction (Chapter 5):

$$Pu^{4+} + 0.25O_2(g) + 1.5H_2O \leftrightarrow PuO_2^{+} + 3H^{+} \qquad \log K = 3.439$$

This second modeling exercise is meant to demonstrate incorporation of the Pu(IV)/Pu(V) redox couple into modeling efforts to provide a more technically accurate model.

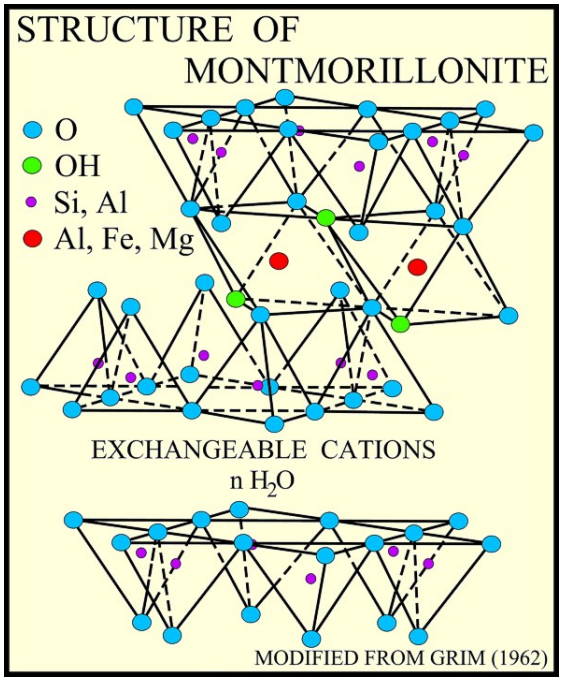

Figure 1.3 Structure of montmorillonite. Image downloaded from http://pubs.usgs.gov/of/2001/of01-041/htmldocs/images/monstru.jpg

2 MATERIALS AND METHODS

2.1 Solid Phase Preparation and Characterization

The current work utilized silica, gibbsite and montmorillonite. The silica was obtained from Unimin Corporation (Spruce Pine, NC) as Iota 8 high purity quartz. Typical contaminant concentrations are shown in Appendix A. The gibbsite (α-$Al(OH)_3$) was obtained from Ward's Natural Science (Rochester, NY). The montmorillonite is sample SWY-1 from the Clay Minerals

Society. All available physical and chemical information provided by the manufacturers is reported in Appendix A. The N_2(g)-BET surface area of all solid phases was measured using a Micrometrics Gemini surface area analyzer. All solid phases were degassed using a nitrogen stream at 110^{o}C for 24 hours prior to measuring surface area.

Unimun Corporation reports a silica particle size range of 75-300 μm. In order to increase the surface area, 2 gram aliquots were ground in a ball-mill for 20 minutes each.
The gibbsite and milled silica were cleaned by adding 10 g of each phase to a 180 mL centrifuge bottle with approximately 180 mL 0.01M NaOH. The suspension was mixed for one hour then centrifuged 60 minutes at 4500 rpm in a swing-bucket rotor (centrifuge: Allegra-22R, rotor: S4180). This left particles less than 150 nm in suspension. The NaOH supernatant was decanted and the solution was replaced with 0.01 M HNO_3, mixed for 1 hour, then centrifuged as described above. The HNO_3 phase was decanted and replaced with ultrapure MQ H_2O. This suspension was mixed by hand for approximately 3 minutes then centrifuged, the aqueous phase decanted, and the procedure repeated 5 times. The final wet solids were transferred to a glass petri dish and dried in an oven at 105 ^{o}C. After drying, the solids were lightly ground with a mortar and pestle to break up aggregates then stored in glass vials. The surface area of the silica and gibbsite were measured as 1.2 m^2 g^{-1} and 1.9 m^2 g^{-1}, respectively.

The SWy-1 montmorillonite was pre-treated by suspending 15 g montmorillonite in 150mL 0.001 M HCl. The suspension was mixed for 30 minutes, 0.50 mL 30% H_2O_2 (J.T. Baker) was then added, and the suspension was mixed for an additional 30 minutes. The suspension was centrifuged for 6 hours at 4500 rpm (centrifuge: Allegra-22R, rotor: S4180). This was calculated to leave particles less than 50 nm in suspension. The supernatant was discarded and the wet solids were transferred to 6000-8000 MWCO dialysis bags which were placed in a 4 L glass beaker with 0.01 M NaCl. The solids were dialyzed for 7 days and the NaCl solution was changed at least once per day. The solids were extruded from the dialysis bags into two 200mL centrifuge bottles and suspended in 150 mL MQ H_2O. These suspensions were mixed overnight to break up particle aggregates formed during dialysis. The suspensions were centrifuged for 5 minutes at 1000 rpm and the supernatant decanted into two clean 200 mL centrifuge bottles. This supernatant phase now contained the <2.0 μm particle size fraction. The suspension was centrifuged 6 hours at 4500 rpm and the supernatant was decanted and discarded to remove >50nm particles. The wet solids (50 nm to 2 μm particles size) were transferred to a glass petri dish and dried for two weeks at 40^{o}C. A remarkable decrease in overall volume of the montmorillonite was observed after drying, presumably due to dehydration of the interlayer. A portion of the dried montmorillonite was resuspended in MQ H_2O to make a suspension with a montmorillonite concentration of 48.06 $g_{montmorillonite}$ $kg^{-1}{}_{solution}$. This was used as a stock montmorillonite suspension. A small portion of the suspension was dried at 40^{o}C and the particles were lightly ground then used for a surface area measurement. The particles had a surface area of 27.1 m^2 g^{-1} which is near the reported value of 31.8 m^2 g^{-1} (Clay Minerals Repository).

XRD patterns for all three solid phases were obtained on a PAD-V x-ray diffractometer (Figures 2.1-2.3). The observed spectra for each of the processed solid phases compares favorably with reference patterns from the ICDD. The diffractometer settings were as follows: 1 mm and 2 mm

tube slit width, 0.3 and 0.2 mm detector slit width, 45kV voltage, 35 mA current, step scan with 0.02 step size, dwell time 1.0s.

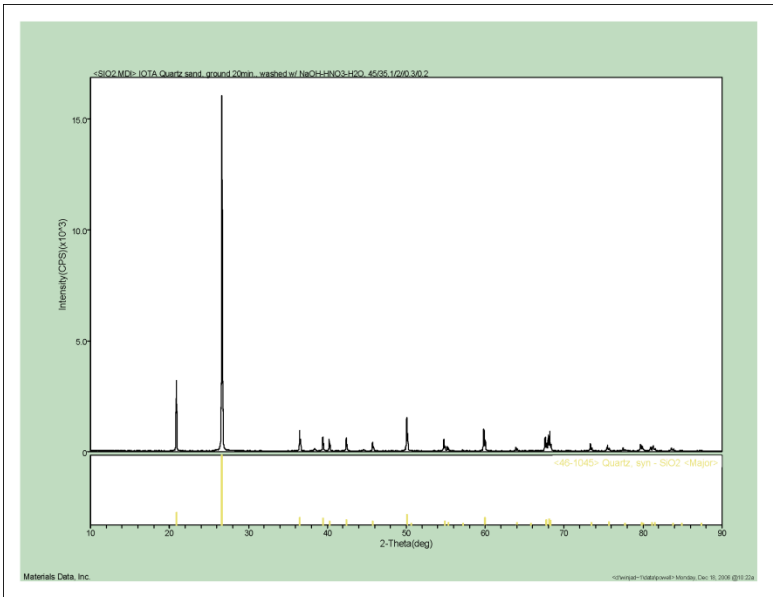

Figure 2.1: XRD pattern of milled and processed silica used in sorption experiments.

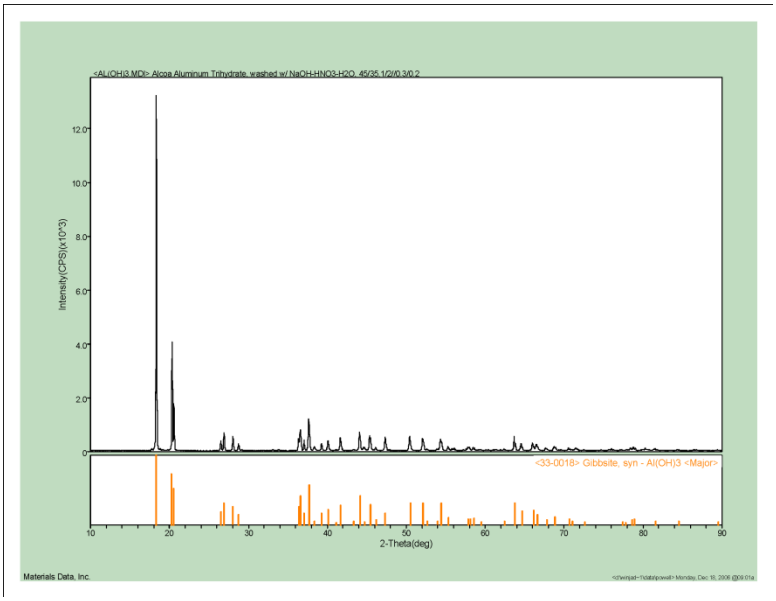

Figure 2.2: XRD pattern of processed gibbsite used in sorption experiments.

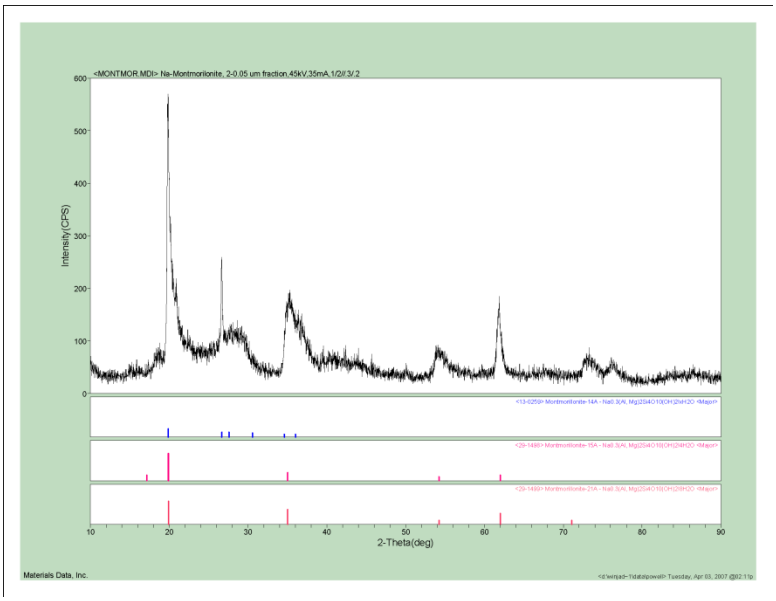

Figure 2.3: XRD pattern of processed montmorillonite used in sorption experiments.

2.2 Plutonium Working Solution Preparation and Characterization

2.2.1 Pu Stock Solution

A 1.2 μM $Pu(NO_3)_4$ stock solution in 1M HNO_3 containing 99.77% ^{238}Pu, 0.16% ^{241}Pu, and 0.04% ^{239}Pu by activity (Isotope Products) was used to prepare the Pu working solutions. The stock solution was purified by anion exchange prior to use to remove the ^{241}Am daughter from ^{241}Pu decay. A full description of the isotopic distribution is located in the Appendix B. Concentrations ^{238}Pu were determined on a Packard Tricarb 2550TR/XL Liquid Scintillation Analyzer in Ecolume (MP Biomedicals) cocktail.

2.2.2 Pu Oxidation State Analysis

The Pu concentration used here was too low to employ more traditional spectroscopic techniques to characterize Pu oxidation state distribution (Cleveland, 1979; Conradson et al., 1998). Instead, oxidation state analysis of the Pu working solution and effluent samples was performed using lanthanum fluoride coprecipitation and solvent extraction. The techniques reported here consider Pu(IV), Pu(V), and Pu(VI). Pu(III) is not considered or quantified in the separation scheme as it will be unstable in the oxic, circumneutral pH solutions used in these experiments (Cleveland, 1979).

Separation of Pu oxidation state by lanthanum fluoride was based on the method described by Kobashi and Choppin (1988). The Pu concentration in the supernatant was determined by LSC and represents the Pu(V/VI) fraction. The Pu(IV) fraction was calculated by difference. Separation of Pu oxidation states by solvent extraction was performed using 0.5 M bis-(ethylhexyl)-phosphoric acid (HDEHP) in xylene and 0.025 M 4-benzyol-3-methyl-1-phenyl-2-pyrazolin-5-one (PMBP) in xylene as the extractants (Bertrand and Choppin, 1982; Foti and Freiling, 1964; Neu et al., 1994; Nitsche et al., 1988). The Pu oxidation state distribution in the

working solution was determined using both HDEHP and PMBP as extractants. The error in the oxidation state distribution can be propagated from nuclear counting methods and is typically in the range of 1%. An estimate of at least 5% error is recommended as these are inherently indirect methods for oxidation state analysis and therefore introduce the possibility of inducing redox changes during measurement.

2.2.3 Pu(V) Working Solution Preparation

To prepare a Pu(V) working solution, a small aliquot of the 1.2 μM $Pu(NO_3)_4$ stock solution was evaporated to dryness then dissolved in 0.5 mL 1.0 M HCl/0.2 mM $KMnO_4$ in a plastic vial. The vial was wrapped in Al foil and left for 8 hours to oxidize all Pu to Pu(VI). The solution was diluted approximately 200× with 5 mM NaCl to pH 2-3. A 10 μL aliquot of 0.01 M $MnCl_2$ was added to precipitate any remaining permanganate. The pH was kept low (<3) during this step to avoid coprecipitating Pu. The solution was then passed through a 100 nm nylon syringe filter into a Teflon bottle, adjusted to pH 3 using NaOH and left for 5 days to allow autoreduction of Pu(VI) to Pu(V). The oxidation state purity of the working solution was verified prior to beginning each experiment (Table 2.1) and a fresh working solution was prepared for each set of experiments. The concentration and oxidation state distribution of these solutions did not change over the course of the experiment indicating the stability of Pu(V) at the trace levels used in these experiments.

Table 2.1 Pu Concentration and Oxidation State in Pu(V) Working Solutions

Experiment - Target Pu Ox. State and Solid Phase	Pu Conc. mol L^{-1}	Solv. Extract. Pu(IV)	Solv. Extract. Pu(V)	Solv. Extract. Pu(VI)	LaF_3-Coprecip Pu(III/IV)	LaF_3-Coprecip Pu(V/VI)
Pu(V)-Gibbsite*	5.90E-09	1.1%	92%	6%	1%	99%
Pu(V)-Silica*	5.90E-09	1.1%	92%	6%	1%	99%
Pu(V)-Gibbsite	1.50E-09	0.3%	97%	2%	2%	98%
Pu(V)-Silica	7.90E-09	1.4%	95%	5%	4%	96%
Pu(V)-Montmorillonite*	5.90E-09	0.6%	96%	2%	2%	96%
Pu(V)-Montmorillonite	8.30E-09	0.6%	96%	1%	0%	100%

*Used in experiments where CO_2(g) was removed

2.2.4 Pu(IV) Working Solution Preparation

New Pu(IV) working solutions were prepared for each experiment. Pu(IV) was prepared by transferring a small aliquot of the ^{238}Pu stock solution to a Teflon vial. The solution was heated until incipient dryness was reached followed by the addition of 0.1 M HCl (less than 1 mL) along with 10 μL 0.1 M $NaNO_2$. To prevent precipitation of $Pu(OH)_4$(s) and to keep Pu in the tetravalent oxidation state, the solution was maintained at pH <1. The total volume was kept low to minimize adjustment of sample pHs following the addition of the Pu(IV) spike. The Pu concentration and oxidation state distribution of each Pu(IV) working solution was determined immediately prior to starting an experiment (Table 2.2).

Table 2.2 Pu Concentration and Oxidation State in Pu(IV) Working Solutions

Experiment - Target Pu Ox. State and Solid Phase	Pu Conc. mol L^{-1}	Solv. Extract. Pu(IV)	Solv. Extract. Pu(V)	Solv. Extract. Pu(VI)	LaF_3-Coprecip Pu(III/IV)	LaF_3-Coprecip Pu(V/VI)
Pu(IV)-Gibbsite*	1.21E-07	96%	2%	1%	98%	2%
Pu(IV)-Silica*	1.21E-07	96%	2%	1%	98%	2%
Pu(IV)-Gibbsite	1.30E-07	95%	3%	2%	99%	1%
Pu(IV)-Silica	1.30E-07	95%	3%	2%	99%	1%
Pu(IV)-Montmorillonite*	1.67E-07	97%	1%	2%	99%	2%
Pu(IV)-Montmorillonite	1.20E-07	99%	1%	1%	99%	1%

*Used in experiments where $CO_2(g)$ was removed

2.3 Sorption Edge Experimental Method

Working suspensions of silica, gibbsite, and montmorillonite were prepared to yield a calculated surface area concentration of approximately 100 $m^2 L^{-1}$. A constant surface area in each solution allows for a more direct comparison of sorption properties. Batch sorption samples were prepared in acid-washed 15mL polypropylene centrifuge tubes by mixing calculated amounts of 0.001 M HCl, 0.001 M NaOH, 0.1 M NaCl, MQ H_2O (distilled-deionized water through Milli-Q system, 18.2 MΩ·cm resistivity), and an aliquot of the silica, gibbsite, or montmorillonite working suspension. The amount of HCl or NaOH was adjusted to achieve a desired pH and the amount of NaCl was adjusted to maintain a constant ionic strength of 0.01 M. The volumes of each solution/suspension used for each experimental system are listed in Appendix B. Although listed as volumes in Tables B1-B4, these values were used as "guides" and the mass of each solution for every sample was monitored gravimetrically to prevent inclusion of pipetting error into calculations. This was especially important when adding a 10μL Pu(IV) spike. Samples were prepared across the pH range 4 to 10. For experiments where $CO_2(g)$ was excluded, all solutions were prepared from MQ H_2O which had been boiled for one hour then cooled while purging the vessel headspace with NaOH-scrubbed $N_2(g)$. All sample preparation and manipulation for $CO_2(g)$-free experiments was performed in a glovebox that was purged with Ar(g) to decrease the $CO_2(g)$ concentration then backfilled with $CO_2(g)$-free air (Ultra Zero Air) such that a constant $O_2(g)$ concentration was maintained in all experiments. Experiments performed under atmospheric conditions ($CO_2(g)$-equilibrated) were prepared as described above except Na_2CO_3 and $NaHCO_3$ were added to ensure equilibration with atmospheric $CO_2(g)$. At pH values greater than 9 the total carbonate concentration was limited to less than 0.01 M to maintain a constant ionic strength.

After preparing the initial suspensions for either $CO_2(g)$-free or $CO_2(g)$-equilibrated experiments, suspensions were spiked with either a Pu(IV) or Pu(V) working solution and the pH adjusted to the target pH using dilute HCl or NaOH. The pH of each suspension was measured with an Orion Ross semi-micro electrode calibrated with standard pH buffers on an Orion 420A meter. After adjusting the pH to the target value, the samples were transferred to a shaking table and mixed at 150 rpm about their longitudinal axis. It is important to note that the shaker table was located outside of the glovebox so samples prepared under $CO_2(g)$ free conditions were mixed outside of the glovebox. Although the samples were sealed, $CO_2(g)$ diffusion into the suspension

became significant at longer time intervals (> 3 days). The diffusion of $CO_2(g)$ caused a notable pH decrease due to formation of bicarbonate during equilibration off the suspension with $CO_2(g)$.

At various time intervals, the pH (and on some occasions E_H) was measured. The aqueous Pu concentration was determined by centrifuging 1.8 mL of the suspension at 10,000 rpm for 2 hours. This centrifuge speed and time was calculated to remove particles greater than 30 nm from the supernatant. A 1.0 mL aliquot of the supernatant was mixed with 5 mL Ecolume LSC cocktail for Pu determination via LSC. In selected cases, additional aliquots were removed and passed through 3k Molecular Weight Cut-Off (MWCO) filters to verify that the centrifugation scheme removed the selected particle size fraction. The Pu oxidation state distribution was measured in the filtrate using the techniques described above.

2.4 Surface Complexation Modeling

To remain consistent with the current modeling efforts and databases employed in UGTA project, the data were modeled using a non-electrostatic surface complexation model. The computer program FIT4FD was used in all modeling efforts. FIT4FD was created by modifying the program FITEQL 4.0 (Herbelin and Westall, 1994) to allow for rapid data input and analysis of complex datasets. The specific details of each modeling exercise are discussed in Chapters 4 and 5.

3 SORPTION EDGE EXPERIMENT RESULTS AND DISCUSSION

3.1 Pu(IV) and Pu(V) Control (Solid-free) Solutions

3.1.1 Pu(V) Control Solutions

Solid-free control samples were included in each sorption experiment. In addition to determining aqueous Pu in each sample, the oxidation state of the aqueous Pu was determined after 2 hours, 24 hours, and 60 days. The aqueous Pu fraction was determined via centrifugation (Figure 3.1). The oxidation state was determined using LaF_3-coprecipitation (Figure 3.2). With the exception of the final sampling event at high pH, Pu(V) solutions remained in the aqueous phase throughout the experiment. The Pu(V) solutions remained predominantly Pu(V) throughout the experiment. The only exception appears to be the high pH system, which also showed a loss of total aqueous Pu after 60 days. The data suggest that some Pu precipitation occurred at this pH.

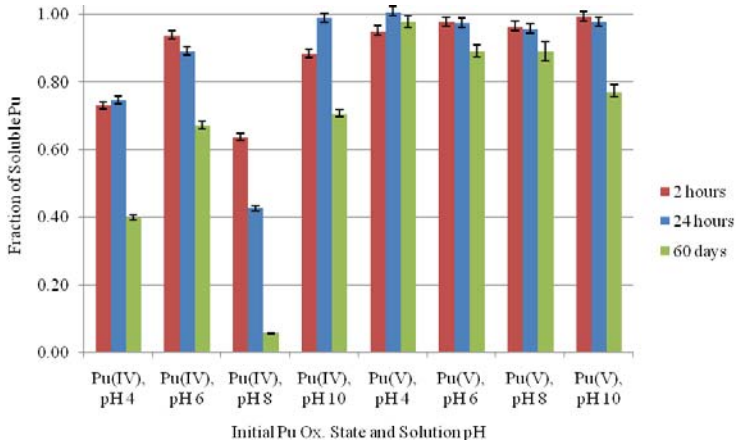

Figure 3.1: Fraction of soluble Pu in Pu(IV) and Pu(V) control solutions (no solid phase present, CO_2(g)-equilibrated system).

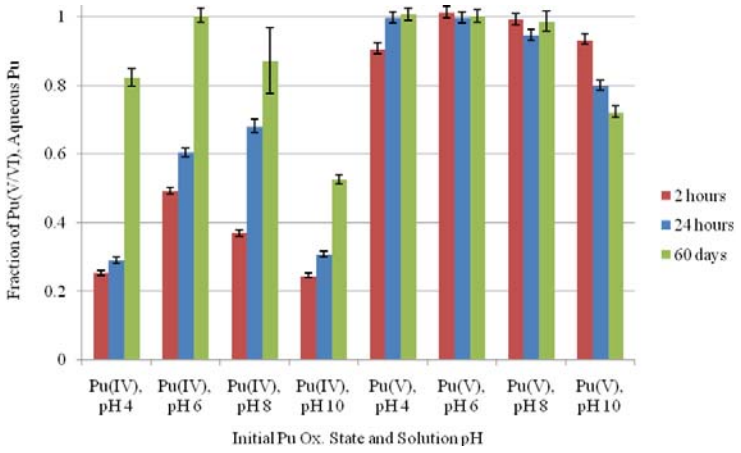

Figure 3.2: Oxidation state distribution of aqueous Pu in Pu(IV) and Pu(V) control solutions (no solid phase present, CO_2(g)-equilibrated system). Note: error bars account for nuclear counting statistics only.

3.1.2 Pu(IV) Control Solutions

The Pu(IV) solutions showed a considerable loss of Pu from the aqueous phase. This is due to either sorption of Pu to the vessel walls or precipitation of $Pu(OH)_4$(s). Using the solubility product for $Pu(OH)_4$(s) reported by Neck and Kim (2001), the Pu(IV) concentration should be limited to approximately 10^{-11} M. However, solubility experiments frequently observe aqueous Pu concentrations ranging from 10^{-11} to 10^{-7} M. The discrepancy is due to oxidation of Pu(IV) to Pu(V) and mischaracterization of colloidal Pu as an aqueous species. Neck et al. (2007) proposed that Pu(V) is formed through oxidation of PuO_2(s) by dissolved oxygen to form the hydrous oxide PuO_{2+x}. They reported that Pu polymers will be present at a constant level of $\log[Pu(IV)]_{coll} = -8.3 \pm 1.0$. Recently, Soderholm et al. (2008) observed monodispere, nanometer sized Pu "nanoclusters" which persisted in solution indefinitely. Colloids of this nature are not expected in this work due to the relatively low Pu concentration (10^{-10} M). However, formation

of some colloidal Pu(IV) cannot be altogether discounted. In light of these observations, there are three main factors that must be considered in the analysis of the Pu(IV) control solutions:

1. Sorption of Pu to the vial walls
2. Oxidation of Pu(IV) to Pu(V) mediated by dissolved oxygen
3. Formation of colloidal Pu(IV) and possible mischaracterization as aqueous Pu

After 2 hours, the aqueous Pu concentration varied with pH. The lowest values were observed at pH 8. A steady decrease in the aqueous Pu concentration was observed for each solution over time. Sorption to the vial walls is expected to occur rapidly. Therefore, the steady loss of aqueous Pu over 60 days is not indicative of sorption to vial walls. Oxidation state analysis of aqueous Pu revealed that even after 2 hours, there was a significant fraction of Pu(V) present. As shown in Table 2.2, the Pu(IV) solutions were initially >95% Pu(IV). Therefore, the observation of Pu(V/VI) in each solution indicates oxidation of Pu(IV) to Pu(V/VI), presumably by dissolved oxygen. The fraction of aqueous Pu characterized as Pu(V/VI) increased over time (Figure 3.2). However, oxidation state data were collected only on the aqueous Pu fraction, not the total Pu. Based on Figure 3.1, there was a corresponding decrease in the total aqueous Pu in the system. Since the concentration and oxidation state distribution of the Pu(V) solutions remained constant, it can be logically assumed that the loss of Pu observed in the Pu(IV) solutions can be attributed to Pu(IV) precipitation. The fraction of Pu(V/VI) as a function of the total Pu concentrations can be calculated by subtracting the concentration of "lost" Pu and the concentration of measured Pu(III/IV) from the total Pu concentrations (Figure 3.3). Except for the pH 8 solution, there was a constant increase in the total Pu(V) in each solution over time. Therefore, despite the initial decrease in the aqueous Pu concentration versus time (Figure 3.1), there was an overall increase in Pu(V/VI) over time. Formation of aqueous Pu(V) from Pu(IV) solutions is vitally important in explaining the observed sorption behavior in this work.

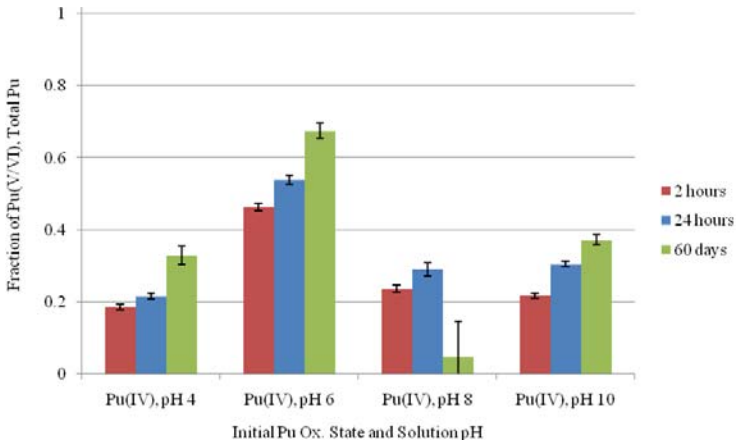

Figure 3.3: Fraction of Pu(V/VI) referenced to total Pu in Pu(IV) control solutions (no solid phase present, CO_2(g)-equilibrated system).

3.2 Pu(IV) and Pu(V) Sorption to Gibbsite

Sorption edges for Pu(V) and Pu(IV) on gibbsite are shown in Figure 3.4. Data for sampling intervals of 24 hours, 62 days, and 306 days are represented by squares, diamonds, and triangles, respectively, in both Pu(IV) and Pu(V) systems. Open symbols were used to represent Pu sorption in CO_2(g) free systems. The CO_2(g)-free data are available for the 24 hours sampling event only. Diffusion of CO_2(g) into the CO_2(g)-free samples limited the reliability of data obtained from longer sampling intervals.

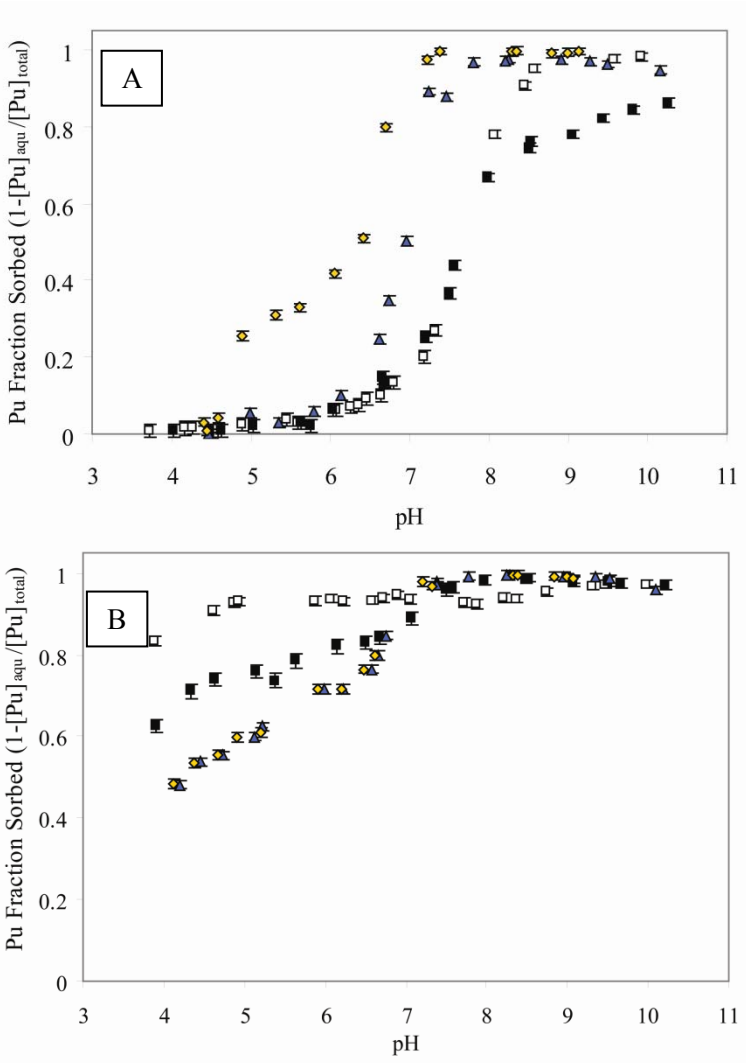

Figure 3.4: Sorption of (A) Pu(V) and (B) Pu(IV) to gibbsite. Data plotted after 24 hours (squares), 62 days (triangles), and 306 days (diamonds). Open squares represent systems where atmospheric CO_2(g) was excluded.

In both Pu oxidation state samples, the fraction sorbed increased with pH. The sorption behavior as a function of pH is due to changing Pu(IV) and Pu(V) solution species as well as the

protonation and deprotonation of the surface hydroxyl groups (AlOH). In acidic solutions, the aluminol sites on the gibbsite surface will be protonated ($AlOH_2^+$), giving the surface and overall net positive charge. As the pH of the solution increases, the aluminol sites depronate to form AlOH and AlO^-. Therefore, the surface transitions to having a net negative charge in basic solutions. The pH at which the net surface charge is zero is called the point of zero charge. This occurs around pH 8 to 9 for gibbsite (Sposito, 1989). This changing surface charge has a profound effect on sorption of charged ions such as Pu(V). At low pH values, Pu(V) is predominantly present as the dioxycation, PuO_2^+. Due to the net positive surface charge carried by the gibbsite in acidic solutions, cationic PuO_2^+ is repelled by the surface and sorption is negligible (Figure 3.4a, 24 hours). The predominant forms of Pu(IV) under environmental conditions are the solution species $Pu(OH)_4(aq)$ and the insoluble hydrolysis product $Pu(OH)_4(s)$. As demonstrated by the strong hydrolysis of Pu(IV) even under acidic conditions, Pu(IV) is strongly attracted to aluminol surface sites and the neutrally charged $Pu(OH)_4(aq)$ species is not repelled by the mineral surface. This allows for strong sorption of Pu(IV) even at low pH values (Figure 3.4b).

The effect of carbonate was only observed in Pu(V) samples. Sorption of Pu(V) becomes significant at circumneutral pH values where the gibbsite surface maintains a neutral or net negative surface charge and where the free $Pu(V)O_2^+$ cation begins to hydrolyze to $Pu(V)O_2OH(aq)$. At approximately pH 8, the effects of carbonate on Pu(V) sorption can be observed. While sorption of Pu(V) steadily increases in the $CO_2(g)$-free system, a marked diversion in the sorption behavior was observed in the $CO_2(g)$-equilibrated system. This is due to the formation of anionic plutonyl-carbonate species such as $PuO_2CO_3^-$ which have a higher affinity for the aqueous phase. Similar behavior at high pH values was not observed for the Pu(IV) systems. Formation of Pu(IV)-carbonates requires relatively high carbonate concentrations as the strength of Pu(IV) hydrolysis is greater than the strength of carbonate complexation.

There is a notable difference in the Pu(IV) $CO_2(g)$-free and $CO_2(g)$-equilibrated experiments at low pH values. This appears to be an experimental artifact due to the oxidation of Pu(IV) to Pu(V). When preparing these suspensions, calculated amounts of acid and base were added to each suspension to achieve a desired pH. In the case of Pu(IV), the exact acid concentration of the stock solution was not known due to the repeated evaporation and re-dissolution of the solution. As a result, insufficient base was initially added to reach the desired pH and several of the Pu(IV) suspensions remained at an acidic pH for as much as 30 minutes. As shown in the Pu(IV) control solutions, some oxidation of Pu(IV) to Pu(V) occurs in acidic and neutral pH solutions at trace Pu concentrations. Over the time at which these samples remained in an acidic solution, some Pu(V) may have formed which would not readily sorb to gibbsite at low pH. *The rate of these changes cannot be predicted using current thermodynamic and kinetic data.* However, it can be stated that the differences in the Pu(IV) datasets under $CO_2(g)$-free and $CO_2(g)$-equilibrated conditions at low pH values are likely due to oxidation of Pu(IV) to Pu(V) during sample preparation. The formation of aqueous Pu(V) was verified in Pu(IV) suspensions in the $CO_2(g)$-equilibrated dataset. It is also noteworthy that similar behavior was observed for the Pu(IV) systems in silica suspensions (discussed in Section 3.3).

The Pu(IV) and Pu(V) data in CO_2(g)-equilibrated systems are plotted together in Figure 3.5. Sorption of Pu(V) to gibbsite increased as a function of time. This is proposed to be due to surface mediated reduction of Pu(V) to Pu(IV). The slope of the sorption edge decreases and appears to more closely resemble that of Pu(IV). There is no significant change in the Pu(IV) data between 62 and 300 days, indicating the system had reached a steady state. The Pu(V) sorption edge had drifted between 62 and 300 days indicating the system had not reached steady state. Presumably, the Pu(V) sorption edge would eventually align with the Pu(IV) sorption edge. It is unclear what the identity of the reductant in this system is. However, based upon the known thermodynamic favorability of Pu(IV) hydroxide species, a plausible hypothesis is that reduction of Pu(V) is based upon a Nerstian behavior where the free energy of the Pu(IV) surface species sufficiently energetically favorable that reduction of Pu(V) to Pu(IV) can be facilitated by water. An alternate hypothesis is that light or alpha particle induced peroxide formation may result in the reduction of Pu(V) to Pu(IV). Reduction of Pu(V) to Pu(IV) on a variety of mineral surfaces has been observed (Keeney-Kennicutt and Morse, 1985; Penrose et al., 1987; Powell et al., 2006; Powell et al., 2004; Powell et al., 2005; Sanchez et al., 1985). Most notably, Pu(V) reduction to Pu(IV) was observed on surfaces expected to be either oxidizing or non-reactive such as pyrolusite (δ-MnO_2), tuff (Pu predominantly associated with ranciete/Mn(IV) phase), hematite (α-Fe_2O_3), goethite (α-FeOOH), and silica (SiO_2) (Powell et al., 2006; Powell et al., 2005). In those studies reduction of Pu(V) was verified using direct (XANES) and indirect (solvent extraction) methods.

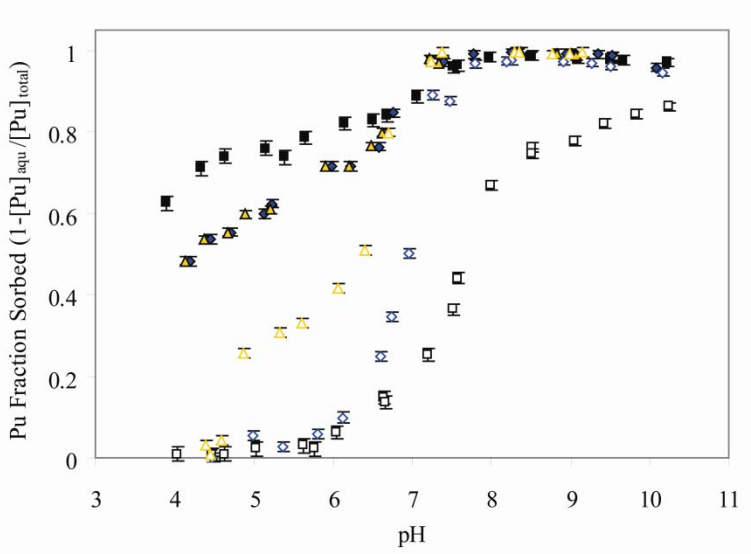

Figure 3.5: Pu(IV) (closed symbols) and Pu(V) (open symbols) sorption to gibbsite at 24 hours (squares), 62 days (diamonds), 300 days (triangles) in CO_2(g)-equilibrated solutions.

Interestingly, there was an increase in the aqueous Pu concentration in Pu(IV) samples between 24 hours and 62 days. Therefore, Pu initially sorbed as Pu(IV) desorbed over time in the pH range 4 to 7. This is likely due to reoxidation of sorbed Pu(IV) to aqueous Pu(V). Surface mediated reduction of Pu(V) to Pu(IV) as discussed above is affected by pH. Powell et al. (2005) found a -0.2 and -0.4 order dependence on the hydrogen ion concentration for the rate of Pu(V) reduction on goethite and hematite, respectively. Therefore, reduction of Pu(V) was expected to

be more favored with increasing pH. Conversely, at low pH values where a significant fraction of Pu is in the aqueous phase, Pu(V) is expected to be the dominant aqueous phase species. This is consistent with the observation of Pu(V) as the stable aqueous oxidation state in slightly acidic to neutral solutions including ocean and lake water and suspensions from Pu(IV) solubility experiments. Additionally, in all Pu sorption experiments where the oxidation state of the aqueous Pu fraction in a solid suspension was measured, Pu(V) was found to be the dominant oxidation state (Banik et al., 2007; Keeney-Kennicutt and Morse, 1985; Penrose et al., 1987; Powell et al., 2006; Powell et al., 2005; Powell et al., 2008; Sanchez et al., 1985). This was found to be the case for this work as well. Selected samples from the Pu(IV) experiments were analyzed after 6 days and after 62 days. The aqueous phase was separated by centrifugation and Pu oxidation state determined using LaF_3-coprecipitation. The data (Table 3.1) clearly show that Pu(V) is the predominant aqueous phase oxidation state. Pu, which initially sorbed as Pu(IV) repartitioned to the aqueous phase as Pu(V) over time. This is consistent with the observed behavior of the control (solid phase free) Pu(IV) and Pu(V) solutions. Assuming that the majority of sorbed Pu was Pu(IV), these Pu(IV)-gibbsite suspensions at 62 and 306 days represent an equilibrium state with regard to all facets of Pu geochemistry including sorption, precipitation, and redox chemistry. The weakly sorbing gibbsite allows for a system to be maintained where significant and measureable quantities of aqueous phase Pu(V) and solid phase Pu(IV) are in equilibrium. This presents a very unique modeling opportunity that will be further explored in Chapter 5.

Table 3.1: Oxidation State Analysis of Pu(IV)-gibbsite CO_2(g)-equilibrated suspensions determined via LaF_3-coprecipitation.

Sample pH	Fraction Sorbed	Fraction Pu(III/IV)	Fraction Pu(V/VI)
After 6 days			
4.3	0.60	0.02 ± 0.03	0.98 ± 0.03
6.5	0.84	0.02 ± 0.05	0.98 ± 0.05
After 62 days			
4.5	0.54	0.01 ± 0.01	0.99 ± 0.01
6.6	0.78	0.05 ± 0.02	0.95 ± 0.01
9.5	0.99	0.00 ± 0.07	1.00 ± 0.07

3.3 Pu(IV) and Pu(V) Sorption to Silica

As with the gibbsite suspensions, Pu sorption to silica generally increased with pH for both Pu(IV) and Pu(V) (Figure 3.6). This is due to electrostatic interactions with silanol (SiOH) surface sites, rather than the aluminol surface. There was a notable difference in the low pH Pu(IV) samples in CO_2(g) and CO_2(g)-equilibrated suspensions after 24 hours. As with the Pu(IV)-gibbsite systems, this difference is believed to be due to oxidation of Pu(IV) to Pu(V) during neutralization of the Pu(IV) working solution. However, this difference was found to be negligible at later sampling intervals as the data for both CO_2(g)-free (data not shown) and CO_2(g)-equilibrated systems were similar after 62 days for all Pu-silica systems (including Pu(V) samples).

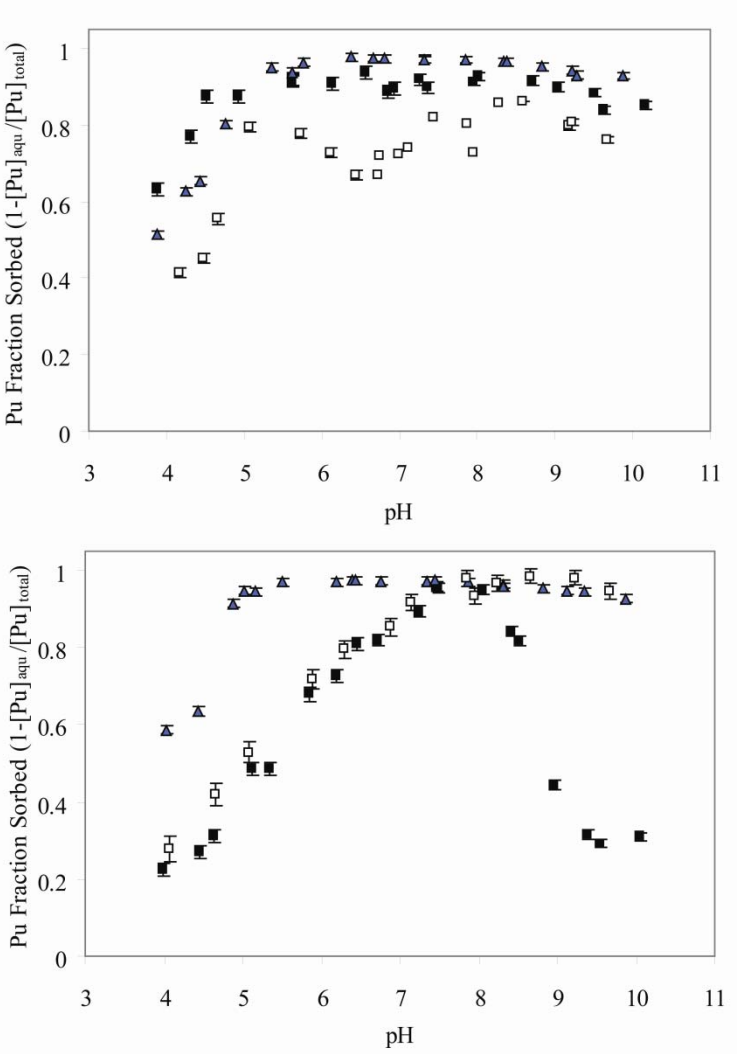

Figure 3.6: Sorption of (A) Pu(IV) and (B) Pu(V) to silica at 24 hours (□, ■) and 62 days (▲). Open symbols represent systems where atmospheric CO_2(g) was excluded.

The Pu(IV) samples showed significant changes in partitioning between 24 hours and 62 days (CO_2(g)-equilibrated samples). Between pH 5 and 9, the fraction of Pu sorbed was ~90% after 24 hours and increased to greater than 95% after 62 days. Due to the low aqueous Pu concentration, oxidation state analysis of the aqueous phase could not be performed. In pH 4 to 5 suspensions, a slight desorption of Pu was observed between the 24 hour and 62 days. Measurement of the oxidation state distribution of the aqueous Pu indicated that oxidized Pu(V/VI) was the predominant oxidation state (Table 3.2). The observed oxidation of Pu to aqueous Pu(V) is proposed to be responsible for the slight "desorption" of Pu between 24 hours and 62 days between pH 4 and 5.

Table 3.2: Oxidation State Analysis of Pu(IV)-silica CO_2(g)-equilibrated suspensions determined via LaF_3-coprecipitation.

Sample pH	Pu Fraction Sorbed	Fraction Pu(III/IV)	Fraction Pu(V/VI)
After 6 days			
3.9	0.64 ± 0.02	0.01 ± 0.03	0.90 ± 0.03
5.8	0.43 ± 0.04	0.13 ± 0.04	0.87 ± 0.04
9.5	0.83 ± 0.01	0.28 ± 0.20	0.72 ± 0.20
After 62 days			
4.4	0.67 ± 0.02	0.04 ± 0.01	0.96 ± 0.01
6.4	0.98 ± 0.02	below level of detection	
9.3	0.97 ± 0.02	below level of detection	

Carbonate did not appear to have a significant influence on Pu(IV) sorption across the high pH region where Pu-carbonate and Pu-hydroxycarbonate species form. Sorption and hydrolysis of Pu(IV) appears to be more energetically favorable than formation of soluble carbonate species. This is expected based upon the relatively low carbonate concentrations used in these experiments and the propensity of Pu(IV) to sorb and/or hydrolyze. Conversely, in the Pu(V) samples, formation of $PuO_2(CO_3)_x^{1-2x}$ species clearly influenced sorption (Figure 3.6b). Between pH 4 and 8 (24 hour data), CO_2(g)-free and CO_2(g)-equilibrated samples behave nearly identically. However, at pH >8, there is a sharp decrease in the Pu fraction sorbed in the CO_2(g)-equilibrated samples. This is consistent with the onset of Pu(V)-carbonate formation (log K^o $PuO_2CO_3^-$ = 5.1, (Clark et al., 1995)). Between pH 9.5 and 10, the effect of carbonate appears to plateau. This is likely due to the fixed carbonate concentration used over this pH range in these samples. The effect of carbonate is more substantial in the silica systems relative to the gibbsite systems. For example, at pH 9 the Pu fraction sorbed was 78% and 44% for the gibbsite and silica systems, respectively. All other system parameters were the same. However, it is noteworthy that the effect of carbonate appears to be transient. At higher pH values, the aqueous phase Pu concentration after 62 days was significantly higher than after 24 hours. The data appear to more closely resemble the CO_2(g)-free system. The decreased sorption due to formation of aqueous Pu(V)-carbonate species will not affect long term sorption behavior under these system conditions (longterm reduction to Pu(IV)).

The Pu(V) samples appear to have undergone redox transformation over the course of the experiment. Similar to the gibbsite systems, the Pu fraction sorbed over time in neutral and acidic pH regions increased with time. The sorption of both Pu(IV) and Pu(V) samples after 24 hours and 62 days is shown in Figure 3.7. The data are dissimilar at 24 hours. However, after 62 days, the data appear to merge suggesting that a steady state has been reached. The shape and slope of the Pu(V) dataset underwent drastic changes to more closely resemble that of the Pu(IV) dataset. This provides circumstantial evidence of the surface mediated reduction of Pu(V) to Pu(IV). The equilibrium distribution of Pu in these silica suspensions appears to be defined as a steady state partitioning between aqueous Pu(V) and solid phase Pu(IV). Measurement of the aqueous Pu in Pu(IV) solutions in the acidic region indicate that the aqueous Pu was Pu(V). The oxidation state of aqueous Pu from the initially Pu(V) experiment was not performed. However, some filtration tests were performed and greater than 96% of the Pu was able to pass through a 3k MWCO centrifugal filter. This verified that Pu was not associated with a colloidal phase and likely a truly soluble species, most likely Pu(V).

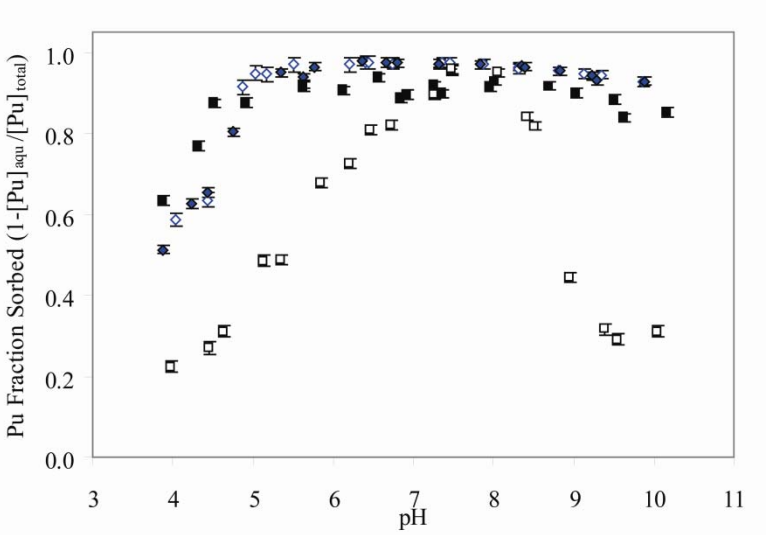

Figure 3.7: Pu(IV) (closed symbols) and Pu(V) (open symbols) sorption to silica after 24 hours (squares) and 62 days (diamonds) in CO_2(g)-equilibrated solutions.

It is interesting to note that sorption of Pu to silica is stronger at low pH values relative to gibbsite. A plot of the Pu distribution at equilibrium (62 days for silica and 300 days for gibbsite) is shown in Figure 3.8. While Pu strongly partitions to both minerals at high pH, sorption of Pu to silica is stronger at low pH. This is proposed to be due to low pK_a of silanol surface sites (log $K \cong 2$) which generate a net negative surface charge which may attract cationic Pu species in low pH suspensions.

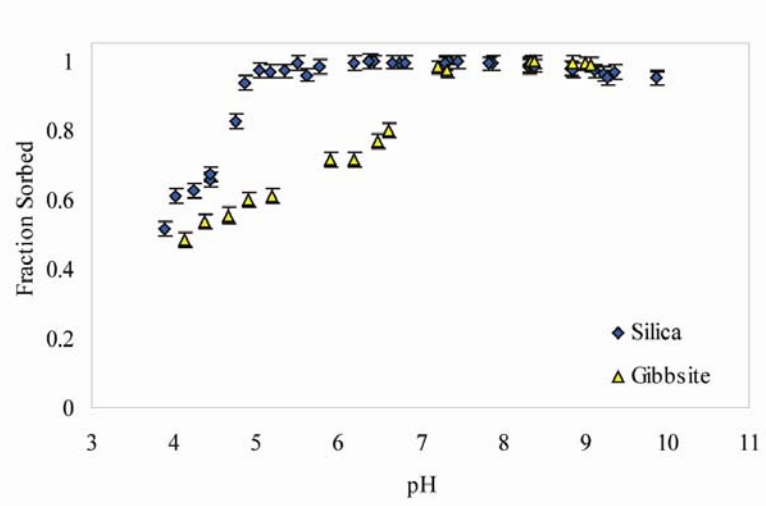

Figure 3.8: Pu sorption to silica (62 days) and gibbsite (300 days) in CO_2(g)-equilibrated solutions.

3.4 Pu(IV) and Pu(V) Sorption to Montmorillonite

The results from Pu(IV) and Pu(V) sorption experiments in montmorillonite suspensions after 24 hours are shown in Figure 3.9. Pu(IV) strongly sorbed to montmorillonite within 24 hours at all pH values examined (Figure 3.9a). Additionally, there appears to be no effect of carbonate on Pu(IV) sorption as both CO_2(g)-equilibrated and CO_2(g)-free samples behave similarly. The partitioning of Pu(V) to montmorillonite after 24 hours was similar to that observed for silica and gibbsite systems (Figure 3.9b). Minimal sorption was observed up to pH 7. Sorption in the CO_2(g)-free system increased between pH 7 and 9. In CO_2(g)-equilibrated suspensions, there was a lower Pu fraction sorbed between pH 8 and 9 relative to the CO_2(g) free system. Similar to silica and gibbsite systems discussed above, it appears formation of $PuO_2(CO_3)_x^{1-2x}$ carbonate species significantly decreases Pu(V) sorption above pH 8.

At higher pH values (8 to 10) Pu(IV) sorption underwent a gradual decrease. There was a slight decrease in the Pu(V) fraction sorbed but this phenomena was considerably more pronounced in the Pu(IV) systems. The decrease in Pu sorption at high pH values is interesting in these systems as it was not observed for silica and gibbsite systems. Similar behavior was observed by Sanchez (1983) but the aqueous chemical species was not determined and no mechanism was proposed. The sorption appeared to achieve a steady state within 24 hours. Further sampling of the Pu(IV)-montmorillonite suspensions after 21, 60, and 90 days showed little change in Pu sorption (Figure 3.10a).

After 160 days the concentration and oxidation state of aqueous Pu was measured. The aqueous Pu concentration was determined by measuring the Pu concentration in the supernatant of a centrifuged sample. For comparison, the Pu concentration was also measured in the filtrate obtained by passing 3mL of the suspensions through a 3k MWCO centrifugal filter (Table 3.3). The results are comparable. The 3k MWCO filters have approximately a 4 nm pore size. Soderholm et al. (2008) found that concentrated Pu solutions form roughly 2 nm particles that may aggregate to greater than 20 nm particles. Recent work in our laboratory has shown that colloidal Pu(IV) sorbs to synthetic goethite crystals in approximately the same size range but is dominated by 2 nm colloids that aggregate to form <20 nm particles. The size of the aggregate is no doubt a function of the initial concentration of Pu in solution. The oxidation state of Pu in the filtrate was measured using LaF_3-coprecipitation and solvent extraction. The results (Table 3.3) indicate that Pu(V/VI) was the predominant aqueous oxidation state.

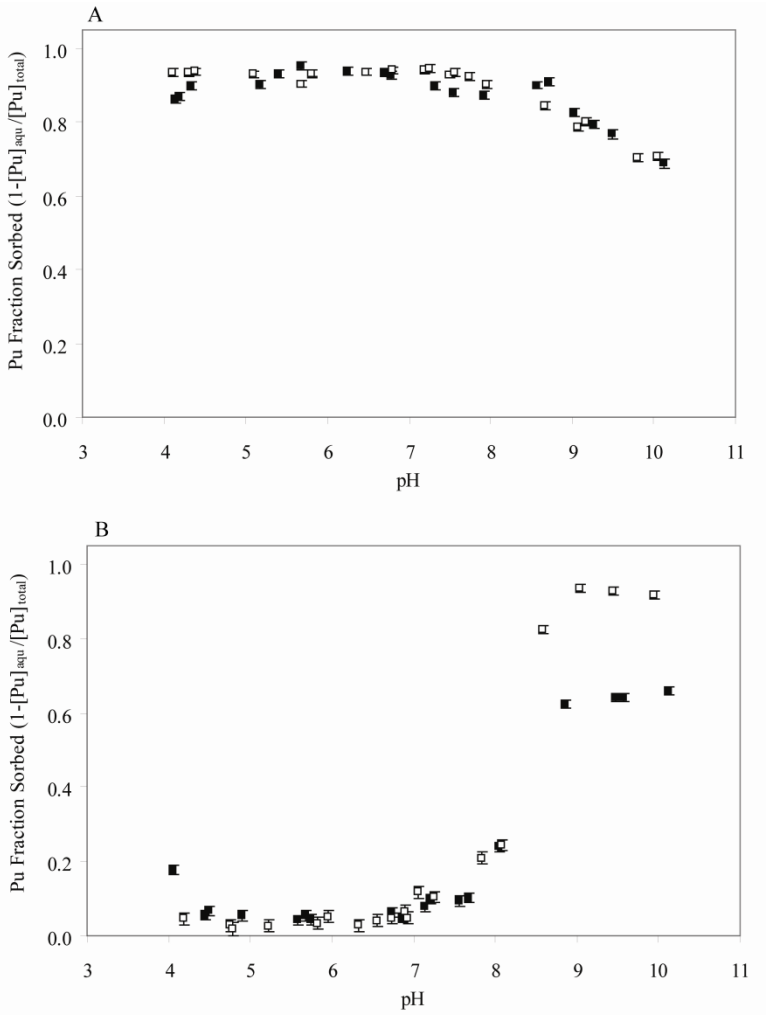

Figure 3.9: Sorption of (A) Pu(IV) and (B) Pu(V) to SWy-1 Na-montmorillonite at 24 hours. Open symbols represent systems where atmospheric CO_2(g) was excluded.

Table 3.3: Fraction of Sorbed Pu and Oxidation State Analysis of Aqueous Pu in Montmorillonite Suspensions after 160 days. Pu(IV)-montmorillonite experiment.

Sample pH	Supernatant Fraction Sorbed[a]	Filtrate Fraction Sorbed[b]	Fraction Pu(III/IV)[c,e]	Fraction Pu(V/VI)[c,e]	Fraction Pu(IV)[d,e]	Fraction Pu(V)[d,e]	Fraction Pu(VI)[d,e]
7.95	0.92 ± 0.05	0.92 ± 0.05	0.09	0.91	0.02	0.91	0.07
8.25	0.91 ± 0.04	0.91 ± 0.04	0.07	0.93	0.03	0.90	0.06
8.31	0.93 ± 0.05	0.93 ± 0.05	0.06	0.94	*error in sample processing*		
9.12	0.79 ± 0.03	0.83 ± 0.03	0.12	0.88	0.22	0.69	0.09
9.9	0.72 ± 0.03	0.78 ± 0.03	0.02	0.98	0.21	0.72	0.07

[a]Phases separated via centrifugation as done during sampling intervals
[b]Phases separated by passing suspension through 3k MWCO centrifugal filter of supernatant
[c]Using LaF_3-coprecipitation technique
[d]Using solvent extraction technique
[e]Due to low concentration of Pu in all samples, minimum error of 10% should be assumed

The surface-area-normalized sorption of Pu(IV) was greater in the montmorillonite suspension than might be expected based on an equivalent mixture of silica and gibbsite. The fraction of Pu sorbed after 24 hours in the montmorillonite, silica, and gibbsite suspensions around pH 4.5 was 86%, 63%, and 62%, respectively. The surface area concentration in silica and gibbsite suspensions was 10 m^2 L^{-1} while the montmorillonite suspensions were 6.3 m^2 L^{-1}. Furthermore, since surface complexation is expected to only occur on the clay edge sites in the montmorillonite suspension, the effective surface area for surface complexation is likely considerably lower for montmorillonite. Apparently, partitioning of Pu(IV) in low pH montmorillonite is controlled by an additional mechanism not available to gibbsite and silica surfaces, such as ion exchange. Given the high effective charge of Pu(IV) and the exchange capacity of the Swy-1 montmorillonite (Appendix A) this appears to be a plausible explanation that will be discussed in greater detail below.

The Pu fraction sorbed in Pu(V) suspensions changed over the course of the experiment (Figure 3.10b). The system did not appear to reach a steady state after 90 days. With the exception of the samples at the highest pH values, the Pu fraction sorbed increased over time. In a similar set of experiments (Zavarin et al., 2008), the rate of Pu(V) sorption to montmorillonite at low pH values (3 to 6) was found to be significantly affected by pH. Pu(V) sorption to montmorillonite was also found to be drastically affected by the background electrolyte concentration. The rate of Pu sorption was inversely related to the NaCl concentration and consistent with an ion exchange mechanism controlling Pu partitioning at low pH. The slow sorption of Pu in the Pu(V) systems was proposed to be due to either cation or proton exchange of Pu coupled with surface mediated reduction of Pu(V) to Pu(IV). The “dip” in the fraction of Pu sorbed between pH 5 and 7 (Figure 3.10b) is indicative of a transition point when ion exchange becomes negligible and surface complexation becomes the primary mechanism controlling Pu partitioning. This “dip” was also observed by Sanchez (1983) when examining Pu sorption to montmorillonite and Banik et al. (2007) when examining Pu sorption to kaolinite.

The Pu fraction sorbed in the Pu(V) systems after 90 days is slightly higher than that of the Pu(IV) systems. This is further circumstantial evience that formation of colloidal Pu(IV) may be controlling a small fraction of Pu in the Pu(IV) experiments. However, based upon the sorption behavior, solid free controls, and the measurement of Pu(V) within the initially Pu(IV) solutions, the fraction of colloidal Pu(IV) is expected to be less than 10%.

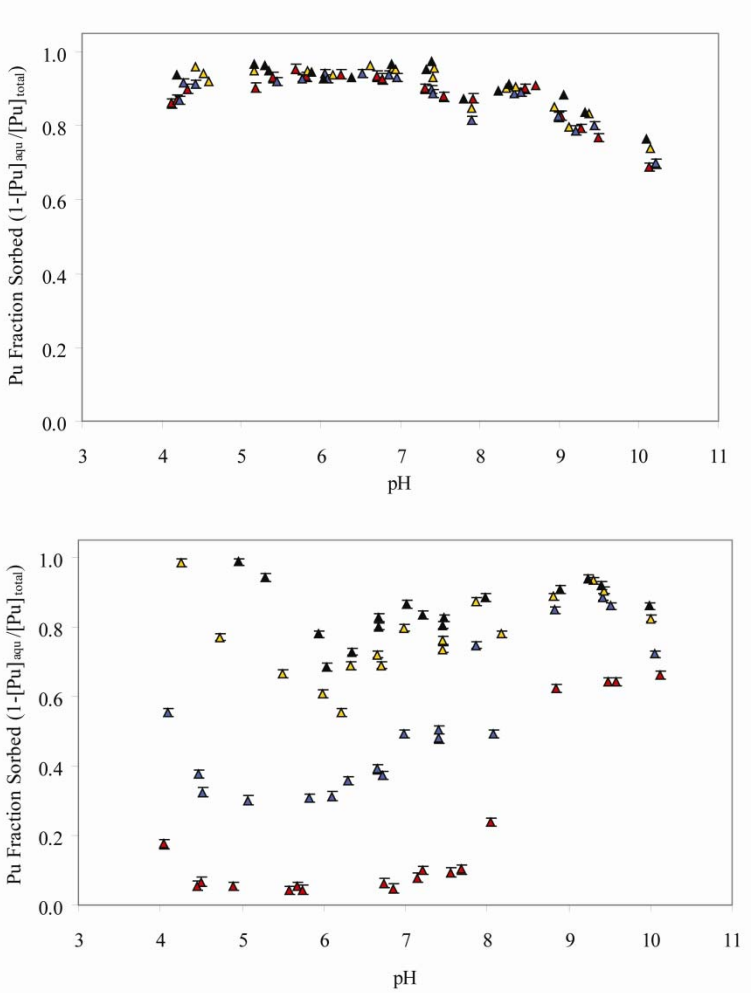

Figure 3.10: Sorption of (A) Pu(IV) and (B) Pu(V) to SWy-1 Na-montmorillonite in carbonate equilibrated solutions at 24 hours (red), 21 days (blue), 60 days (orange), and 90 days (black).

4 SURFACE COMPLEXATION MODELING USING EXISTING UGTA CONCEPTUAL MODEL

4.1 Description of Current UGTA Non-Electrostatic Surface Complexation Model

A listing of the relevant aqueous species thermodynamic constants from the current UGTA thermochemical database is shown in Table 4.1. The ion sizes listed are used in the extended Debye-Huckel activity coefficent model (also known as the B-dot model). Modeling efforts in this work utilized the Davies equation with constants 0.509 and 0.30, respectively. A value for the Pu(V)/Pu(IV) redox couple is reported in Table 4.1 but it has not been explicitly incorporated into current modeling efforts described in this chapter in order to remain consistent with the current UGTA database. Efforts have been made in Chapter 5 to fix a redox potential of the system and allow the Pu(IV/V) couple to come to equilibrium.

Table 4.1 Summary of Aqueous Complex Thermodynamic Constants in Current UGTA Database*

Species	Reaction	Ion Size (A)**	log K (25°C)
Complexation			
OH^-	$H_2O \leftrightarrow OH^- + H^+$	3.5	-14
$CO_2(aq)$	$H+ + HCO_3^- \leftrightarrow CO_2(aq)$	3	6.34
CO_3^{--}	$HCO_3^- \leftrightarrow H+ + CO_3^{--}$	4.5	-10.33
NaCl(aq)	$Na+ + Cl^- \leftrightarrow NaCl(aq)$	3	-0.777
$NaCO_3^-$	$Na+ + HCO_3^- \leftrightarrow H^+ + NaCO_3^-$	4	-9.814
$NaHCO_3(aq)$	$Na+ + HCO_3^- \leftrightarrow NaCO_3^-$	3	0.154
NaOH(aq)	$Na+ + H_2O \leftrightarrow NaOH(aq) + H^+$	3	-14.205
$PuOH^{+++}$	$Pu^{4+} + H_2O \leftrightarrow PuOH^{+++} + H^+$	5	-0.78
$Pu(OH)_2^{++}$	$Pu^{4+} + 2H_2O \leftrightarrow Pu(OH)_2^{++} + 2H^+$	4.5	-1.66
$Pu(OH)_3^+$	$Pu^{4+} + 3H_2O \leftrightarrow Pu(OH)_3^+ + 3H^+$	4	-4.62
$Pu(OH)_4(aq)$	$Pu^{4+} + 4H_2O \leftrightarrow Pu(OH)_4(aq) + 4H^+$	3	-8.85
$Pu(OH)_2(CO_3)_2^{--}$	$Pu^{4+} + 2H_2O + 2HCO_3^- \leftrightarrow Pu(OH)_2(CO_3)^{2--} + 4H^+$	4	-2.75
$Pu(OH)_4(CO_3)_{2----}$	$Pu^{4+} + 4H_2O + 2HCO_3^- \leftrightarrow Pu(OH)_4(CO_3)^{2--} + 6H^+$	5	-25.53
$Pu(CO_3)_4^{----}$	$Pu^{4+} + 4HCO_3^- \leftrightarrow Pu(CO_3)_4^{4-} + 4H^+$	5	-4.62
$Pu(CO_3)_5^{6-}$	$Pu^{4+} + 5HCO_3^- \leftrightarrow Pu(CO_3)_5^{6-} + 5H^+$	5	-16.3
$PuO_2OH(aq)$	$PuO_2^+ + H_2O \leftrightarrow PuO_2OH(aq) + H^+$	3	-9.7
$PuO_2CO_3^-$	$PuO_2^+ + HCO_3^- \leftrightarrow PuO_2CO_3^- + H^+$	4	-5.21
$PuO_2(CO_3)_2^{---}$	$PuO_2^+ + 2HCO_3^- \leftrightarrow PuO_2(CO_3)_2^{3-} + 2H^+$	4	-14.12
$PuO_2(CO_3)_3^{5-}$	$PuO_2^+ + 3HCO_3^- \leftrightarrow PuO_2(CO_3)_3^{5-} + 3H^+$	5	-26
Redox			
PuO_2^+/Pu^{++++}	$Pu^{++++} + 0.25O_2(g) + 1.5H_2O \leftrightarrow PuO_2^+ + 3H^+$	4	3.439

*Constants predominantly taken from DATACOM.V8.R6 of the GEMBOCHS thermodynamic database (Turner et al., 1998) and associated revisions (Carle et al., 2006; Pawloski et al., 2000; Pawloski et al., 2001; Tompson et al., 1999).

A summary of the relevant Non-electrostatic Surface Complexation Constants in the current UGTA database is listed in Table 4.2. We initially present predicted Pu sorption to silica, gibbsite, and montmorillonite using the current UGTA database (Tables 4.1 and 4.2). The data are later re-fit and non-electrostatic surface complexation constants updated.

Mineral characteristics used in surface complexation modeling are presented in Table 4.3. The site density of 2.3 sites per nm^2 used for gibbsite and silica is the recommended value for all minerals suggested by Davis and Kent (1990). It is assumed that the edge sites of montmorillonite are the locations for reactive surface sites. These sites represent 10% of the total available surface area (Turner et al., 1998). Therefore, the site density was decreased to 0.23 sites per nm^2 when calculating the aluminol and silanol site concentrations. White and Zelazny (1988) proposed an Al:Si ratio of 0.83 for the edge sites on montrmorillonite. This ratio was used to adjust the surface site distribution as shown in Table 4.3.

Table 4.2: Summary of non-electrostatic surface complexation constants from current UGTA database

Species	Reaction	Current UGTA Database, log K*
AlO^-	$AlOH \leftrightarrow AlO^- + H^+$	-9.73
$AlOH_2^+$	$AlOH + H^+ \leftrightarrow AlOH_2^+$	8.33
$AlOPu(OH)_2^+$	$AlOH + Pu^{4+} + 2\,H_2O \leftrightarrow AlOPu(OH)_2^+ + 3H^+$	5.95
$AlOPu(OH)_4^-$	$AlOH + Pu^{4+} + 4H_2O \leftrightarrow AlOPu(OH)_4^- + 5H^+$	-11.93
$AlOPuO_2^o$	$AlOH + PuO_2^+ \leftrightarrow AlOPuO_2^o + H+$	-3.09
SiO^-	$SiOH \leftrightarrow SiO^- + H^+$	-7.2
$SiOPu(OH)_2^+$	$SiOH + Pu^{4+} + 2H_2O \leftrightarrow SiOPu(OH)_2^+ + 3H^+$	2.32
$SiOPuO_2^o$	$SiOH + PuO_2^+ \leftrightarrow SiOPuO_2^o + H^+$	-6.43
$SiOPuO_2OH^-$	$SiOH + H_2O + PuO_2^+ \leftrightarrow SiOPuO_2OH^- + 2H^+$	-14.8

* Non-electrostatic Surface Complexation Model Constants from Zavarin and Bruton (2004).

Table 4.3: Mineral characteristics used in surface complexation modeling

Mineral	Surface Area ($m^2\ g^{-1}$)	Site Density	Site Type	Estimated Site Concentration in 10 $m^2\ L^{-1}$ Suspension (mol L^{-1})
Silica	1.18	2.3	>SiOH	3.85E-5
Gibbsite	1.85	2.3	>AlOH	3.85E-5
Montmorillonite	27.17	0.23	>SiOH (0.45)* >AlOH (0.55)*	>SiOH, 9.64E-7 >AlOH, 8.00E-7 Total, 1.76E-6

*Fraction of Total Sites based upon assumed Al:Si ratio of 0.83 (White and Zelazny, 1988)

4.2 Prediction of Pu Sorption Using Current UGTA Database

4.2.1 Prediction of Pu Sorption to Gibbsite

Using the current UGTA database (Tables 4.1 and 4.2) along with the mineral characteristics (Table 4.3), Pu(IV) and Pu(V) sorption to gibbsite was predicted and compared with sorption data. The 24 hour data was used to minimize effects of Pu(IV) oxidation and Pu(V) reduction in sorption data. The model output is shown in Figure 4.1. A table listing the concentrations for all species in each system that used to generate the model input files is reported in Appendix C.

Sorption of Pu(IV) was over-predicted at low pH values and provided a reasonable fit to the data at high pH values. As discussed earlier, the low Pu sorption at low pH may be the result of Pu(IV) oxidation by dissolved oxygen. Since Pu(V) was not considered in this model, this is considered a modeling artifact. The Pu(IV)-AlOH constants listed in Table 4.2 were calculated by Zavarin and Bruton (2004) based upon the data of Righetto et al. (1991) and Allard et al. (1982). Neither of the earlier studies measured or attempted to control the oxidation state of Pu used in their experiments. Therefore, Zavarin and Bruton (2004) were required to deduce the Pu oxidation state based upon sorption behavior. In this manner, constants for both Pu(IV) and Pu(V) were calculated from the data reported by Righetto et al. (1991) and constants for Pu(IV) were calculated based on the data of Allard et al. (1982).

Sorption of Pu(V) was accurately predicted for the CO_2(g)-free system (Figure 4.1c). The good agreement supports the assumption of Zavarin and Bruton (Zavarin and Bruton, 2004) that Pu(V) was present in the experiments performed by Righetto et al. (1991). Prediction of Pu(V) sorption in the presence of carbonate was under-predicted. This may be due to uncertainty in the thermodynamic constants for Pu(V)-carbonates or due to an underprediction of the stability of the $AlOPuO_2^o$ surface complex.

4.2.2 Prediction of Pu Sorption to Silica

Predictions of Pu(IV) and Pu(V) sorption to silica using the current UGTA database are shown in Figure 4.2. The constants within the current database cannot accurately predict Pu sorption to silica. Sorption of Pu(IV) is simulated using only one surface species, $SiOPu(OH)_2^+$. This species is predicted to sorb significantly at low pH. However, no additional Pu(IV)-SiOH species are included in the model so no sorption of Pu(IV) is predicted at high pH. The poor SiOH-Pu(IV) predition is primarily due to insufficient data available for Pu(IV)-silica system. Zavarin and Bruton (2004) estimated the $SiOPu(OH)_2^+$ constant from data describing Pu(IV) sorption to montmorillonite. In that model fit, Pu(IV)-AlOH species were assumed to predominate in the high pH region. Therefore, there was little need for additional Pu(IV)-SiOH species in the model.

Constants for the two Pu(V)-SiOH species included in the current database were fitted to data collected in a single sorption experiment (Sanchez, 1983). Sanchez (1983) examined Pu(V) sorption to silica gel and observed minimal sorption even up to pH 9 in a solution with a total Pu concentration of 10^{-14} M. The weak sorption coupled with a low total Pu concentration and very high silica gel surface areas resulted in relatively low fitted constants for the $SiOPuO_2^o$ and $SiOPuO_2OH^-$ species.

4.2.3 Prediction of Pu Sorption to Montmorillonite

Prediction of Pu(IV) sorption to montmorillonite provides acceptable fits to the data but several of the subtle effects of pH are not accurately predicted (Figure 4.3). The model incorrectly predicts a decrease in sorption at low pH. Additionally, the model does not predict the decrease in sorption observed at high pH. As discussed in Chapter 3, the aqueous Pu at high pH regions was likely a mixture of Pu(V) and colloidal Pu(IV). Since the model does not consider formation of either of these species, it would not be expected to provide a good fit to the data.

Due to the low constants for Pu(V)-SiOH species, sorption of Pu(V) to montmorillonte at low pH is drastically underpredicted (Figure 4.3). As the pH of the system increases, sorption of Pu(V) to aluminol sites increases and the model fit improves. However, an acceptable prediction of the Pu(V)-montmorillonite sorption data was not possible with the constants available in the current database.

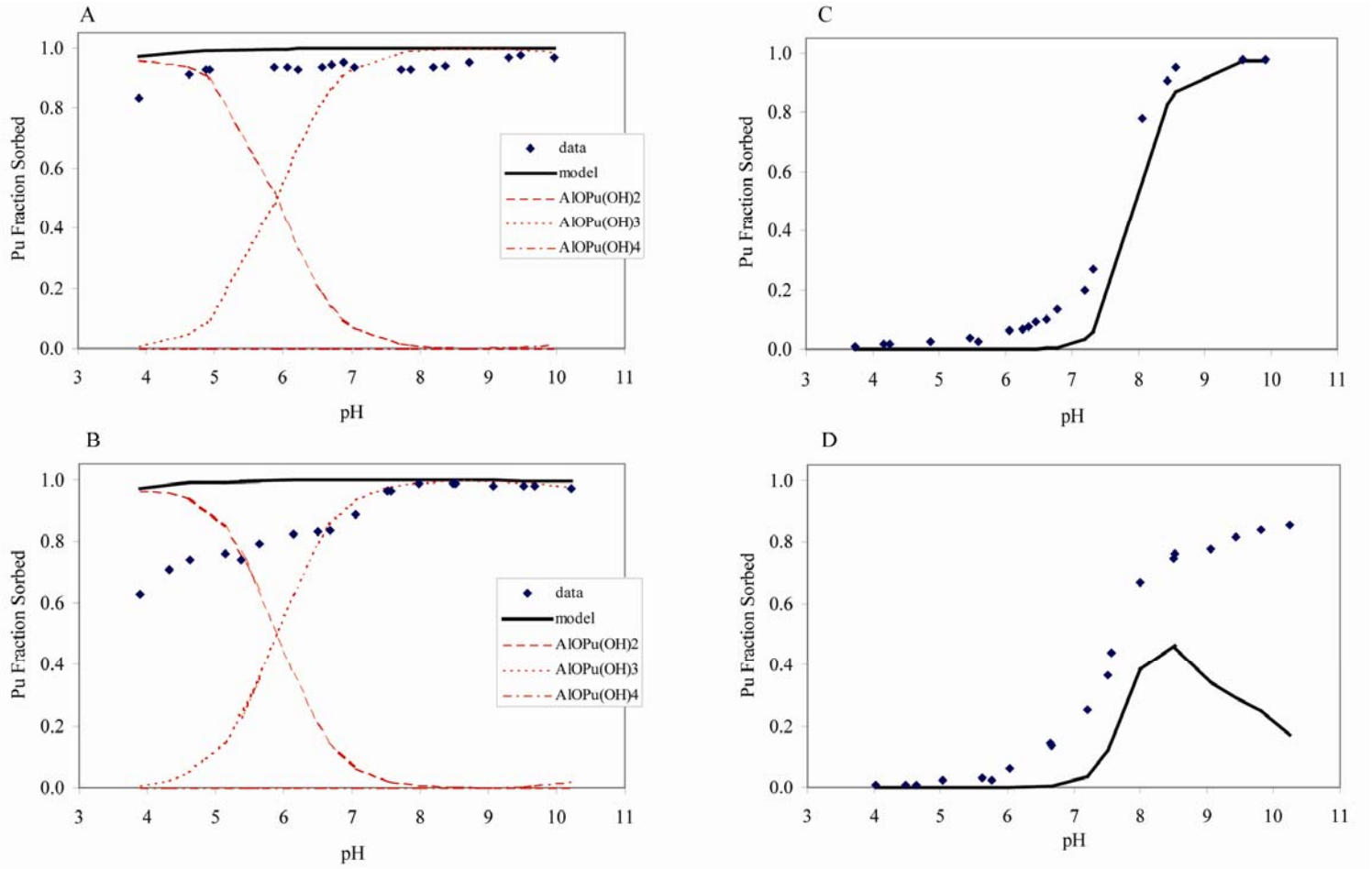

Figure 4.1: Prediction of Pu sorption to gibbsite after 24 hours using non-electrostatic surface complexation constants defined in the current UGTA database for (A) initially Pu(IV)-CO_2(g)free, (B) initially Pu(IV), CO_2(g)-equilibrated, (C) initially Pu(V), CO_2(g)-free, and (D) initially Pu(V), CO_2(g)-equilibrated sorption data. Speciation in Pu(V) systems is not displayed as $AlOPuO_2^0$ is the only surface complex defined in the current UGTA model.

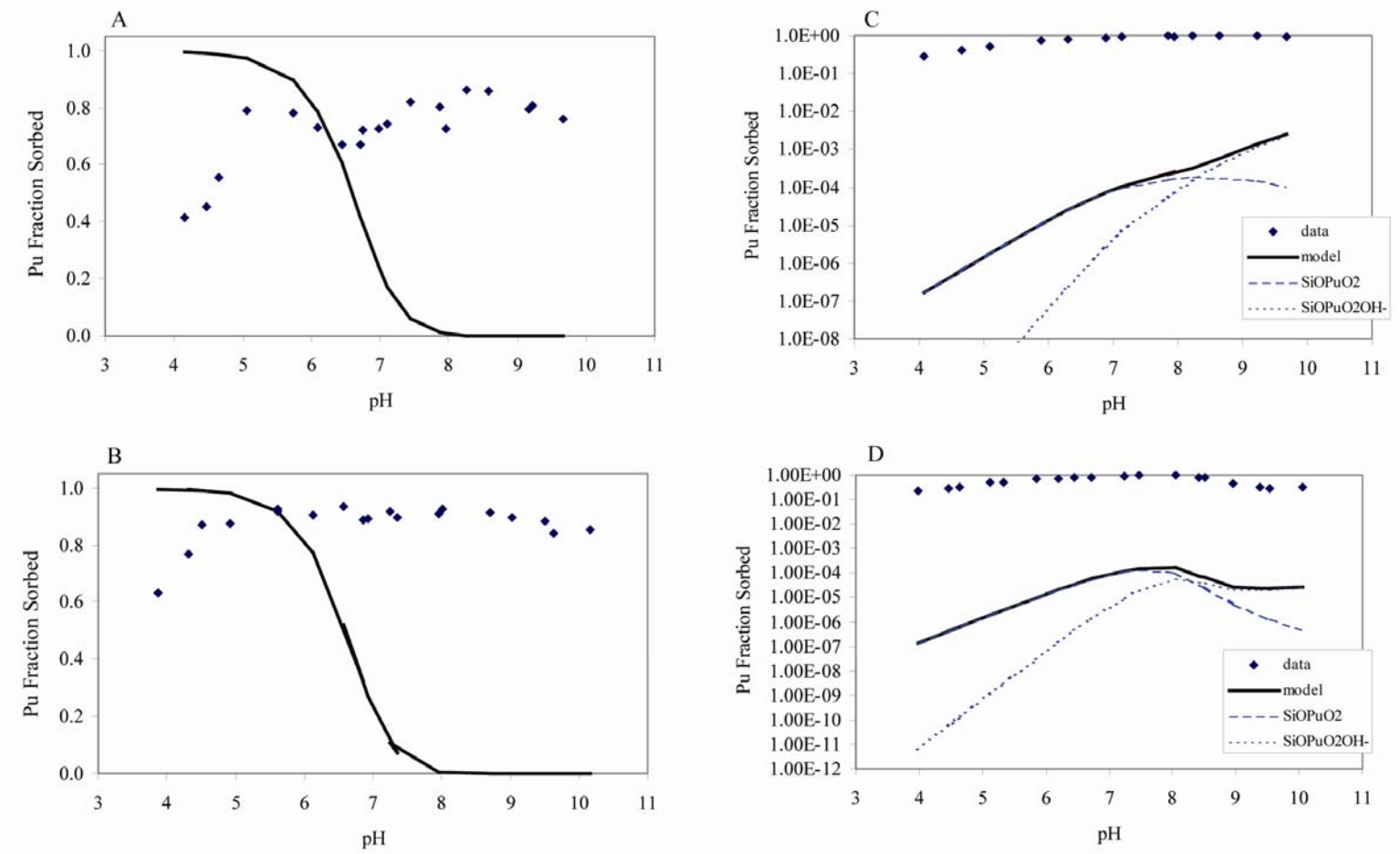

Figure 4.2: Prediction of Pu sorption to silica after 24 hours using non-electrostatic surface complexation constants defined in the current UGTA database for (A) initially Pu(IV)-CO_2(g)free, (B) initially Pu(IV), CO_2(g)-equilibrated (C) initially Pu(V), CO_2(g)-free, and (D) initially Pu(V), CO_2(g)-equilibrated sorption data. Speciation in Pu(IV) systems is not displayed as only one surface complex is defined in the current UGTA model.

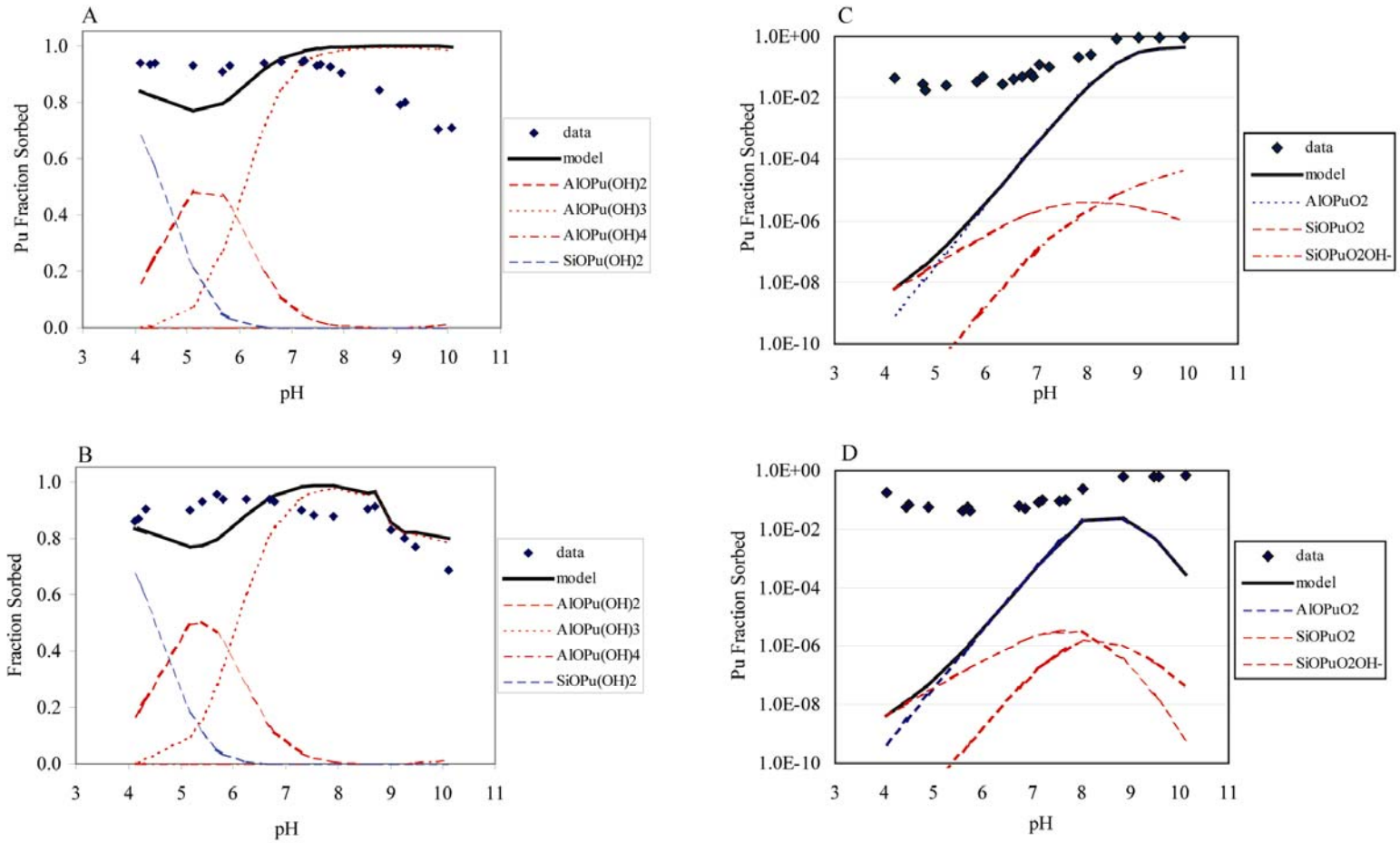

Figure 4.3: Prediction of Pu sorption to montmorillonite after 24 hours using non-electrostatic surface complexation constants defined in the current UGTA database for (A) initially Pu(IV)-CO_2(g)free (B) initially Pu(IV), CO_2(g)-equilibrated (C) initially Pu(V), CO_2(g)-free, and (D) initially Pu(V), CO_2(g)-equilibrated sorption data.

4.3 Determination of Revised Sorption Constants

Pu(IV) and Pu(V) sorption to silica and gibbsite were fit to obtain new non-electrostatic SCM constants for use in a revised UGTA database. To remain compatible with the current database, the aqueous thermodynamic constants listed in Table 4.1 and the protonation/deprotonation constants for aluminol and silanol groups (Table 4.2) were used. Changing these constants would require refitting of the entire database prior to incorporation of the revised Pu constants.

When modeling Pu(V) systems, only the data from CO_2(g)-free systems was used to generate sorption constants. Those constants were used to simulate the CO_2(g)-equilibrated system without additional fitting as a test of the reliability of the constants. Unfortunately, due to the observed instability of aqueous Pu(IV), we were not able to implement this approach when modeling Pu(IV) sorption data. Sorption constants were determined from each dataset and compared to determine the most "reliable" constant. It is important to note that similar considerations should be made for the Pu(V) dataset due to surface mediated reduction to Pu(IV). However, reduction of Pu(V) on non-redox active surfaces such as the gibbsite and silica used here is expected to be relatively slow, as demonstrated by the slow shift in the sorption edge in Pu(V) sorption experiments (Figures 3.5 and 3.10). Modeling of Pu(V) constants was only performed using sorption data obtained after 24 hours where the fraction of Pu(IV) on the surface would be minimal. This may not be a valid assumption. However, the alternative is to couple Pu(V/IV) in the sorption model which is beyond the scope of the modeling effort presented in this chapter. (*Note: Such a modeling effort will require reconsideration of the conceptual framework of Pu sorption in the current UGTA database. Such a revised model is proposed in Chapter 5.*) A list of the constants determined from each dataset is shown in Table 4.4. Model fits for each dataset and relevant discussion are presented below.

4.3.1 Pu(IV) Sorption to Gibbsite

Three separate model fits to Pu(IV)-gibbsite sorption data are shown in Figure 4.4. As discussed in Chapter 3, there was an observed difference between the sorption of Pu(IV) after 24 hours in CO_2(g)-free and CO_2(g)-equilibrated systems at low pH values. The constants obtained from fits to each dataset are shown in Table 4.4. In all systems the dominant surface species at low pH was $AlOPu(OH)_2^+$. In accordance with the observed sorption behavior at low pH values the log K for $AlOPu(OH)_2^+$ was 5.1 for the CO_2(g)-free system and 4.55 for the CO_2(g)-equilibrated system. The log K fitted for the 62 day sorption data further decreased to 4.1 due to the net desorption of Pu observed. The log K of 5.1 obtained for the CO_2(g)-free 24 hour sorption dataset compared most favorably with the value of 5.95 in the current UGTA database. Since it was shown that the aqueous Pu in the CO_2(g)-equilibrated datasets was predominantly Pu(V), the log K values for Pu(IV) sorption constants in that range will be artificially low. Therefore, the log K value of 5.1 for the $AlOPu(OH)_2^+$ species is recommended as a lower limit.

The log K values for the neutrally charged $AlOPu(OH)_3^o$ species were –3.37 and –3.52 for the 24 hours datasets in CO_2(g)-free and CO_2(g)-equilibrated systems, respectively. There is no corresponding neutrally charged species considered in the current UGTA database.

Table 4.4: Summary of Surface Complexation Constants Determined for Pu-silica and Pu-gibbsite Interactions. The corresponding constants from the current UGTA database are provided for comparison.

Dataset	Reaction Time	$CO_2(g)$	Reaction	Species	Revised log K	log K from Current UGTA Database*
Pu(IV)-gibbsite	24h	free	$AlOH + Pu^{4+} + 2H_2O \leftrightarrow AlOPu(OH)_2^+ + 3H^+$	$AlOPu(OH)_2^+$	5.1	5.95
			$AlOH + Pu^{4+} + 3H_2O \leftrightarrow AlOPu(OH)_3^o + 4H^+$	$AlOPu(OH)_3^o$	-3.37	
			$AlOH + Pu^{4+} + 4H_2O \leftrightarrow AlOPu(OH)_4^- + 5H^+$	$AlOPu(OH)_4^-$	-12.3	-11.93
Pu(IV)-gibbsite	24h	equilibrated	$AlOH + Pu^{4+} + 2H_2O \leftrightarrow AlOPu(OH)_2^+ + 3H^+$	$AlOPu(OH)_2^+$	4.55	5.95
			$AlOH + Pu^{4+} + 3H_2O \leftrightarrow AlOPu(OH)_3^o + 4H^+$	$AlOPu(OH)_3^o$	-3.52	
			$AlOH + Pu^{4+} + 4H_2O \leftrightarrow AlOPu(OH)_4^- + 5H^+$	$AlOPu(OH)_4^-$	-9.81	-11.93
Pu(IV)-gibbsite	62d	equilibrated	$AlOH + Pu^{4+} + 2H_2O \leftrightarrow AlOPu(OH)_2^+ + 3H^+$	$AlOPu(OH)_2^+$	4.16	5.95
			$AlOH + Pu^{4+} + 3H_2O \leftrightarrow AlOPu(OH)_3^o + 4H^+$	$AlOPu(OH)_3^o$	-2.64	
			$AlOH + Pu^{4+} + 4H_2O \leftrightarrow AlOPu(OH)_4^- + 5H^+$	$AlOPu(OH)_4^-$	-9.47	-11.93
Pu(IV)-silica	24h	equilibrated	$SiOH + Pu^{4+} + 2H_2O \leftrightarrow SiOPu(OH)_2^+ + 3H^+$	$SiOPu(OH)_2^+$		2.32
			$SiOH + Pu^{4+} + 3H_2O \leftrightarrow SiOPu(OH)_3^o + 4H^+$	$SiOPu(OH)_3^o$	-3.55	
			$SiOH + Pu^{4+} + 4H_2O \leftrightarrow SiOPu(OH)_4^- + 5H^+$	$SiOPu(OH)_4^-$	-9.05#,-10.71	
Pu(IV)-silica	62d	equilibrated	$SiOH + Pu^{4+} + 2H_2O \leftrightarrow SiOPu(OH)_2^+ + 3H^+$	$SiOPu(OH)_2^+$		
			$SiOH + Pu^{4+} + 3H_2O \leftrightarrow SiOPu(OH)_3^o + 4H^+$	$SiOPu(OH)_3^o$	-3.94	
			$SiOH + Pu^{4+} + 4H_2O \leftrightarrow SiOPu(OH)_4^- + 5H^+$	$SiOPu(OH)_4^-$	-8.77#, -9.07	
Pu(V)-gibbsite	24h	free	$AlOH + PuO_2^+ \leftrightarrow AlOHPuO_2^+$	$AlOHPuO_2^+$	5.36	
			$AlOH + PuO_2^+ \leftrightarrow AlOPuO_2^o + H^+$	$AlOPuO_2^o$	-3.09	-3.09
			$AlOH + H_2O + PuO_2^+ \leftrightarrow AlOPuO_2OH^- + 2H^+$	$AlOPuO_2OH^-$	-11.6	
Pu(V)-silica	24h	free	$SiOH + PuO_2^+ \leftrightarrow SiOHPuO_2^+$	$SiOHPuO_2^+$	4.11	
			$SiOH + PuO_2^+ \leftrightarrow SiOPuO_2^o + H^+$	$SiOPuO_2^o$	-1.10	-6.43
			$SiOH + H_2O + PuO_2^+ \leftrightarrow SiOPuO_2OH^- + 2H^+$	$SiOPuO_2OH^-$	-11.3	-14.80

* Non-electrostatic Surface Complexation Model Constants from (Zavarin and Bruton, 2004).
#Constants determined while suppressing formation of Pu(IV)-carbonate and Pu(IV)-hydroxycarbonate species.

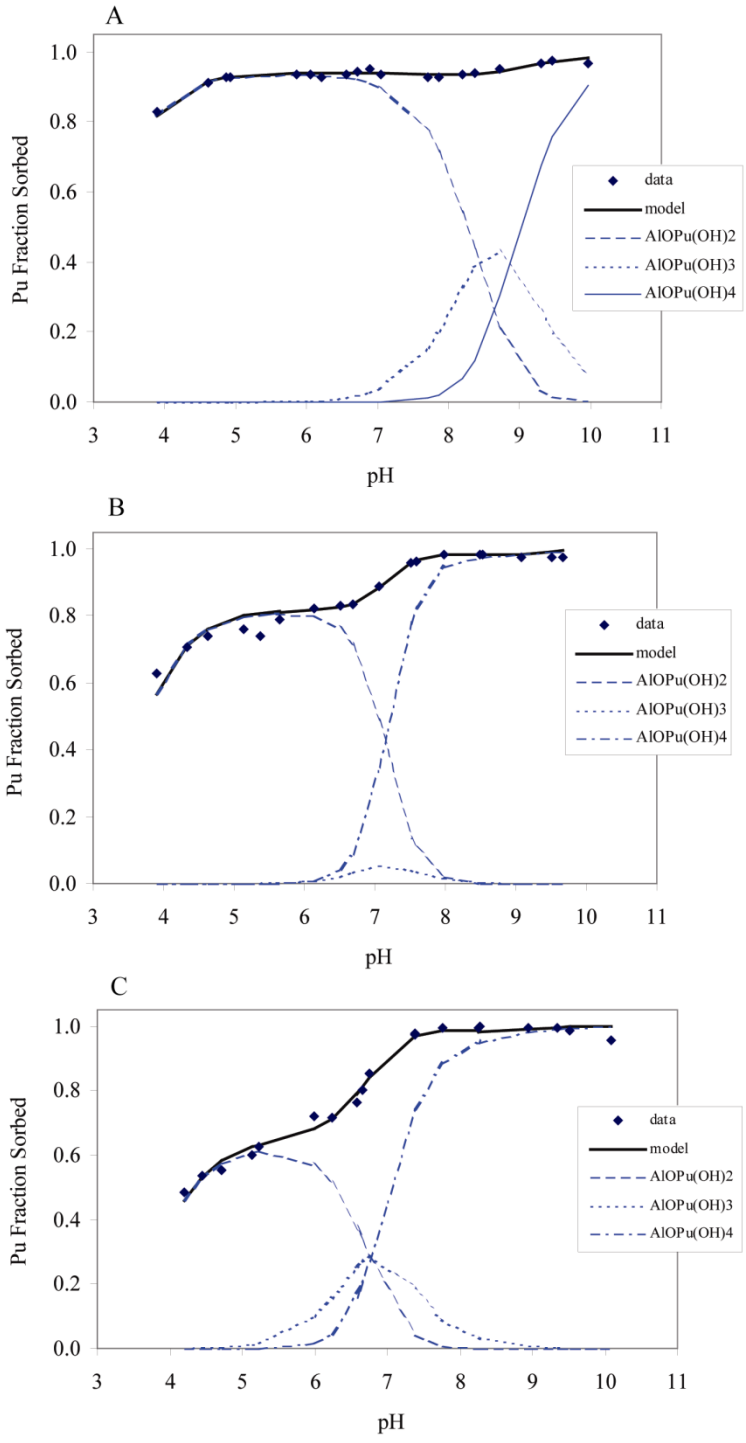

Figure 4.4: Sorption of Pu(IV) to gibbsite for (A) 24 hours CO_2(g)-free (B) 24 hours CO_2(g)-equilibrated, and (C) 62 days CO_2(g)-equilibrated sorption data. Solid black lines represent total model fit to data and broken blue lines represent individual species distribution within model.

The log K values for the Pu species predominating at high pH vary significantly due to the influence of carbonate when determining the constants. The log K of –12.3 obtained from the 24hour CO_2(g)-free dataset is most consistent with the value of –11.93 from the current UGTA database. The log K constants of –9.8 and –9.5 for the CO_2(g)-equilibrated datasets after 24 hours and 62 days, respectively, appear to be artificially low due to inclusion of carbonate species when determining the constants. In the high pH regions, there does not appear to be an observable difference in the sorption behavior in CO_2(g)-free and CO_2(g)-equilibrated systems. Therefore, either Pu(IV)-carbonate/hydroxycarbonate species have similar sorption affinities as Pu(IV)-hydroxides or aqueous Pu(IV)-carbonates/hydroxycarbonates did not form in sufficient quantities to significantly affect sorption. The log K values determined for CO_2(g)-equilibrated systems may have been artificially increased to negate the formation of Pu(IV)-carbonates/hydroxycarbonates.

4.3.2 Pu(IV) Sorption to Silica

As discussed above, the current UGTA database is unable to accurately predict Pu sorption to silica since $SiOPu(OH)_2^+$ is the only assumed surface species and it is not predicted to sorb at high pH values. Attempts to fit the data with only $SiOPu(OH)_2^+$ were unsuccessful. The best model fits were obtained assuming $SiOPu(OH)_3^o$ and $SiOPu(OH)_4^-$ as the sorbing species. An acceptable fit to the data could also be achieved by including $SiOPu(OH)_2^+$ as a sorbing species but $SiOPu(OH)_3^o$ provided a better fit to the data. Based on known Pu(IV) solution chemistry, the predominance of a fully hydrolyzed Pu(IV) hydroxide species at the silica surface at circumneutral pH is more plausible.

Constants for Pu(IV)-silanol species were only determined for the datasets equilibrated with carbonate. As discussed above, the data from CO_2(g)-free experiments are proposed to contain a significant fraction of Pu(V) and therefore be unrepresentative of Pu(IV) sorption. This is supported by the measurement of Pu(V/VI) as the predominant oxidation state of aqueous Pu in low pH silica suspensions. Therefore, the most reliable data are from the CO_2(g)-equilibrated dataset after 62 days as it contained the largest fraction of Pu(IV). This assumption is supported by the convergence of the initially Pu(IV) and initially-Pu(V) datasets after 62 days. The model fits for the CO_2(g)-equilibrated dataset after 24 hours are shown for reference. Both datasets yielded similar log K values. The log K for $SiOPu(OH_3)^o$ decreased from –3.55 to –3.94 due to the slight desorption of Pu observed in these systems over between 24 hours and 62 days, respectively. Since the aqueous Pu was determined to be predominantly Pu(IV), the higher log K value of –3.55 from the 24 hour dataset is proposed to be more representative of Pu(IV). There was a more significant difference in the log K values for $SiOPu(OH)_4^-$. As discussed for the gibbsite datasets above, formation of $Pu(OH)_2(CO_3)_2^{2-}$ significantly affects the results. For the 62 day dataset, the log K decreased from –8.77 to –9.07 when $Pu(OH)_2(CO_3)_2^{2-}$ was excluded. For the 24 day dataset, $Pu(OH)_2(CO_3)_2^{2-}$ has a greater effect on the sorption constants due to the higher concentration of aqueous Pu at high pH values. The similarity of the values for both datasets when $Pu(OH)_2(CO_3)_2^{2-}$ is included indicates that the most accurate value may be approximately -9.

4.3.3 Pu(V) Sorption to Gibbsite

Sorption constants for Pu(V)-aluminol species were determined from the dataset obtained after 24 hours. Again, the assumption in this modeling effort is that surface mediated reduction of Pu(V) to Pu(IV) is kinetically hindered and the data are most representative of Pu(V) sorption. A good fit was obtained assuming three surface complexes as noted in Table 4.4. The model fit is shown in Figure 4.6a. The current model includes only one sorbing species, $AlOPuO_2^o$ with a log K of –3.09. Attempts to model the Pu(V)-gibbsite sorption data with only one species were unsuccessful.

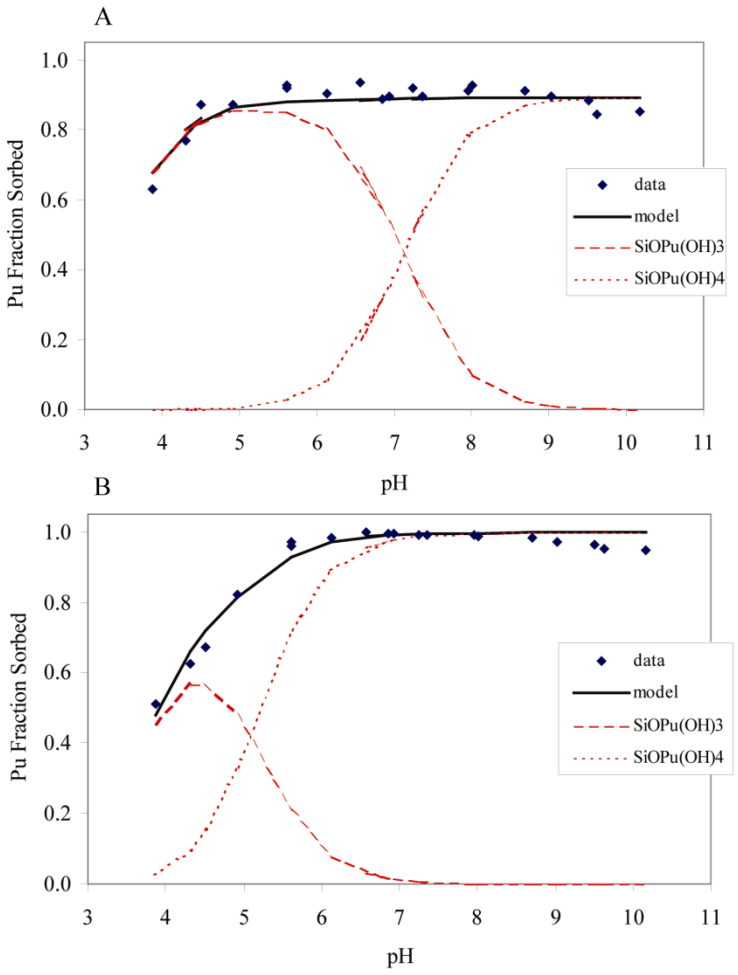

Figure 4.5: Sorption of Pu(IV) to silica under the following conditions a). 24 hours, CO_2(g)-equilibrated and b). 62 days, CO_2(g)-equilibrated. Solid black lines represent total model fit to data and broken red lines represent individual species distribution within model.

The log K value of $AlOPuO_2^o$ was fixed at –3.09 to remain consistent with the current UGTA database and the constants for $AlOHPuO_2^+$ and $AlOPuO_2OH^-$ were fitted (Figure 4.6a). Using these constants to predict the effect of carbonate on Pu(V) sorption to gibbsite resulted in a reasonable fit to the data (Figure 4.6b). The model accurately predicts the "sorption edge" and

general shape of the curve. It is noteworthy that the HCO_3^-/CO_3^{2-} concentration used in these experiments is in equilibrium with atmosphereic $CO_2(g)$ up to pH 9. Thereafter, the concentration is limited to 10 mM total carbonate. There is a notable divergence between $CO_2(g)$-free and $CO_2(g)$-equilibrated Pu(V) systems at pH 7 to 8 as the formation of Pu(V)-carbonate complexes becomes favorable. As the pH rises above 8, competition between formation of Pu(V)-carbonates and Pu(V)-hydroxide occurs and the effect of carbonate on Pu(V) sorption is diminished.

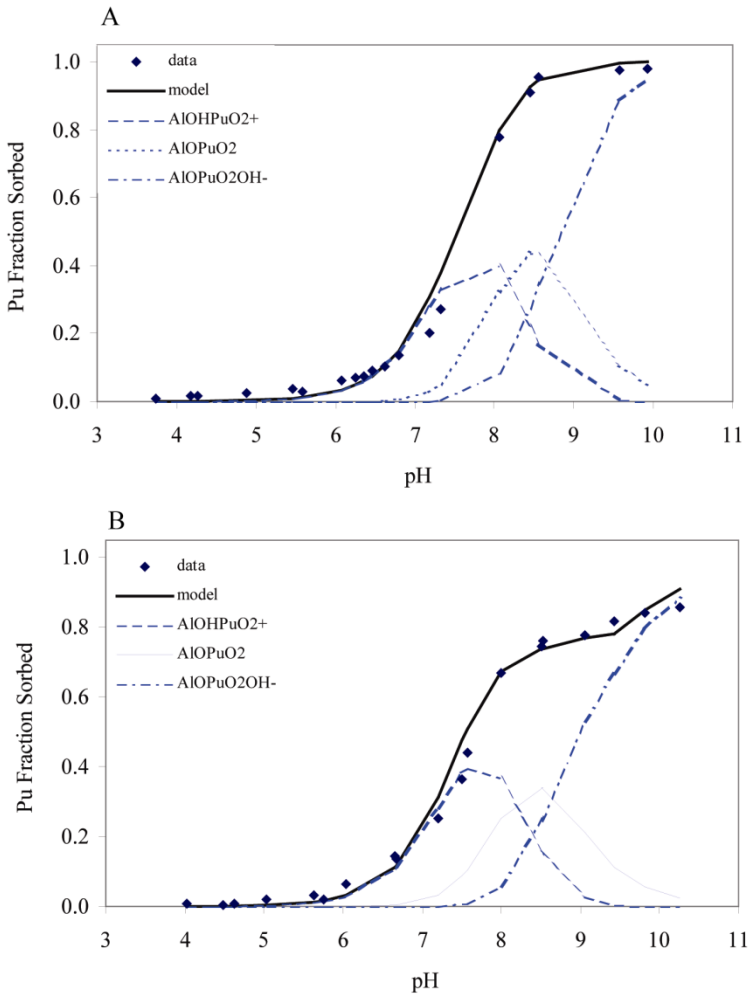

Figure 4.6: Sorption of Pu(V) to gibbsite after 24 hours for (A) $CO_2(g)$-free and (B) $CO_2(g)$-equilibrated sorption data. Solid black lines represent total model fit to data and broken red lines represent individual species distribution within model.

4.3.4 Pu(V) Sorption to Silica

Pu(V) sorption to silica was accurately modeled assuming three solid phase species, $SiOHPuO_2^+$, $SiOPuO_2^0$, and $SiOPuO_2OH^-$. The log K values for the $SiOPuO_2^o$ and $SiOPuO_2OH^-$ species are 5.3 and 3.5 orders of magnitude higher, respectively, than the corresponding species in the

current UGTA database. Pu(V) sorption was drastically under-predicted using the current UGTA database (Figures 4.2c and 4.2d). Efforts to model the data using only the two Pu(V)-silanol species assumed in the current UGTA database provided a good fit to the data in the high pH region but overpredicted sorption at neutral pH values. Therefore, an additional sorbing species was added, $SiOHPuO_2^+$. The single datapoint at pH 4 was found to be very influential on the log K value for $SiOHPuO_2^+$ and impeded model convergence. The $SiOHPuO_2^+$ species was manually adjusted to –4.1 to achieve the fit shown in Figure 4.7. Alternatively, by omitting the single datapoint at pH 4, FIT4FD was able to converge on all three surface species. The log K values for $SiOPuO_2^o$ and $SiOPuO_2OH^-$ did not significantly change but the log K for $SiOHPuO_2^+$ increased to 4.4. Due to the sensitivity of the log K value for $SiOHPuO_2^+$, an error of at least 0.5 log units is recommended. It is noteworthy that the sensitivity of this value is also linked to the assumed SiOH deprotonation constant of –7.0. As shown in Figure 4.7b, the revised constants were able to accurately predict the effect of carbonate on Pu(V) sorption to silica.

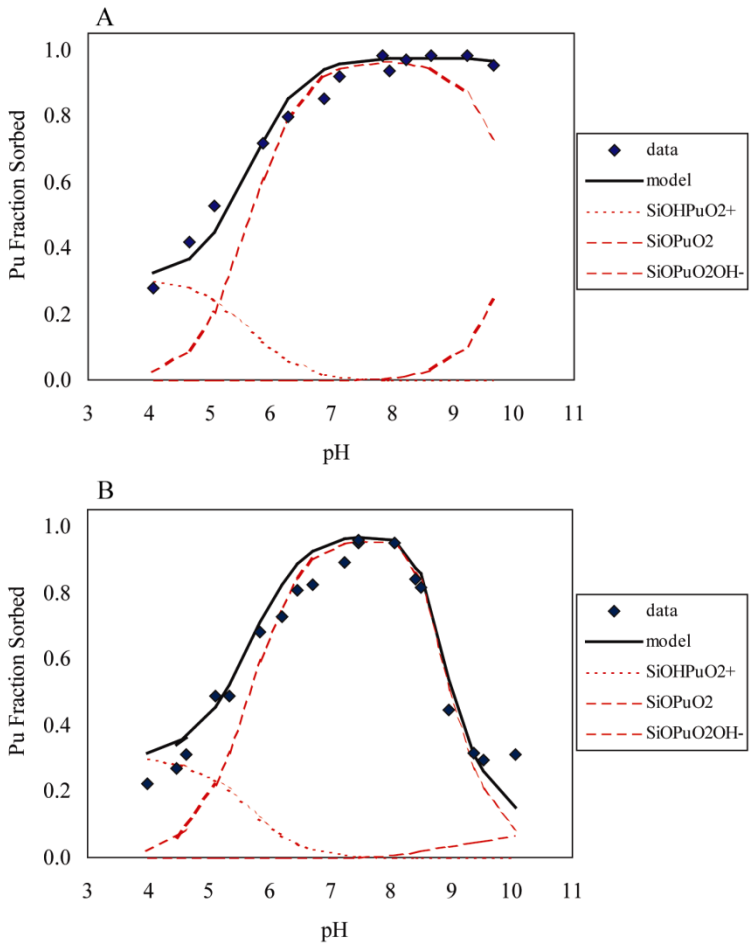

Figure 4.7: Sorption of Pu(V) to silica after 24 hours for (A) CO_2(g)-free and (B) CO_2(g)-equilibrated sorption data. Solid black lines represent total model fit to data and broken red lines represent individual species distribution within model.

4.4 Modeling Pu Sorption to Montmorillonite using Revised Sorption Constants

4.4.1 Pu(V) Sorption to Montmorillonite

The Pu(V)-silanol and Pu(V)-aluminol constants listed in Table 4.5 were selected from the modeling effort described above to perform predictive modeling of the Pu(V)-montmorillonite sorption data. These constants were selected as the most reliable based on the discussion above. The constants were utilized in FIT4FD along with the montmorillonite surface data listed in Table 4.3 to generate the model shown in Figure 4.8a. All constants and surface site concentrations were fixed in this model to evaluate how well constants derived from silica and gibbsite sorption data could predict Pu(V) sorption to montmorillonite. As shown in Figure 4.8a, the model approximates the shape of the sorption curve but does not accurately predict the data. The model overpredicts sorption in the pH range 6 to 8 through predominance of $SiOPuO_2^o$. Additionally, the model underpredicts sorption at high pH values and is not able to accurately fit the slight decrease in sorption at pH greater than 9.

Additional modeling exercises were preformed to determine sensitivity of log K values (Table 4.5). Reasonable fits to the data were achieved in two cases. In both cases, the constant for $SiOPuO_2^o$ was changed to approximately –1.9. However reasonable fits to the high pH data were achieved by adjusting the log K values for either $SiOPuO_2OH^-$ or $AlOPuO_2OH^-$ (Table 4.5). The best fit was obtained by adjusting $SiOPuO_2^o$ and $AlOPuO_2OH^-$ simultaneously. The model fit using these constants is shown in Figure 4.8b. It is important to note that this is purely a fitting exercise with no evidence to support preferentially modifying either Pu-aluminol or Pu-silanol surface complexation constants. Using the constants from "Adjusted Model 1" (Table 4.5), the effect of $CO_2(g)$ was reasonably predicted as shown in Figure 4.9.

Overall, the use of sorption constants derived from Pu(V)-gibbsite and Pu(V)-silica experiments appears to be capable of qualitatively predicting sorption of Pu(V) to montmorillonite. By adjusting two constants by approximately one log unit, a substantially better fit to the data could be achieved.

Table 4.5: Pu(V)- Surface Complexation Constants Used in Montmorillonite Sorption Modeling

Dataset	Species	Selected Constants from Table 4.4	Adjusted Model 1	Adjusted Model 2
Pu(V)-gibbsite	$AlOHPuO_2^+$	5.36	same, fixed	same, fixed
	$AlOPuO_2$	-3.09	same, fixed	same, fixed
	$AlOPuO_2(OH)^-$	-11.6	-10.5	same, fixed
Pu(V)-silica	$SiOHPuO_2^+$	4.11	same, fixed	same, fixed
	$SiOPuO_2$	-1.1	-1.91	-1.94
	$SiOPuO_2OH^-$	-11.3	same, fixed	-9.95

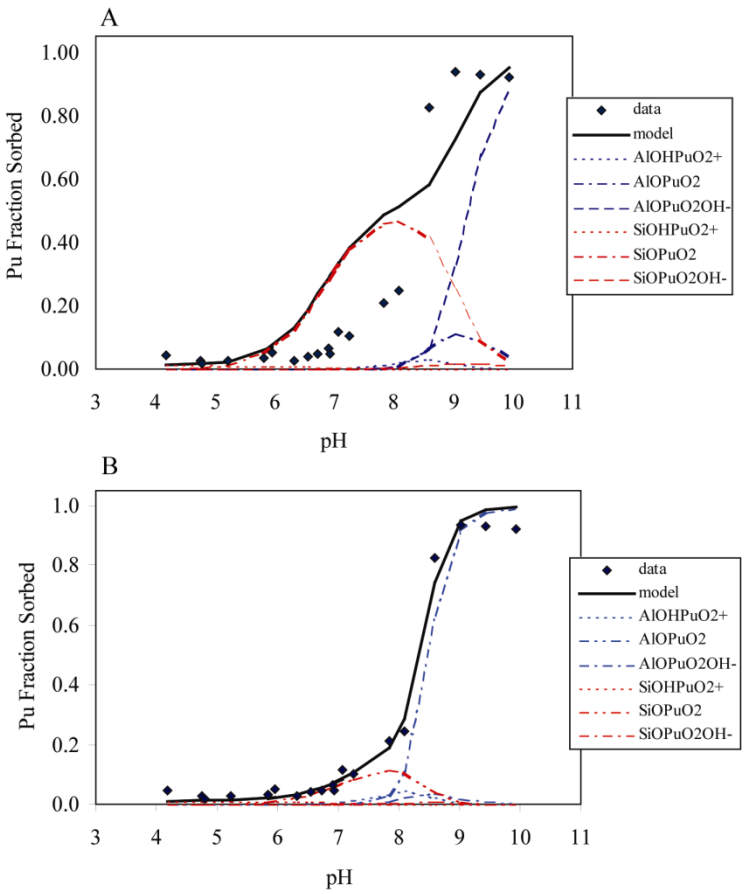

Figure 4.8: Pu(V) sorption to montmorillonite under CO_2(g) free conditions after 24 hours using (A) constants determined from Pu(V)-gibbsite and Pu(V)-silica studies and (B) revised constants for $SiOPuO_2^o$ and $AlOPuO_2OH^-$. Surface complexation constants used in model are listed in Table 4.5.

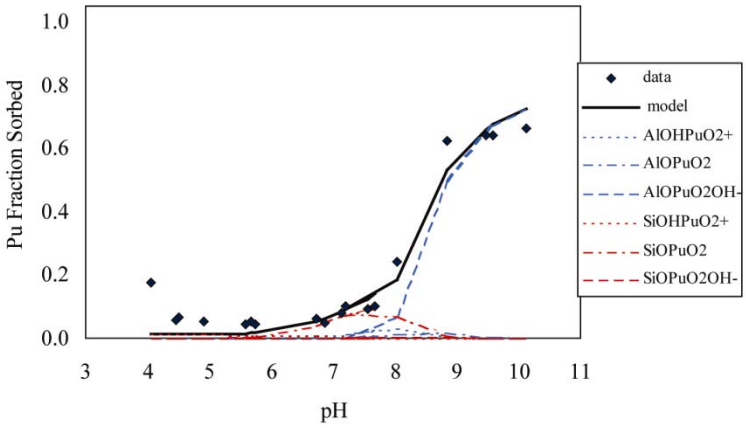

Figure 4.9: Prediction of Pu(V) sorption to montmorillonite after 24 hours under CO_2(g) equilibrated conditions using adjusted model constants listed in Table 4.4.

4.4.2 Pu(IV) Sorption to Montmorillonite

Predictions of Pu(IV) sorption to montmorillonite are shown in Figure 4.9. The Pu(IV)-aluminol and Pu(IV)-silanol constants selected from the silica and gibbsite model fits are listed in Table 4.6. Overall the model did a poor job of fitting using the Pu(IV)-aluminol and Pu(IV)-silanol constants determined from gibbsite and silica studies. At low pH, sorption of Pu was drastically under-predicted and at high pH sorption was over-predicted.

Some additional modeling exercises were performed to determine sensitivity of log K values. The surface complexation constants determined from some of these exercises are listed in Table 4.6 and fits to the data are shown in Figure 4.10. When performing these modeling exercises, not all surface species were considered at once. Within individual exercises, only selected surface complexes were considered. From Figure 4.10, it is clear that acceptable fits to the data can be obtained using several non-unique sets of constants.

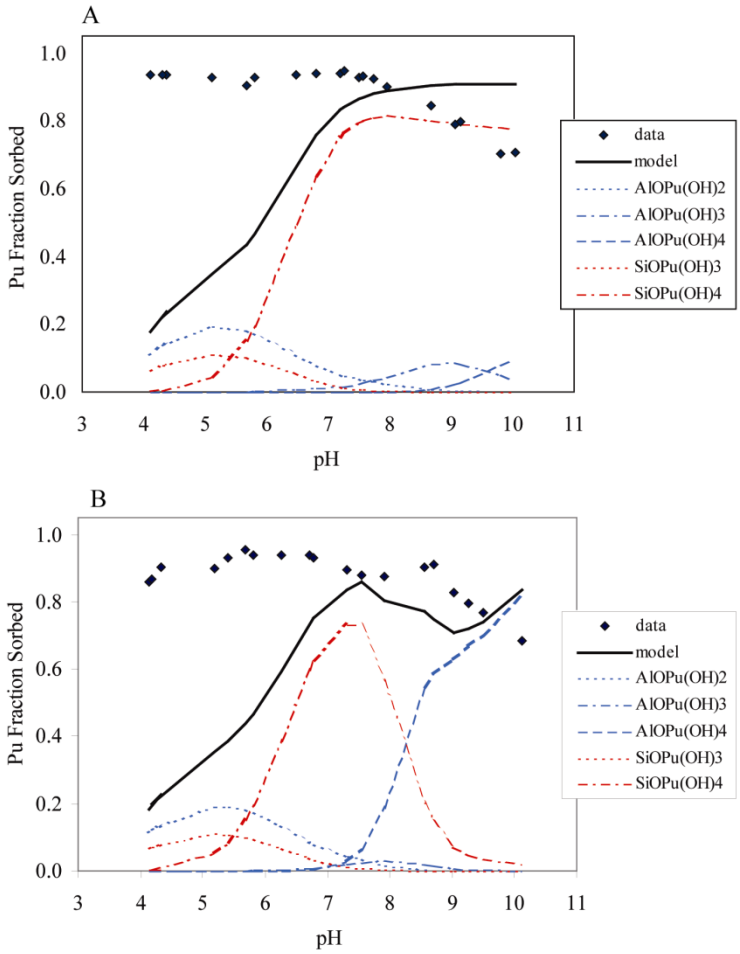

Figure 4.9: Pu(IV) sorption to montmorillonite after 24 hours under (A) CO_2(g)-free and (B) CO_2(g)-equilibrated conditions using constants determined from Pu(IV)-gibbsite and Pu(IV)-silica studies. Surface complexation constants used in model are listed in Table 4.6.

Table 4.6: Pu(IV) Surface Complexation Constants Used in Montmorillonite Sorption Modeling

Species	Selected for Montmorillonite Sorption Modeling	Adjusted Model 1	Adjusted Model 2	Adjusted Model 3	Adjusted Model 4	Adjusted Model 5	Adjusted Model 6	Adjusted Model 7
$AlOPu(OH)_2^+$	5.10		6.93		6.66	6.93	6.61	
$AlOPu(OH)_3^o$	-2.64			-2.07	-1.98			
$AlOPu(OH)_4^-$	-12.3		-11.92	-12.45				-11.97
$SiOPu(OH)_2^+$		2.66	2.27		2.70			
$SiOPu(OH)_3^o$	-3.55			-1.27			-1.80	-0.46
$SiOPu(OH)_4^-$	-9.10	-9.67				-9.69	-9.66	

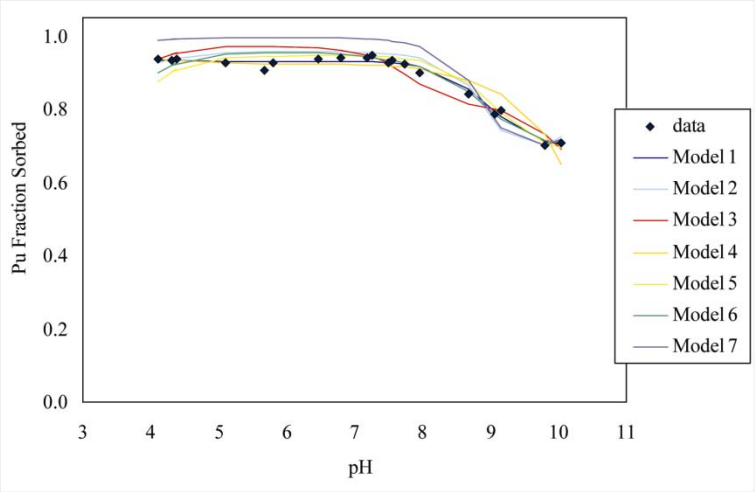

Figure 4.10: Additional model fits to Pu(IV) montmorillonite sorption data assuming various Pu(IV) surface complexes as listed in Table 4.6.

Finding multiple solutions to a sorption dataset is a common problem in surface complexation modeling. Turner et al. (1998) calculated Np-silanol and Np-aluminol surface complexation constants based solely on montmorillonite sorption data. A good fit was achieved using only two species: $AlONpO_2^o$ and $SiOHNpO_2^+$. However, the possibility of this being a non-unique solution was not discussed. These surface complexation constants cannot be assumed to represent true surface species as they represent non-unique solutions. However, general trends can be observed. In order to account for the drastic under-prediction of Pu sorption at low pH, the log K values for the $SiOPu(OH)_3^o$ and $AlOPu(OH)_2^+$ species were required to increase by approximately 1.5 log units. Additionally, the $SiOPu(OH)_2^+$ species could be assumed to account for the high sorption at low pH. Although Figure 4.9 shows that the model over-predicted Pu sorption at high pH, the surface complexation constants for $AlOPu(OH)_4^-$ and $SiOPu(OH)_4^-$ species are relatively consistent for all models listed in Table 4.6.

There are a number of factors contributing to the under-prediction of Pu sorption at low pH and the over-prediction at high pH. The high degree of Pu(IV) sorption at low pH is not expected based upon the observations from the Pu(IV)-gibbsite and Pu(IV)-silica datasets. As shown in Figure 3.4 (gibbsite) and Figure 3.6 (silica), at pH <5 less than 90% of the Pu is sorbed after 62 days for both systems. For the Pu(IV)-gibbsite system, less than 60% of the Pu is sorbed after 62

days. The silica and gibbsite suspensions were estimated to have 3.85 x 10^{-5} mol L^{-1} total surface sites while the montmorillonite suspensions were estimated to have 1.76 x 10^{-6} mol L^{-1}. Since the total number of surface sites in the montmorillonite suspensions are a factor of 30 lower than the silica and gibbsite suspensions, the sorption observed in the montmorillonite suspension cannot be attributed to equivalent reactions on gibbsite or silica. There are two very important assumptions in the above analysis that do not correctly describe the systems. They are:

1. Pu(IV) is the only Pu oxidation state in the system. While this was assumed for the gibbsite and silica systems, this was shown to be incorrect through chemical oxidation state analysis for all systems. In most cases, Pu(V) was the predominant aqueous oxidation state. There is also some evidence that Pu(IV) hydroxide polymer may have formed at high pH (see control samples Figure 3.1). By assuming Pu(IV) is the only oxidation state present in the silica and gibbsite suspensions, the Pu(IV) surface complexation constants are artificially lowered because they assume the aqueous Pu is Pu(IV) while it is actually Pu(V).

2. The only mechanism for sorption is surface complexation. This neglects ion exchange processes known to occur with montmorillonite clays, particularly at low pH. Therefore, the increased sorption at low pH could very well be the result of ion exchange.

5 SURFACE COMPLEXATION MODELING WITH INCORPORATION OF Pu(IV)/Pu(V) REDOX COUPLE

5.1 Incorporation of Active Pu(IV)/Pu(V) Redox Couple in Surface Complexation Model

A revised conceptual model of Pu aqueous chemistry and sorption behavior can be devised from the following general observations of Pu solution chemistry and sorption behavior.

1. Pu(V/VI)) is the predominant aqueous phase oxidation state even in the presence of minimal dissolved oxygen. This was demonstrated during $Pu(OH)_4(s)$ and $PuO_2(s)$ solubility experiments in which the aqueous phase oxidation state was measured (Neck et al., 2007; Rai, 1984; Rai et al., 2001; Rai et al., 1980)
2. Following sorption of Pu initially added as Pu(V), reduction to Pu(IV) progresses at various rates ranging from minutes to months. This has been shown using both indirect chemical separation oxidation state analysis techniques as well as direct x-ray absorption spectroscopy for the following solids:
    - magnetite, Fe_3O_4 (Powell et al., 2003)
    - goethite, α-FeOOH (Keeney-Kennicutt and Morse, 1985; Penrose et al., 1987; Powell et al., 2005; Sanchez et al., 1985)
    - hematite, α-Fe_2O_3 (Keeney-Kennicutt and Morse, 1985; Powell et al., 2005)
    - silica, SiO_2 (Sanchez, 1983) indirectly inferred
    - gibbsite, α-$Al(OH)_3$ (Sanchez, 1983) indirectly inferred
    - hausmannite, Mn_3O_4 and manganite, γ-MnOOH (Powell et al., 2003; Shaughnessey et al., 2003)

- pyrolusite, β-MnO_2 and ranceite (incorporated in Yucca Mountain tuff (Powell et al., 2006)
- sandy soils, (Kaplan et al., 2004)

3. Desorption of Pu(IV) appears to be coupled with reoxidation to Pu(V) at a rate approximately 5 orders of magnitude slower than the forward reduction rate. This yields a constant distribution of aqueous Pu(V) and sorbed Pu(IV) which appears to be significantly affected by pH. This has been clearly demonstrated in Zavarin et al. (2008) with a series of batch flow-through experiments examining Pu sorption to goethite. Additionally, a similar difference in relative rates was required in a reactive transport model to predict the observed long-term Pu mobility (Kaplan et al., 2004).
4. Based upon preliminary results reported by Zavarin et al. (2008), ion exchange appears to significantly contribute to Pu(IV) sorption at low pH but has little contribution to Pu(V) sorption at intermediate and high ionic strengths.

A revised modeling scheme was developed based on the known Pu behavior. A flowsheet of the modeling scheme is shown in Figure 5.1. First, the surface complexation constants for Pu(V) are determined from the 24 hours sorption datasets for gibbsite and silica assuming Pu(V) is the predominant oxidation state. Note that inherent in this assumption is a further assumption that surface mediated reduction of Pu(V) to Pu(IV) is negligible within the first 24 hours. This step has already been performed as discussed above. The surface complexation constants are listed in Table 4.5.

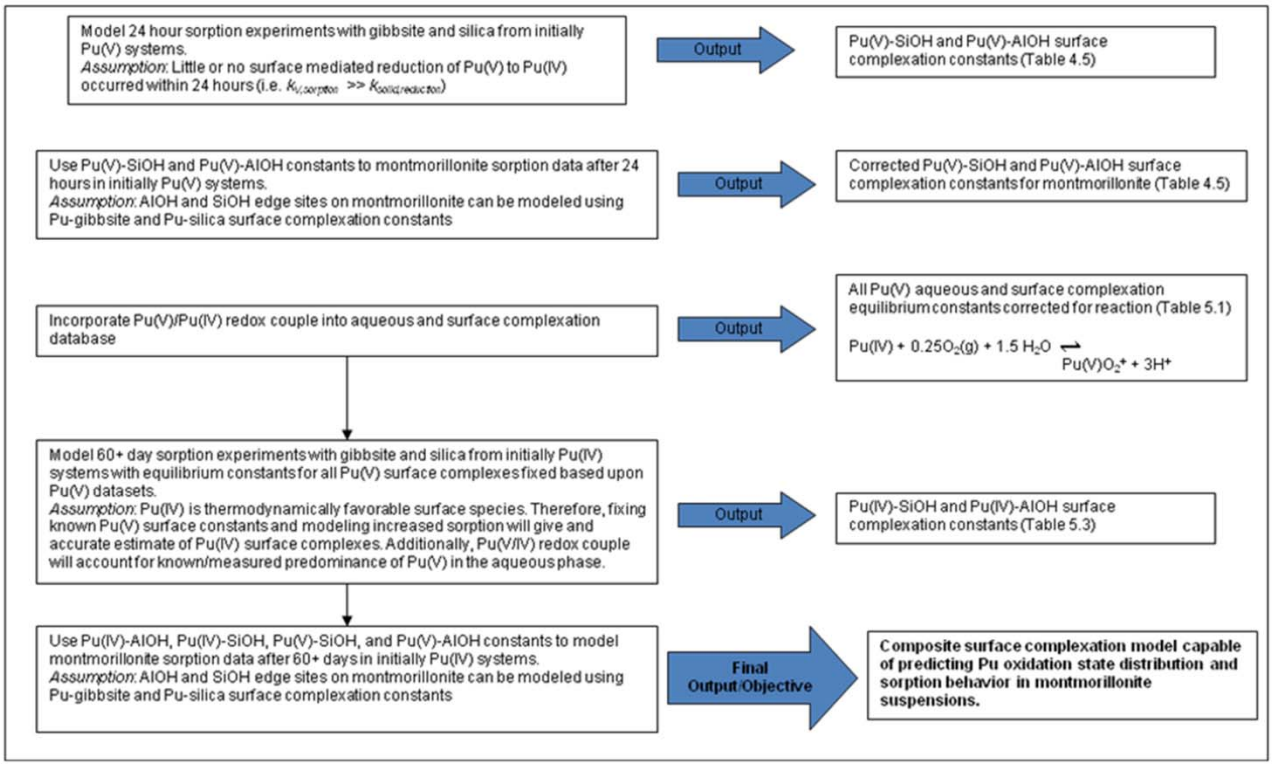

Figure 5.1: Flowsheet of revised surface complexation modeling approach.

In the next step, the thermodynamic databases used in surface complexation modeling were rewritten such that the Pu(V)/Pu(IV) redox couple was considered. To accomplish this, the aqueous Pu(V) species were all rewritten in terms of the Pu(IV)/Pu(V) redox equation below:

$$Pu^{4+} + 0.25O_2(g) + 1.5H_2O \leftrightarrow PuO_2^{+} + 3H^{+} \quad \log K = 3.439 \qquad (5.1)$$

It is important to note that this modeling effort is limited in that only the Pu(IV/V) redox couple is allowed and it is coupled with dissolved oxygen. This is necessary for simplicity in this preliminary modeling effort. However, further consideration of Pu chemistry including solubility, additional Pu oxidation states, and disproportionation reactions may be warranted. Table 5.1 below shows the revised log K values used for aqueous species. Only the constants for Pu(V) species were changed from those presented in Table 4.1.

Table 5.1 Summary of Thermodynamic Constants for Aqueous Complexes in Current UGTA Database*

Species	Reaction	Ion Size (A)**	log K (25°C)
Complexation			
OH^-	$H_2O \leftrightarrow OH^- + H^+$	3.5	-14
$CO_2(aq)$	$H+ + HCO_3^- \leftrightarrow CO_2(aq)$	3	6.34
CO_3^{--}	$HCO_3^- \leftrightarrow H+ + CO_3^{--}$	4.5	-10.33
NaCl(aq)	$Na+ + Cl^- \leftrightarrow NaCl(aq)$	3	-0.777
$NaCO_3^-$	$Na+ + HCO_3^- \leftrightarrow H^+ + NaCO_3^-$	4	-9.814
$NaHCO_3(aq)$	$Na+ + HCO_3^- \leftrightarrow NaCO_3^-$	3	0.154
NaOH(aq)	$Na+ + H_2O \leftrightarrow NaOH(aq) + H^+$	3	-14.205
$PuOH^{+++}$	$Pu^{4+} + H_2O \leftrightarrow PuOH^{+++} + H^+$	5	-0.78
$Pu(OH)_2^{++}$	$Pu^{4+} + 2H_2O \leftrightarrow Pu(OH)_2^{++} + 2H^+$	4.5	-1.66
$Pu(OH)_3^+$	$Pu^{4+} + 3H_2O \leftrightarrow Pu(OH)_3^+ + 3H^+$	4	-4.62
$Pu(OH)_4(aq)$	$Pu^{4+} + 4H_2O \leftrightarrow Pu(OH)_4(aq) + 4H^+$	3	-8.85
$Pu(OH)_2(CO_3)_2^{--}$	$Pu^{4+} + 2H_2O + 2HCO_3^- \leftrightarrow Pu(OH)_2(CO_3)^{2--} + 4H^+$	4	-2.75
$Pu(OH)_4(CO_3)_{2----}$	$Pu^{4+} + 4H_2O + 2HCO_3^- \leftrightarrow Pu(OH)_4(CO_3)^{2--} + 6H^+$	5	-25.53
$Pu(CO_3)_4^{----}$	$Pu^{4+} + 4HCO_3^- \leftrightarrow Pu(CO_3)_4^{4-} + 4H^+$	5	-4.62
$Pu(CO_3)_5^{6-}$	$Pu^{4+} + 5HCO_3^- \leftrightarrow Pu(CO_3)_5^{6-} + 5H^+$	5	-16.3
$PuO_2OH(aq)$	$Pu^{4+} + 0.25O_2(g) + 2.5H_2O \leftrightarrow PuO_2OH(aq) + 4H^+$	3	-6.261
$PuO_2CO_3^-$	$Pu^{4+} + 0.25O_2(g) + 1.5H_2O + HCO_3^- \leftrightarrow PuO_2CO_3^- + 4H^+$	4	-1.771
$PuO_2(CO_3)_2^{---}$	$Pu^{4+} + 0.25O_2(g) + 1.5H_2O + 2HCO_3^- \leftrightarrow PuO_2(CO_3)_2^{3-} + 5H^+$	4	-10.681
$PuO_2(CO_3)_3^{5-}$	$Pu^{4+} + 0.25O_2(g) + 1.5H_2O + 3HCO_3^- \leftrightarrow PuO_2(CO_3)_3^{5-} + 6H^+$	5	-22.561
Redox			
PuO_2^+/Pu^{++++}	$Pu^{++++} + 0.25O_2(g) + 1.5H_2O \leftrightarrow PuO_2^+ + 3H^+$	4	3.439

*Constants predominantly taken from DATACOM.V8.R6 of the GEMBOCHS thermodynamic database (Turner et al., 1998) and associated revisions (Carle et al., 2006; Pawloski et al., 2000; Pawloski et al., 2001; Tompson et al., 1999).

The solid phase thermodynamic database was similarly changed to incorporate the Pu(V)/Pu(IV redox couple. The Pu(V) surface complexation constants from the silica and gibbsite experiments listed in Table 4.5 were rewritten as shown in Table 5.2.

Table 5.2: Pu(V)-aluminol and Pu(V)-silanol Surface Complexation Constants Written in Terms of the Pu(V)/Pu(IV) Redox Couple.

Species	Reaction	log K
$SiOHPuO_2^+$	$SiOH + Pu^{4+} + 0.25\ O_2(g) + 1.5\ H_2O \leftrightarrow SiOHPuO_2^+ + 3H^+$	7.549
$SiOPuO_2^o$	$SiOH + Pu^{4+} + 0.25\ O_2(g) + 1.5\ H_2O \leftrightarrow SiOPuO_2^o + 4H^+$	2.339
$SiOPuO_2OH^-$	$SiOH + Pu^{4+} + 0.25\ O_2(g) + 2.5\ H_2O \leftrightarrow SiOPuO_2OH^- + 5H^+$	-7.861
$AlOHPuO_2^+$	$AlOH + Pu^{4+} + 0.25\ O_2(g) + 1.5\ H_2O \leftrightarrow AlOHPuO_2^+ + 3H^+$	8.799
$AlOPuO_2^o$	$AlOH + Pu^{4+} + 0.25\ O_2(g) + 1.5\ H_2O \leftrightarrow AlOPuO_2^o + 4H^+$	0.349
$AlOPuO_2OH^-$	$AlOH + Pu^{4+} + 0.25\ O_2(g) + 2.5\ H2O \leftrightarrow AlOPuO_2OH^- + 5H^+$	-8.161

As written in Equation 5.1, the Pu(V)/Pu(IV) redox couple is dependent on $O_2(g)$ fugacity. As a result, the surface complexation constants will be dependent on the input $O_2(g)$ fugacity. It is possible to estimate the $O_2(g)$ fugacity from redox measurements. Unfortunately, redox measurements were not made for all samples at the time of sampling. Therefore, an empirical equation was fit to the known measurements to estimate the $O_2(g)$ fugacity for all samples to be used in modeling efforts. Figure 5.2 shows the measured redox potentials versus the pH of each suspension. Although there is a considerable amount of scatter in the data, there is a clear trend that can be fit to a linear model.

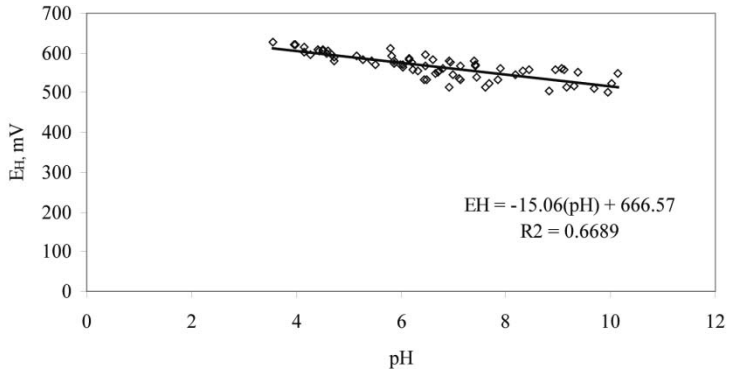

Figure 5.2: Measured redox potential versus suspension pH from samples in Pu sorption experiments.

Using that empirical equation, the E_H of each sample was calculated based upon the measured solution pH. Then the $O_2(g)$ fugacity was calculated from the E_H value using the two relationships:

$$O_2(g) + 4H+ + 4e^- \Leftrightarrow 2H_2O \quad \log K = 20.78 \tag{5.2}$$

$$E_H = 59.16pe^- \tag{5.3}$$

The log $O_2(g)$ fugacity for each sample was calculated from the sample pH at the time of measurement by combining Equations 5.2 and 5.3 to obtain Equation 5.4:

$$\log O_2(g) = -20.78 + pH + 0.25*(E_H/59.16) \quad (5.4)$$

The E_H value in Equation 5.4 was calculated using the empirical relationship determined from the data in Figure 5.2.

$$E_H = -15.06*pH + 666.57 \quad (5.5)$$

This calculation yielded log $O_2(g)$ values ranging from –15 to –8. While these values are considered oxidizing, estimations of log $O_2(g)$ fugacity do not reflect the molar concentration of dissolved oxygen. This is important to consider as Equation 5.1 indicates a 0.25 order dependence of $O_2(g)$ on the Pu(IV/V) couple. Therefore the high $O_2(g)$ fugacities are more realistic when considering the dissolved oxygen concentration. To independently test this approach, some Pu solubility measurements of Rai et al. (2001) were modeled. Rai et al. (2001) reported total dissolved Pu in equilibrium with hydrous plutonium oxide as well as the distribution of the aqueous oxidation states. A model was developed with the total dissolved Pu concentration, pH, and estimated log $O_2(g)$ concentration (Figure 5.2). Using this approach of estimating the log $O_2(g)$ fugacity, a reasonable fit to the data reported by Rai et al. (2001) was achieve as shown in Figure 5.3.

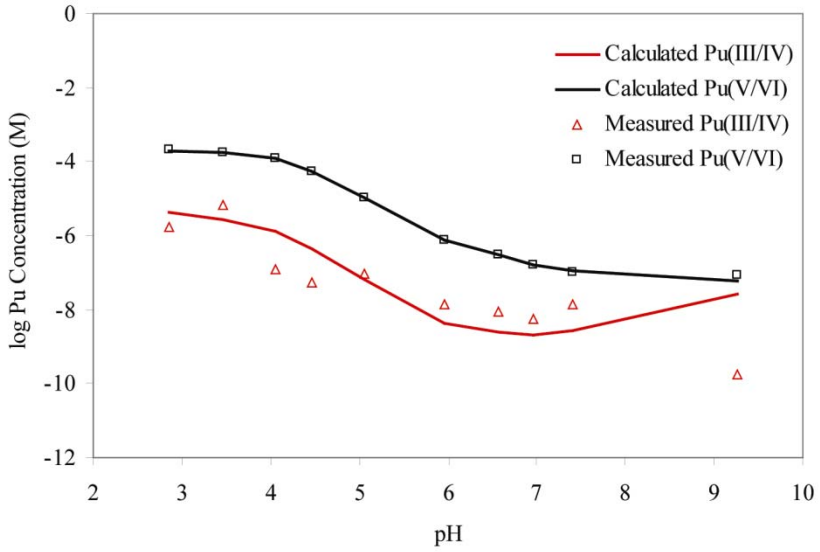

Figure 5.3: Fit of Pu solution species to solubility data of (Rai et al., 2001) assuming log $O_2(g)$ fugacity calculated from Equation 5.4.

5.2 Refinement of Model with Active Pu(IV)/Pu(V) Redox Couple

Using the revised constants shown in Tables 5.1 and 5.2, the Pu(IV)-aluminol and Pu(IV)-silanol surface complexation constants were refitted. Data from the initially Pu(IV) sorption experiments with silica and gibbsite after 62 days were used in the model because they are assumed to

represent the equilibrium distribution between Pu(IV) and Pu(V) in each system. One unfortunate results of using these datasets was that the effect of carbonate must also be incorporated in the model. As discussed above the carbonate concentrations that were used in the model were input based upon the initial amounts of carbonate added to each sample. However, additional carbonate was added to each sample through addition of NaOH during pH adjustments and through diffusion of $CO_2(g)$ through the vial walls. Therefore, the input carbonate concentration should be assumed to have at least a 10% uncertainty. This uncertainty must be carried over to the surface complexation constants as they are indirectly dependent on the total carbonate concentration. The carbonate concentrations used in the model input along with other system parameters (Total Pu concentration, Sorbed Pu concentration, and pH) are listed for each dataset in Appendix C.

The data and model fit describing Pu(IV) sorption to silica after 62 days is shown in Figure 5.4. The model closely predicted the measured sorbed concentration. The Pu(IV) surface complexes are shown in red and the Pu(V) surface complexes are shown in blue. Consistent with the expected behavior of sorbed Pu, the model predicted that the majority of sorbed Pu will be Pu(IV). Furthermore, Pu(V) was correctly predicted to be the dominant aqueous phase oxidation state (as $PuO_2^+(aq)$ and $PuO_2CO_3^-(aq)$). Therefore, in addition to accurately predicting the aqueous and solid phase Pu concentrations, the revised surface complexation model was able to closely predict the expected oxidation state distribution of Pu in the system where the solid phase was dominated by Pu(IV) and the aqueous phase was dominated by Pu(V). The revised non-electrostatic surface complexation constants are shown in Table 5.3. In order to predict the appearance of solid phase Pu(IV) in the presence of $O_2(g)$, the constants for both of the assumed Pu(IV)-silanol species increased. The log K values for $SiOPu(OH)_3$ increased from –3.55 to 0.14 and the value for $SiOPu(OH)_4^-$ increased from –9.10 to –7.58. These values are consistent with the presumed thermodynamic favorability of sorbed Pu(IV) complexes.

Similar behavior was observed for the Pu-gibbsite sorption dataset and model (Figure 5.5). After incorporation of the Pu(IV/V) redox couple, the model accurately predicted both the solid and aqueous phase Pu concentrations. Additionally, the oxidation state of sorbed Pu was dominated by Pu(IV) except for the high pH region, where a significant fraction of sorbed Pu was predicted to be the $AlOPuO_2OH^-$ surface species. Similar to the silica model discussed above, the aqueous phase Pu was predominantly Pu(V) as PuO_2^+ and $PuO_2CO_3^-$.

In order to achieve the fit shown in Figure 5.5, the predicted surface speciation had to be changed. Without coupling Pu(IV/V), the best fit to the available data was found using $\equiv AlOPu(OH)_2^+$, $\equiv AlOPu(OH)_3$, and $\equiv AlOPu(OH)_4^-$ species. The $\equiv AlOPu(OH)_4^-$ species was not required when coupling Pu(IV/V) but a less hydrolyzed $\equiv AlOPu(OH)^{++}$ species was required to fit the low pH data. While developing the uncoupled model, it was found that the $\equiv AlOPu(OH)^{++}$ species could be included and a slightly better fit could be obtained. However, the increase in model complexity (addition of a fourth surface species) was not justified for the slightly better fit. Similar to the Pu(IV)-silanol constants, the log K values for Pu(IV)-aluminol constants increased when adding the Pu(IV/V) couple. The log K value for $\equiv AlOPu(OH)_2^+$ increased from 5.10 to 7.34 and the value for $\equiv AlOPu(OH)_3$ increased from –2.64 to –0.10.

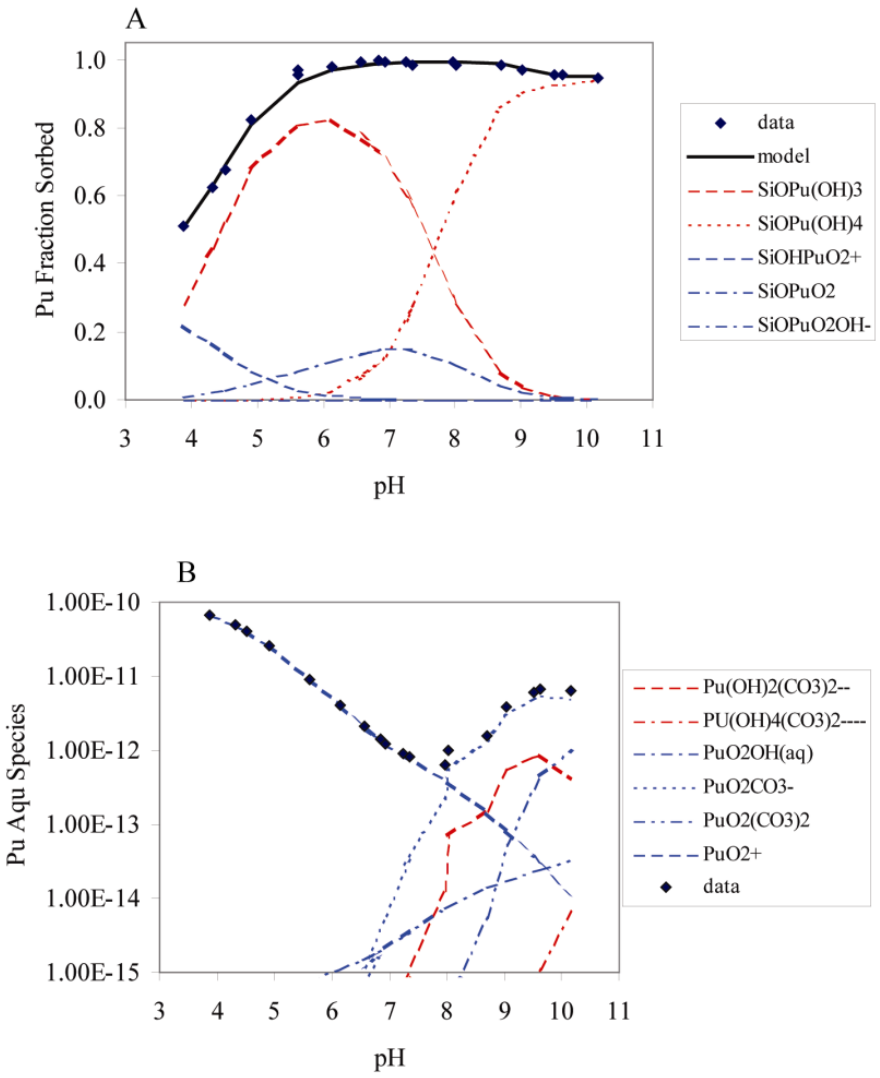

Figure 5.4 Model Prediction of Pu (a) solid phase and (b) aqueous phase distribution in silica suspension after 62 days with carbonate present. Revised SCM constants listed in Table 5.3 used to obtain fit.

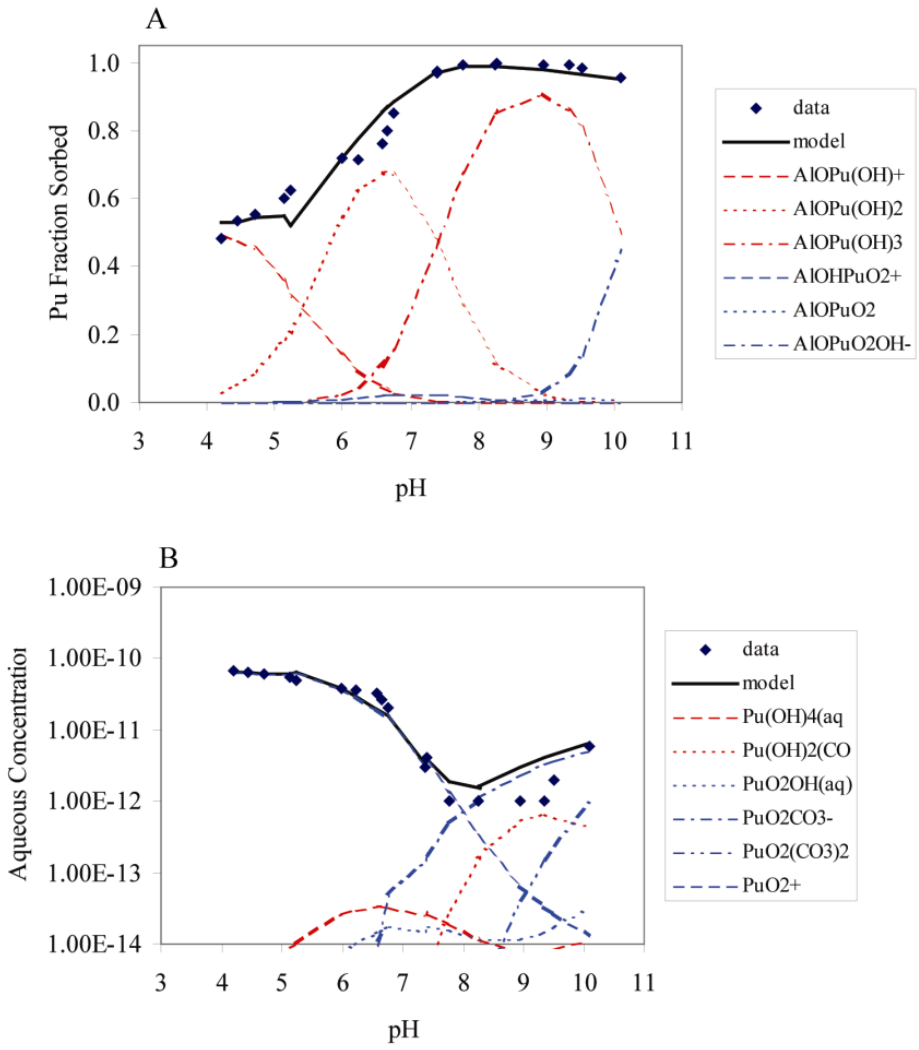

Figure 5.5 Model Prediction of Pu (a) solid phase and (b) aqueous phase distribution in silica suspension after 62 days with carbonate present. Revised SCM constants listed in Table 5.3 used to obtain fit.

Table 5.3: Revised Pu-aluminol and Pu-silanol Surface Complexation Constants written in terms of the Pu(V)/Pu(IV) redox couple.

Species	Reaction	log K
$SiOHPuO_2^+$	$SiOH + Pu^{4+} + 0.25\ O_2(g) + 1.5\ H_2O \leftrightarrow SiOHPuO_2^+ + 3H^+$	7.55
$SiOPuO_2^o$	$SiOH + Pu^{4+} + 0.25\ O_2(g) + 1.5\ H_2O \leftrightarrow SiOPuO_2^o + 4H^+$	2.34
$SiOPuO_2OH^-$	$SiOH + Pu^{4+} + 0.25\ O_2(g) + 2.5\ H_2O \leftrightarrow SiOPuO_2OH^- + 5H^+$	-7.86
$AlOHPuO_2^+$	$AlOH + Pu^{4+} + 0.25\ O_2(g) + 1.5\ H_2O \leftrightarrow AlOHPuO_2^+ + 3H^+$	8.80
$AlOPuO_2^o$	$AlOH + Pu^{4+} + 0.25\ O_2(g) + 1.5\ H_2O \leftrightarrow AlOPuO_2^o + 4H^+$	0.35
$AlOPuO_2OH^-$	$AlOH + Pu^{4+} + 0.25\ O_2(g) + 2.5\ H2O \leftrightarrow AlOPuO_2OH^- + 5H^+$	-8.16
$AlOPu(OH)^{++}$	$AlOH + Pu^{4+} + H_2O \leftrightarrow AlOPu(OH)^{++} + 2H^+$	12.82
$AlOPu(OH)_2^+$	$AlOH + Pu^{4+} + 2H_2O \leftrightarrow AlOPu(OH)_2^+ + 4H^+$	7.34
$AlOPu(OH)_3^o$	$AlOH + Pu^{4+} + 3H_2O \leftrightarrow AlOPu(OH)_3^o + 4H^+$	-0.10
$SiOPu(OH)_3^o$	$SiOH + Pu^{4+} + 3H_2O \leftrightarrow SiOPu(OH)_3^o + 4H^+$	0.14
$SiOPu(OH)_4^-$	$SiOH + Pu^{4+} + 4H_2O \leftrightarrow SiOPu(OH)_4^- + 5H^+$	-7.58

5.3 Modeling Pu Sorption to Montmorillonite with Active Pu(IV)/Pu(V) Redox Couple

Since the experiments in montmorillonite systems which were initially Pu(V) did not appear to reach a steady-state within the time of these experiments (Figure 3.10b), only the initially Pu(IV) dataset was used for this modeling comparison. Using the surface complexation constants listed in Table 5.3 and the thermodynamic constants listed in Table 5.1 (including the Pu(IV/V) redox couple, sorption of Pu(IV) to montmorillonite was predicted. The model output is shown in Figure 5.6 below and plotted with the initially Pu(IV)-montmorillonite dataset obtained after 62 days under $CO_2(g)$ equilibrated conditions. The model does an acceptable job of fitting the data at high pH values. As discussed above, the difficultly of predicting Pu(IV) sorption in the presence of carbonate and the uncertainty in the exact carbonate concentrations are believed to be responsible for the poor fit at the highest pH values. Of greater concern is the very poor fit observed at low pH. The most significant predicted sorbing species is $\equiv SiOPu(OH)_3$ but the predicted sorbed concentration is significantly lower than the observed concentration.

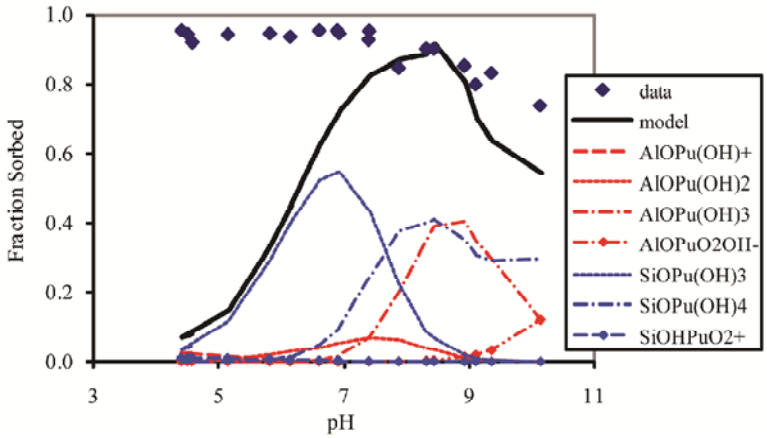

Figure 5.6 Model prediction of Pu sorption to montmorillonite after 62 days with carbonate present. Pu surface complexation constants fixed from Pu-silanol and Pu-aluminol species as listed in Table 5.3.

An examination of estimated surface site concentrations for each mineral and the sorption behavior at steady-state (Figrue 5.7) for Pu(IV) systems in gibbsite, silica, and montmorillonite suspensions provides some insight regarding the poor montmorillonite fit at low pH. There are two possible explanations for the observed behavior and apparent inconsistency in the model:

1. Sorption of Pu to montmorillonite is occurring by a process other than compelxation with aluminol and silanol groups
2. The assumption that ≡SiOH and ≡AlOH sites make up 10% of the available surface area is incorrect

It is highly unlikely that the montmorillonite edge sites which make the majority of ≡SiOH and ≡AlOH site account for exactly 10% of the measured surface area as is assumed in the model. However, even if 100% of the measured surface area was assumed to be ≡SiOH and ≡AlOH groups, the total surface site concentration (1.8×10^{-5} M) is still 2x less than the assumed surface site concentration in the silica and gibbsite suspensions. Therefore, it is likely that another process is controlling Pu sorption to montmorillonite at low pH. The most likely mechanism is ion exchange.

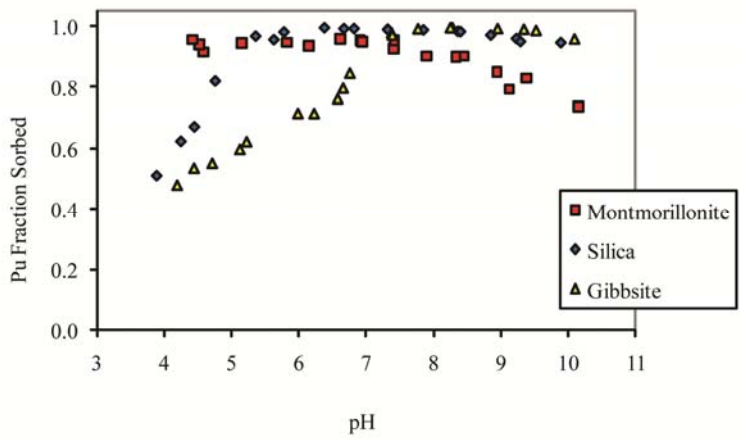

Figure 5.7: Measured Pu sorption at steady-state in gibbsite, silica, and montmorillonite suspensions from initially Pu(IV), CO_2(g) equilibrated solutions.

Using the Vaneslow model for ion exchange (Sposito, 1977), exchange reactions of Pu^{4+} were modeled relative to Na^+ (Equations 5.6 and 5.7). The cation exchange capacity of 76.4 meq/100g reported for the SWy-1 montmorillonite by the Clay Minerals Society (Appendix A) was used to calculate an ion exchange site concentration of 1.3×10^{-4} M. This exchange site concentration and the surface complexation constants for Pu-aluminol and Pu-silanol groups listed in Table 5.3 were held constant during the modeling exercise. It appears that a steady state Pu distribution was achieved after approximately 24 hours. Therefore, the 24 hours and 62 day sorption dataset from initially Pu(IV) systems in the presence of CO_2(g) were used to determine the ion exchange constant.

$$X^- + Pu^{4+} + 3H_20 \rightarrow X^-Pu(OH)_3^+ + 3H^+ \qquad \log K = -1.45 \qquad (5.6)$$

$$X^- + Na^+ \rightarrow X^-Na^+ \qquad \log K = 0 \qquad (5.7)$$

The best fit was obtained by assuming exchange with $Pu(OH)_3^+$ (Equation 5.8 and Figure 5.8). To calculate the direct exchange constant, the Pu^{4+} hydrolysis reaction was subtracted out as follows:

$$\begin{array}{l} Pu(OH)_3^+ + 3H^+ \rightarrow Pu^{4+} + 3H_2O \quad \log K = 4.62 \\ + X^-Na^+ + Pu^{4+} + 3H_20 \rightarrow X^-Pu(OH)_3^+ + Na^+ + 3H^+ \quad \log K = -1.45 \\ \hline X^-Na^+ + Pu(OH)_3^+ \rightarrow X^-Pu(OH)_3^+ + Na^+ \quad \log K = 3.17 \end{array} \qquad (5.8)$$

The high exchange constant (3.17) is indicative of a strong affinity of Pu for montmorillonite basal plane ion-exchange sites. Similar high values have been reported for Cs, which is known to have strong ion exchange interaction with this mineral. There is insufficient experimental data in this dataset to confirm that ion exchange is occurring. The discussion of the surface site density provides only circumstantial evidence to justify incorporation of ion exchange into this model. However, evidence of Pu ion exchange on SWy-1 montmorillonite was recently reported (Zavarin et al., 2008). The slight increase in Pu sorption at low pH values (Figure 3.10) is also indicative of Pu(V) reduction followed by ion exchange.

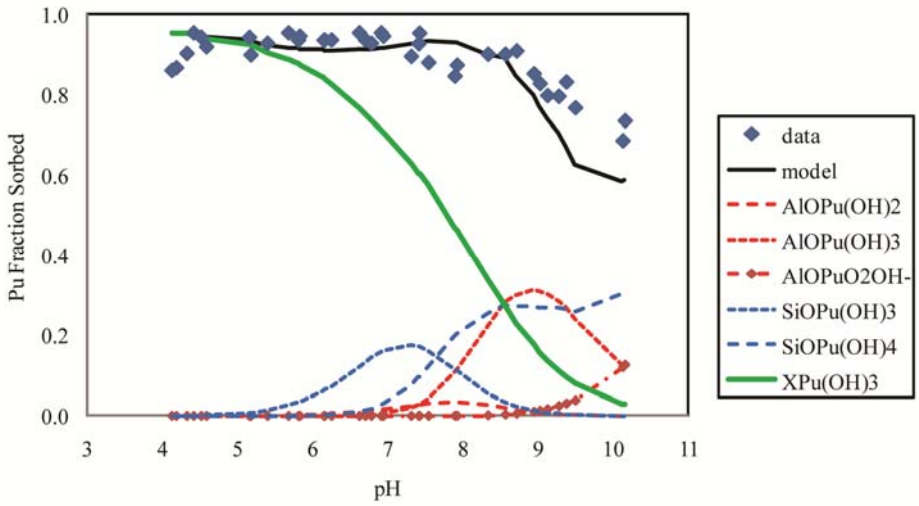

Figure 5.8 Model prediction of Pu sorption to montmorillonite after 24 hours and 62 days with carbonate present assuming both ion exchange and surface complexation. Pu surface complexation constants fixed from Pu-silanol and Pu-aluminol species as listed in Table 5.3. Ion exchange shown as green solid line.

6 SUMMARY

Data describing Pu sorption to silica verified previous observations that Pu(V) sorption is relatively weak while Pu(IV) sorption is strong. Similar results were observed for Pu sorption to gibbsite. However, it was interesting that in this work Pu appears to have a stronger affinity for silica relative to gibbsite. Based on these sorption experiments, a series of Pu-aluminol and Pu-silanol non-electrostatic surface complexation models (Tables 4.5 and 4.6) were developed to

describe Pu interactions with silica and gibbsite. These constants were used to predict sorption of Pu(IV) and Pu(V) to montmorillonite. Overall, the constants can predict Pu(V) sorption to montmorillonite across a wide pH range. This is not the case for Pu(IV) sorption to montmorillonite at low pH values although a good fit was obtained in neutral pH. Further incorporation of Pu(IV) ion exchange could be used to obtain a better fit for Pu(IV) sorption to montmorillonite. The constants listed in Tables 4.5 and 4.6 can be directly incorporated into the UGTA database. However, some of the inherent complexity of Pu geochemical behavior is not captured in these systems because they assume that Pu is present in only one oxidation state, either Pu(IV) or Pu(V). Additional modeling was performed in an attempt to capture some of the redox processes that are known to influence Pu geochemical behavior.

By examining sorption of Pu to relatively weakly sorbing minerals, the equilibrium distribution and oxidation state of aqueous Pu in mineral suspensions were more accurately quantified. Due to the strong degree of sorption observed when performing sorption experiments with strongly sorbing minerals such as iron and manganese oxides, the concentration of aqueous Pu is typically too low to allow for accurate oxidation state analysis. Verification of aqueous Pu(V) in silica and gibbsite suspensions which were initially Pu(IV) indicated that the equilibrium distribution between aqueous Pu(V) and solid phase Pu(IV) must be carefully considered during modeling efforts.

In the current literature, all attempts to develop Pu(IV) surface complexation models have been done assuming Pu(IV) is the only oxidation state present. The observation of aqueous Pu(V) in equilibrium with solid phase Pu(IV) requires for a change in the modeling approach when analyzing Pu sorption data and describing Pu subsurface transport. *The modeling approach described in Chapter 5 where the Pu(IV)/Pu(V) redox couple was included is proposed as a starting point for further model development. The constants are not intended to represent exact values. Rather, the revised modeling effort is proposed for future development and will require further laboratory experiments and modeling exercises.* One of the most important considerations regarding this modeling effort is that the Pu(IV) surface complexation constants are highly dependent on the dissolved oxygen fugacity used in the model. Thus, the constants reported in Table 5.3 are conditional constants applicable only under the simulated log $O_2(g)$ values used in the model input.

Whether the surface complexation model presented here is used with or without the Pu(IV)/Pu(V) couple active, it is very important to note that there is no spectroscopic evidence in the present work to verify the assumed solid phase oxidation state distribution or interfacial species. These analyses are necessary for the development of a rigorous surface complexation model. Based upon the model output and experimental data presented in this report, three areas for future research are necessary for a comprehensive model describing Pu sorption to montmorillonite. These three areas are:

1. Rigorous characterization of Pu oxidation state speciation at trace Pu concentrations in homogenous (no solid phase) ground water solutions
2. Spectroscopic verification of the predominance of solid phase Pu(IV) on non-redox active solid phases such as the gibbsite and silica used in this work. Additionally, experiments at higher Pu concentration that will allow for EXAFS analysis of the Pu chemical environment would greatly aid model development.

3. Detailed evaluation of Pu ion exchange with smectite clays including studies of possible interlayer collapse leading to the formation of "irreversibly" bound Pu within the clay interlayer. Similar to the discussion above, this work will require both batch sorption experiments as well as spectroscopic evaluation.

7 REFERENCES

Allard, B., Kipatsi, H., Lilijenzin, J.O., 1980. Expected species of uranium, neptunium and plutonium in neutral aqueous-solutions. Journal of Inorganic and Nuclear Chemistry 42, 1015-1027.

Allard, B., Olofsson, U., Torstenfelt, B., Kipatsi, H., Andersson, K., 1982. Sorption of actinides in well-defined oxidation states on geologic media, in: Lutze, W. (Ed.), Scientific basis for radioactive waste management - V. Elsevier Science Pub. Co., pp. 775-782.

Banik, N.L., Buda, R.A., Burger, S., Kratz, J.V., Trautmann, N., 2007. Sorption of tetravalent plutonium and humic substances onto kaolinite. Radiochimica Acta 95, 569-575.

Bertrand, P.A., Choppin, G.R., 1982. Separation of actinides in different oxidation states by solvent extraction. Radiochimica Acta 31, 135-137.

Bradbury, M.H., Baeyens, B., 2005. Modelling the sorption of Mn(II), Co(II), Ni(II), Zn(II), Cd(II), Eu(III), Am(III), Sn(IV), Th(IV), Np(V) and U(VI) on montmorillonite: Linear free energy relationships and estimates of surface binding constants for some selected heavy metals and actinides. Geochimica et Cosmochimica Acta 69, 875-892.

Carle, S.F., Maxwell, R.M., Pawloski, G.A., Shumaker, D.E., Tompson, A.F.B., Zavarin, M., 2006. Evaluation of the Transient Hydrologic Source Term for the Cambric Underground Nuclear Test at Frenchman Flat, Nevada Test Site, UCRL-TR-226916, Lawrence Livermore National Laboratory, Livermore, CA.

Clark, D.L., Hobart, D.E., Neu, M.P., 1995. Actinide carbonate complexes and their importance in actinide environmental chemistry. Chemical Reviews 95.

Clark, D.L., Janecky, D.R., Lane, L.J., 2006. Science-based cleanup of Rocky Flats. Physics Today 59, 34-40.

Cleveland, J.M., 1979. The Chemistry of Plutonium. American Nuclear Society, La Grange Park.

Conradson, S.D., Mahamid, I.A., Clark, D.L., Hess, N.J., Hudson, E.A., Neu, M.P., Palmer, P.D., Runde, W.H., Tait, C.D., 1998. Oxidation state determination of plutonium aquo ions using x-ray absorption spectroscopy. Polyhedron 17, 599-602.

Davis, J.A., Kent, D.B., 1990. Surface complexation modeling in aqueous geochemistry. Reviews in Mineralogy 23, 177-260.

Foti, S.C., Freiling, E.C., 1964. The determination of the oxidation states of tracer uranium, neptunium, and plutonium in aqueous media. Talanta 11, 385-392.

Herbelin, A.L., Westall, J.C., 1994. FITEQL, A computer program for determination of chemical equilibrium constants from experimental data, 3.1 ed. Department of Chemistry, Oregon State University.

Kaplan, D.I., Powell, B.A., Demirkanli, D.I., Fjeld, R.A., Molz, F.J., Serkiz, S.M., Coates, J.T., 2004. Influence of oxidation states on plutonium mobility during long-term transport through an unsaturated subsurface environment. Environmental Science & Technology 38, 5053-5058.

Keeney-Kennicutt, W.L., Morse, J.W., 1985. The redox chemistry of Pu(V)O2+ interaction with common mineral surfaces in dilute solutions and seawater. Geochimica et Cosmochimica Acta 49, 2577-2588.

Kobashi, A., Choppin, G.R., 1988. A study of techniquioes for separating plutonium in different oxidation states. Radiochimica Acta 43, 211-215.

Lemire, R.J., Fuguer, J., Nitsche, H., Potter, P., Rand, M.H., Rydberg, J., Spahiu, K., Sullivan, J.C., Ullman, W.J., Votorge, P., Warner, H., 2001. Chemical Thermodymamics of Neptunium and Plutonium. Elsevier, Amsterdam, The Netherlands.

McKinley, J.P., Zachara, J.M., Smith, S.C., Turner, G.D., 1995. The influence of uranyl-hydrolysis and multiple site-binding reaction on adsorption of U(VI) to montmorillonite. Clays and Clay Minerals 45, 586-598.

Neck, V., Altmaier, M., Seibert, A., Yun, J.I., Marquardt, C.M., Fanghanel, T., 2007. Solubility and redox reactions of Pu(IV) hydrous oxide: Evidence for the formation of PuO2+x(s, hyd). Radiochimica Acta 95, 193-207.

Neck, V., Kim, J.I., 2001. Solubility and hydrolysis of tetravalent actinides. Radiochimica Acta 89, 1-16.

Neu, M., Hoffman, D.C., Roberts, K.E., Nitsche, H., Silva, R.J., 1994. Comparison of chemical extractions and laser photoacoustic spectroscopy for the determination on plutonium species in near-neutral carbonate solutions. Radiochimica Acta 66/67, 251-258.

Nitsche, H., Lee, S.C., Gatti, R.C., 1988. Determination of plutonium oxidation states at trace levels pertinent to nuclear waste disposal. Journal of Radioanalytical and Nuclear Chemistry 124, 171-185.

Pawloski, G.A., Tompson, A.F.B., Bruton, C.J., Zavarin, M., 2000. Evaluation of the Hydrologic Source Term from Underground Nuclear Tests in Frenchman Flat at the Nevada Test Site (U), UCRL-ID-138007-DR, Lawrence Livermore National Laboratory, Livermore, CA.

Pawloski, G.A., Tompson, A.F.B., Carle, S.F., 2001. Evaluation of the hydrologic source term from underground nuclear tests on Pahute Mesa at the Nevada Test Site: The CHESHIRE test, UCRL-ID-147023, Lawrence Livermore National Laboratory, Livermore, CA.

Penrose, W.R., Metta, D.N., Hylko, J.M., Rinckel, L.A., 1987. Chemical speciation of plutonium in natural waters. Journal of Environmental Radioactivity 5, 169-184.

Peretrukhin, V.F., Spitsyn, W.I., 1982. Electrochemical determination of the oxidation potentials and the thermodynamic stability of the valence states of the trans-uranium elements in aqueous alkaline media. Izv. Adad. Nauk. SSR, Ser. Khim. 31, 726-730.

Powell, B.A., Duff, M.C., Kaplan, D.I., Fjeld, R.A., Newville, M., Hunter, D.B., Bertsch, P.M., Coates, J.T., Eng, P., Rivers, M.L., Serkiz, S.M., Sutton, S.R., Triay, I.R., Vaniman, D.T., 2006. Plutonium oxidation and subsequent reduction by Mn(IV) minerals in Yucca Mountain tuff. Environmental Science & Technology 40, 3508-3514.

Powell, B.A., Fjeld, R.A., Kaplan, D.I., Coates, J.T., 2003. Plutonium reduction on synthetic magnetite (Fe3O4) and hematite (alpha-Fe2O3). Abstr Pap Am Chem S 226, U77-U77.

Powell, B.A., Fjeld, R.A., Kaplan, D.I., Coates, J.T., 2004. Plutonium reduction on synthetic magnetite (Fe3O4). Abstr Pap Am Chem S 227, U77-U77.

Powell, B.A., Fjeld, R.A., Kaplan, D.I., Coates, J.T., Serkiz, S.M., 2005. PU(V)0(2)(+) adsorption and reduction by synthetic hematite and goethite. Environmental Science & Technology 39, 2107-2114.

Powell, B.A., Kersting, A.B., Zavarin., M., 2008. Sorption and desorption rates of neptunium and plutonium on goethite, in: M. Zavarin, e.a., Editors. (Ed.), Hydrologic resources management program and underground test area project, FY 2006 progress report,. Lawrence Livermore National Laboratory, Livermore, CA, pp. UCRL-TR-404620.

Rai, D., 1984. Solubility product of Pu(IV) hydrous oxide and equilibrium constants of Pu(IV)/Pu(V), Pu(IV)/Pu(VI), and Pu(V)/Pu(VI) couples. Radiochimica Acta 35, 97-106.

Rai, D., Hess, N.J., Felmy, A.R., Moore, D.A., Yui, M., Vitorge, P., 1999. A thermodynamic model for the solubility of PuO2(am) in the aqueous K+-HCO3--CO32--OH--H2O system. Radiochimica Acta 86, 89-99.

Rai, D., Moore, D.A., Felmy, A.R., Choppin, G.R., Moore, R.C., 2001. Thermodynamics of the PuO2+-Na+-OH--Cl--ClO4--H2O system: Use of NpO2+ pitzer parameters for PuO2+. Radiochimica Acta 89, 491-498.

Rai, D., Serne, R.J., Swanson, J.L., 1980. Solution species of Pplutonium in the environment. Journal of Environmental Quality 9, 417-420.

Righetto, L., Bidoglio, G., Azimonti, G., Bellebono, I.R., 1991. Competitive actinide interaction in colloidal humic acid-mineral oxide systems. Environmental Science and Technology 25, 1913-1919.

Sanchez, A.L., 1983. Chemical speciation and adsorption behavior of plutonium in natural waters, Oceanography. University of Washington, Seattle, p. 191.

Sanchez, A.L., Murray, J.W., Sibley, T.H., 1985. The adsorption of plutonium IV and V on goethite. Geochimica et Cosmochimica Acta 49, 2297-2307.

Shaughnessey, D.A., Nitsche, H., Booth, C.H., Shuh, D.K., Waychunas, G.A., Wilson, R.E., Gill, H., Cantrell, K.J., Serne, R.J., 2003. Molecular interfacial teactions between Pu(VI) and manganese oxide minerals manganite and hausmannite. Environmental Science & Technology 37, 3367-3374.

Soderholm, L., Almond, P.M., Skanthakumar, S., Wilson, R.E., Burns, P.C., 2008. The structure of the plutonium oxide nanocluster [Pu38O56Cl54(H2O)(8)](14-). Angew. Chem.-Int. Edit. 47, 298-302.

Sposito, G., 1977. The gapon and vanselow selectivity coefficients. Soil Science Society of America Journal 41, 1205.

Sposito, G., 1989. The Chemistry of Soils. Oxford University Press, New York.

Stoller-Navarro, 2008. Phase II Transport Model for Corrective Action Unit 98: Frenchman Flat, Nevada Test Site, Nye County, Nevada, Las Vegas, NV.

Tompson, A.F.B., Bruton, C.J., Pawloski, G.A., 1999. Evaluation of the hydrologic source term from the underground nuclear tests in Frenchman Flat and the Nevada Test Site: The CAMBRIC test, Lawrence Livermore National Laboratory, Livermore, CA.

Turner, D.R., 1995. A uniform approach to surface complexation modeling of radionuclide sorption, cnwra 95-001, Center for Nuclear Waste Regulatory Analyses, San Antonio.

Turner, D.R., Pabalan, R.T., Bertetti, F.P., 1998. Neptunium(V) sorption on montmorillonite: An experimental and surface complexation modeling study. Clays and Clay Minerals 46, 256-269.

Vaniman, D., Furlano, A., Chipera, S., Thompson, J., Triay, I., 1996. Microautoradiography in studies of Pu(V) sorption by trace and fracture minerals in tuff. Materials Research Society Symposium Proceedings Vol 412, 639-645.

White, G.N., Zelazny, L.W., 1988. Analysis and implications of the edge structure of dioctahedral phyllosilicates. Clays and Clay Minerals 36, 141-146.

Zavarin, M., Bourbin, M., Kersting, A.B., Powell, B.A., Zhao, P.Z., 2008. GEOC 226-Examination of the effects of ionic strength and pH on neptunium(V) and plutonium(V) sorption to montmorillonite. Abstr Pap Am Chem S 235, 226-GEOC.

Zavarin, M., Bruton, C.J., 2004. A Non-Electrostatic Surface Complexation Approach to Modeling Radionuclide Migration at the Nevada Test Site: Aluminosilicates, UCRL-TR-208672, Lawrence Livermore National Laboratory, Livermore, California.

APPENDIX A - Solid Phase Charachterization Data Provided by Manufacturer

Data for Na-Montmorillonite SWy-1 reported by Clay Minerals Repository.
(website: http://www.agry.purdue.edu/cjohnston/sourceclays/chem.htm, accessed 01/23/2008)

ORIGIN: Newcastle formation, (cretaceous)
County of Crook, State of Wyoming, USA

LOCATION: NE 1/4 SE 1/4 Sec.18, T 57 N, R 65 W; 8, Topographic map: Seeley(15'), The upper 63 of recently stripped area was removed to expose clean,green upper Newcastle, Collected from which samples was taken, October 3,1972.

CHEMICAL COMPOSITION (%): SiO_2: 62.9, Al_2O_3: 19.6, TiO_2: 0.090, Fe_2O_3:3.35, FeO: 0.32, MnO: 0.006, MgO: 3.05, CaO: 1.68, Na_2O: 1.53, K_2O: 0.53,F: 0.111, P_2O_5: 0.049, S: 0.05, Loss on heating: -550°C: 1.59; 550-1000°C:4.47, CO_2: 1.33.

CATION EXCHANGE CAPACITY (CEC): 76.4 meq/100g, principal exchange cations Na^+ and Ca^{2+}.

SURFACE AREA: N_2 area: 31.82 +/- 0.22 m^2/g

THERMAL ANALYSIS: DTA: endotherms at 185°C (shoulder at 235°C), desorptionof water: 755°C, dehydroxylation; shoulder at 810°C, exotherms at 980°C. TG: Loss in dehydroxylation range: 5.53% (theory: 5%).

INFRARED SPECTROSCOPY: Typical spectrum for Wyoming bentonite with a moderate Fe^{+3} content (band at 885 cm^{-1}). Quartz is detectable (band at 780, 800,698, 400, and 373 cm^{-1}), a trace of carbonate (band at 1425 cm^{-1}).

STRUCTURE:$(Ca_{0.12}\ Na_{0.32}\ K_{0.05})[Al_{3.01}\ Fe(III)_{0.41}\ Mn_{0.01}\ Mg_{0.54}Ti_{0.02}][Si_{7.98}\ Al_{0.02}]O_{20}(OH)_4$,Octahedral charge:-0.53, Tetrahedral charge:-0.02,Interlayer charge:-0.55, Unbalanced charge:0.05,

Data for IOTA Quartz Sand provided by Unimin Corporation

TECHNICAL DATA

IOTA® HIGH PURITY QUARTZ

FEATURES AND BENEFITS

IOTA STANDARD
IOTA-4
IOTA-6

SPRUCE PINE, NC

A unique orebody coupled with statistically controlled production techniques enable Unimin to produce the purest grades of natural quartz. These materials are known worldwide as IOTA® Quartz.

IOTA STANDARD is the material of choice for the manufacture of quartz tubing used in halogen and high intensity discharge lamps.

IOTA-4 and IOTA-6 are ultra-high purity grades used for the production of semiconductor quartz glass such as CZ Crucibles, diffusion tubes, quartz rods, and ingots.

A full range of analytical services is provided by Unimin's on-site laboratories.

PARTICLE SIZE ANALYSIS AND PROPERTIES
Mean Values. These Do Not Represent A Specification.

1. Particle Size:

   1% Max. +50 Mesh (>300 micron)
   1% Max. -200 Mesh (<75 micron)

2. Chemistry (ppm):

ELEMENT	IOTA STANDARD Mean	IOTA STANDARD Max.	IOTA-4 Mean	IOTA-4 Max.	IOTA-6 Mean	IOTA-6 Max.
Al	15.2	22.0	7.9	10.0	7.9	9.5
Ca	0.4	1.5	0.6	1.0	0.5	0.7
Fe	0.3	1.5	0.6	1.0	0.2	0.3
Li	0.7	1.5	0.2	1.0	0.2	0.3
Na	0.9	1.5	1.0	1.3	0.1	0.2
K	0.7	1.5	0.4	1.0	0.1	0.2
B	0.08	0.10	0.04	0.05	0.03	0.04

TECHNICAL DATA

IOTA® HIGH PURITY QUARTZ

FEATURES AND BENEFITS

IOTA®-8

Unimin's introduction of Iota-8 in 1999 represents a major technical breakthrough in the purity level obtained from natural quartz sands. Iota-8 was developed with the target of reducing alkali and transition metals to their lowest possible levels. The ultra high purity of Iota-8 improves devitrification and thermal stability properties, making Iota-8 the ideal raw material for large diameter crucibles and as a crucible lining.

PARTICLE SIZE ANALYSIS AND PROPERTIES

Mean Values. These Do Not Represent A Specification.

1. Particle Size: 1% max > 300 µm (+50 mesh)
   2% max < 75 µm (-200 mesh)

2. Typical Chemical Values (ppm):

Element	Iota-8
Al	7.0
B	<0.04
Ca	0.5
Cr	<0.003
Cu	0.002
Fe	<0.03
K	<0.04
Li	<0.02
Mg	<0.02
Mn	<0.02
Na	0.03
Ni	<0.02
P	0.05
Ti	1.2
Zr	<0.10

APPENDIX B - Volumes of NaCl, HCl, NaOH, Mineral Suspensions, Pu Working Solutions, and Carbonate Solutions Used for Sample Preparation at I = 0.01 M.

Table B1: Volumes of each solution/suspension required to prepared 10mL samples at constant ionic strength for initially Pu(IV) suspensions without carbonate. For control solutions, an additional 1 mL of MQ H_2O was added in place of the aliquot of mineral or clay suspension.

Target pH	0.001 M HCl	0.10 M NaCl	0.001 M NaOH	MQ H_2O	Mineral/Clay Suspension*	$^{238}Pu(V)$**
4	5.000	0.950	0.000	2.800	1.000	0.250
4.5	1.666	0.980	0.000	6.104	1.000	0.250
5	0.500	0.990	0.000	7.260	1.000	0.250
5.5	0.167	1.000	0.000	7.583	1.000	0.250
6	0.050	1.000	0.000	7.700	1.000	0.250
6.5	0.016	1.000	0.000	7.734	1.000	0.250
7		1.000	0.005	7.745	1.000	0.250
7.5		1.000	0.005	7.745	1.000	0.250
8		1.000	0.025	7.725	1.000	0.250
8.5		1.000	0.050	7.700	1.000	0.250
9		1.000	0.100	7.650	1.000	0.250
9.5		0.990	0.500	7.260	1.000	0.250
10		0.990	1.000	6.760	1.000	0.250

*Based on 100 $m^2 L^{-1}$ silica and gibbsite suspensions and 46 $m^2 L^{-1}$ montmorillonite suspension

**See Table 2.1 for exact concentrations, volume was changed to maintain 1.2 x 10^{-10} M Pu total concentration. Difference in volume was made up by adding or subtracting water to maintain total volume of 10 mL.

Table B2: Volumes of each solution/suspension required to prepared 10mL samples at constant ionic strength for initially Pu(IV) suspensions without carbonate. For control solutions, an additional 1 mL of MQ H_2O was added in place of the aliquot of mineral or clay suspension.

Target pH	0.001 M HCl	0.10 M NaCl	0.001 M NaOH	MQ H_2O	Mineral/Clay Suspension	$^{238}Pu(IV)$**
4	5.000	1.000	0.000	7.990	1.000	0.010
4.5	1.666	1.000	0.500	7.490	1.000	0.010
5	0.500	0.990	0.900	7.100	1.000	0.010
5.5	0.167	0.990	0.950	7.050	1.000	0.010
6	0.050	0.990	0.990	7.010	1.000	0.010
6.5	0.016	0.990	0.995	7.005	1.000	0.010
7		0.990	1.001	6.999	1.000	0.010
7.5		0.990	1.005	6.995	1.000	0.010
8		0.990	1.010	6.990	1.000	0.010
8.5		0.990	1.050	6.950	1.000	0.010
9		0.990	1.100	6.900	1.000	0.010
9.5		0.980	1.500	6.510	1.000	0.010
10		0.980	2.000	6.010	1.000	0.010

*Based on 100 $m^2 L^{-1}$ silica and gibbsite suspensions and 46 $m^2 L^{-1}$ montmorillonite suspension

**See Table 2.2 for exact concentrations, volume was changed to maintain 1.2 x 10^{-10} M Pu total concentration. Difference in volume was made up by adding or subtracting water to maintain total volume of 10 mL.

Table B3: Volumes of each solution/suspension required to prepared 10mL samples at constant ionic strength for initially Pu(V) suspensions with carbonate present. Note: Initial $CO_2(g)$ limited to approximately 0.01 M HCO_3^- in pH >9 suspensions to maintain ionic strength of 0.01 M. For control solutions, an additional 1 mL of MQ H_2O was added in place of the aliquot of mineral or clay suspension.

Target pH	0.001 M HCl	0.1 M NaCl	0.10 M $NaHCO_3$	0.10 M Na_2CO_3	MQ H_2O	Mineral/Clay Suspension*	$^{238}Pu(V)$**
4	5.000	1.000	0.002		2.898	1.000	0.100
4.5	1.666	1.000	0.002		6.232	1.000	0.100
5	0.500	1.000	0.002		7.398	1.000	0.100
5.5	0.167	1.000	0.002		7.732	1.000	0.100
6	0.050	1.000	0.002		7.848	1.000	0.100
6.5	0.016	1.000	0.004		7.880	1.000	0.100
7		1.000	0.009		7.891	1.000	0.100
7.5		1.000	0.025		7.875	1.000	0.100
8		1.000	0.077		7.823	1.000	0.100
8.5		0.800	0.239	0.000	7.860	1.000	0.100
9		0.250	0.749	0.005	7.895	1.000	0.100
9.5		0.200	0.779	0.022	7.899	1.000	0.100
10			0.851	0.065	7.985	1.000	0.100

*Based on 100 $m^2 L^{-1}$ silica and gibbsite suspensions and 46 $m^2 L^{-1}$ montmorillonite suspension
**See Table 2.1 for exact concentrations, volume was changed to maintain 1.2 x 10^{-10} M Pu total concentration. Difference in volume was made up by adding or subtracting water to maintain total volume of 10 mL.

Table B4: Volumes of each solution/suspension required to prepared 10mL samples at constant ionic strength for initially Pu(IV) suspensions with carbonate present. Note: Initial $CO_2(g)$ limited to approximately 0.01 M HCO_3^- in pH >9 suspensions to maintain ionic strength of 0.01 M. For control solutions, an additional 1 mL of MQ H_2O was added in place of the aliquot of mineral or clay suspension.

Target pH	0.001 M HCl	0.1 M NaCl	0.10 M $NaHCO_3$	0.10 M Na_2CO_3	MQ H_2O	Mineral/Clay Suspension*	$^{238}Pu(IV)$**
4	5.000	0.900	0.002		3.088	1.000	0.010
4.5	1.666	0.900	0.002		6.422	1.000	0.010
5	0.500	0.900	0.002		7.588	1.000	0.010
5.5	0.167	0.900	0.002		7.922	1.000	0.010
6	0.050	0.900	0.002		8.038	1.000	0.010
6.5	0.016	0.900	0.004		8.070	1.000	0.010
7		0.900	0.008		8.082	1.000	0.010
7.5		0.900	0.025		8.065	1.000	0.010
8		0.900	0.077		8.013	1.000	0.010
8.5		0.700	0.239	0.000	8.050	1.000	0.010
9		0.150	0.749	0.005	8.085	1.000	0.010
9.5		0.100	0.779	0.022	8.089	1.000	0.010
10			0.851	0.065	8.075	1.000	0.010

*Based on 100 $m^2 L^{-1}$ silica and gibbsite suspensions and 46 $m^2 L^{-1}$ montmorillonite suspension
**See Table 2.2 for exact concentrations, volume was changed to maintain 1.2 x 10^{-10} M Pu total concentration. Difference in volume was made up by adding or subtracting water to maintain total volume of 10 mL.

APPENDIX C - Sorption Data and Species Concentrations Used for Development of Surface Complexation Model Input Files

Table C1: Pu(IV) sorption to gibbsite under $CO_2(g)$ equilibrated conditions. Note: Reported HCO_3^-/CO_3^{2-} concentrations based on initial solution conditions. Some diffusion of $CO_2(g)$ occurred over the course of the experiment.

Total Sample Mass (g)	$[Na^+]$	$[Cl^-]$	$[\alpha\text{-}Al(OH)_3]$ ($m^2\ L^{-1}$)	$[HCO_3^-]/[CO_3^{2-}]$	$[Pu]_{Total}$	pH after 24 hours	$[Pu]_{aqu}$* after 24 hours	Error $[Pu]_{aqu}$* after 24 hours	pH after 62 days	$[Pu]_{aqu}$* after 62 days	Error $[Pu]_{aqu}$* after 62 days	pH after 300 days	$[Pu]_{aqu}$* after 300 days	Error $[Pu]_{aqu}$* after 300 days
10.136	0.01	0.01	10.24	1.4E-07	1.33E-10	3.9	5.00E-11	8.75E-13	4.2	6.92E-11	5.52E-13	4.13	6.89E-11	5.50E-13
9.945	0.01	0.01	10.42	4.4E-07	1.35E-10	4.33	3.91E-11	7.39E-13	4.45	6.24E-11	5.11E-13	4.37	6.26E-11	5.13E-13
10.050	0.01	0.01	10.39	4.4E-07	1.34E-10	4.63	3.49E-11	6.86E-13	4.72	5.98E-11	4.96E-13	4.67	5.97E-11	4.96E-13
10.047	0.01	0.01	10.33	1.3E-06	1.34E-10	5.14	3.22E-11	6.53E-13	5.13	5.37E-11	4.59E-13	4.9	5.39E-11	4.60E-13
9.945	0.01	0.01	10.62	4E-06	1.34E-10	5.64	2.88E-11	6.09E-13	5.23	5.06E-11	4.35E-13	5.2	5.25E-11	4.52E-13
10.024	0.01	0.01	10.34	4E-06	1.34E-10	5.38	3.53E-11	6.94E-13	5.99	3.82E-11	3.63E-13	5.9	3.82E-11	3.63E-13
9.983	0.01	0.01	10.41	1.2E-05	1.30E-10	6.14	2.33E-11	5.36E-13	6.23	3.70E-11	3.55E-13	6.2	3.70E-11	3.55E-13
9.989	0.01	0.01	10.34	3.7E-05	1.35E-10	6.5	2.30E-11	5.31E-13	6.66	2.73E-11	2.93E-13	6.62	2.73E-11	2.93E-13
10.020	0.01	0.01	10.33	3.7E-05	1.35E-10	6.68	2.14E-11	5.09E-13	6.58	3.19E-11	3.23E-13	6.48	3.17E-11	3.22E-13
9.961	0.01	0.01	10.42	0.00011	1.35E-10	7.06	1.52E-11	4.23E-13	6.76	2.08E-11	2.50E-13			
9.967	0.01	0.01	10.38	0.00034	1.28E-10	7.51	5.21E-12	2.67E-13	7.38	2.83E-12	1.07E-13			
10.033	0.01	0.01	10.30	0.00034	1.37E-10	7.58	4.96E-12	2.64E-13	7.39	4.00E-12	1.19E-13	7.21	2.82E-12	1.07E-13
9.921	0.01	0.01	10.45	0.00104	1.42E-10	7.98	2.36E-12	2.15E-13	7.77	1.23E-12	8.97E-14	7.33	4.00E-12	1.19E-13
9.941	0.01	0.01	10.44	0.00316	1.34E-10	8.49	1.96E-12	2.06E-13	8.28	6.51E-13	8.23E-14	8.33	6.49E-13	8.20E-14
9.950	0.01	0.01	10.42	0.00316	1.36E-10	8.52	1.52E-12	1.98E-13	8.25	6.73E-13	8.26E-14	8.38	6.71E-13	8.24E-14
10.059	0.01	0.01	10.33	0.0072	1.30E-10	9.08	2.75E-12	2.21E-13	8.95	1.03E-12	8.71E-14	8.84	1.03E-12	8.72E-14
9.971	0.01	0.01	10.42	0.00846	1.32E-10	9.51	2.73E-12	2.21E-13	9.34	1.33E-12	9.06E-14	9	1.32E-12	9.01E-14
10.017	0.01	0.01	10.38	0.00846	1.32E-10	9.67	3.16E-12	2.29E-13	9.52	1.84E-12	9.65E-14	9.07	1.83E-12	9.60E-14
9.955	0.01	0.01	10.43	0.00974	1.32E-10	10.22	3.82E-12	2.44E-13	10.09	5.50E-12	1.33E-13			

* Measured aqueous phase concentration at sampling time determined via LSC.

Table C2: Pu(IV) sorption to silica under CO_2(g) equilibrated conditions. Note: Reported HCO_3^-/CO_3^{2-} concentrations based on initial solution conditions. Some diffusion of CO_2(g) occurred over the course of the experiment.

Total Sample Mass (g)	$[Na^+]$	$[Cl^-]$	$[SiO_2]$ (m^2 L^{-1})	$[HCO_3^-]$ /$[CO_3^{2-}]$	$[Pu]_{Total}$	pH after 24 hours	$[Pu]_{aqu}$* after 24 hours	Error $[Pu]_{aqu}$* after 24 hours	pH after 62 days	$[Pu]_{aqu}$* after 62 days	Error $[Pu]_{aqu}$* after 62 days
10.070	0.01	0.01	10.35	1.44E-07	1.36E-10	3.87	4.99E-11	8.73E-13	3.88	6.61E-11	4.97E-13
10.069	0.01	0.01	10.35	4.38E-07	1.33E-10	4.51	1.68E-11	4.47E-13	4.44	4.36E-11	3.96E-13
10.012	0.01	0.01	10.35	4.38E-07	1.35E-10	4.31	3.11E-11	6.37E-13	4.24	5.05E-11	4.68E-13
10.042	0.01	0.01	10.35	1.33E-06	1.34E-10	4.92	1.68E-11	4.45E-13	4.75	2.38E-11	2.70E-13
10.044	0.01	0.01	10.35	4.03E-06	1.34E-10	5.62	1.13E-11	3.68E-13	5.62	5.66E-12	1.34E-13
10.018	0.01	0.01	10.35	4.03E-06	1.35E-10	5.62	1.07E-11	3.58E-13	5.35	4.16E-12	1.20E-13
10.006	0.01	0.01	10.35	1.22E-05	1.36E-10	6.13	1.27E-11	3.88E-13	5.77	2.34E-12	1.01E-13
9.945	0.01	0.01	10.35	3.72E-05	1.35E-10	6.85	1.55E-11	4.30E-13	6.66	8.17E-13	8.40E-14
10.037	0.01	0.01	10.35	3.72E-05	1.36E-10	6.57	8.42E-12	3.23E-13	6.37	4.30E-13	7.91E-14
10.076	0.01	0.01	10.35	1.13E-04	1.32E-10	6.93	1.38E-11	4.06E-13	6.81	7.82E-13	8.35E-14
10.019	0.01	0.01	10.35	3.43E-04	1.35E-10	7.36	1.36E-11	4.02E-13	7.31	1.10E-12	8.74E-14
10.025	0.01	0.01	10.35	3.42E-04	1.35E-10	7.25	1.10E-11	3.63E-13	7.31	1.31E-12	9.01E-14
10.056	0.01	0.01	10.35	1.04E-03	1.35E-10	7.96	1.16E-11	3.73E-13	7.84	1.40E-12	9.12E-14
10.090	0.01	0.01	10.35	3.15E-03	1.35E-10	8.02	9.73E-12	3.44E-13	8.35	2.00E-12	9.79E-14
9.974	0.01	0.01	10.35	3.16E-03	1.36E-10	8.7	1.13E-11	3.68E-13	8.39	2.15E-12	9.95E-14
10.028	0.01	0.01	10.35	7.20E-03	1.35E-10	9.03	1.36E-11	4.02E-13	8.84	3.68E-12	1.15E-13
10.083	0.01	0.01	10.35	8.47E-03	1.36E-10	9.51	1.57E-11	4.33E-13	9.22	5.24E-12	1.30E-13
10.000	0.01	0.01	10.35	8.47E-03	1.33E-10	9.63	2.15E-11	5.13E-13	9.28	6.47E-12	1.52E-13
10.062	0.01	0.01	10.35	9.77E-03	1.35E-10	10.17	1.99E-11	4.92E-13	9.88	7.06E-12	1.46E-13

* Measured aqueous phase concentration at sampling time determined via LSC.

Table C3: Pu(IV) Sorption to gibbsite under CO_2(g)-free conditions. Note: Data at 62 days is shown but was not used in the report or modeling efforts due to CO_2(g) diffusion into the vial.

Total Sample Mass (g)	$[Na^+]$	$[Cl^-]$	$[\alpha\text{-}Al(OH)_3]$ (m^2 L^{-1})	$[Pu]_{Total}$	pH after 24 hours	$[Pu]_{aqu}$* after 24 hours	Error $[Pu]_{aqu}$* after 24 hours	pH after 62 days	$[Pu]_{aqu}$* after 62 days	Error $[Pu]_{aqu}$* after 62 days
10.006	0.01	0.01	9.99	1.24E-10	3.89	2.07E-11	4.98E-13	4.22	2.21E-11	5.33E-13
10.091	0.01	0.01	9.91	1.23E-10	4.62	1.12E-11	3.77E-13	4.49	2.36E-11	5.50E-13
10.092	0.01	0.01	9.91	1.23E-10	4.87	8.79E-12	3.43E-13	4.76	2.79E-11	5.98E-13
10.001	0.01	0.01	10.00	1.24E-10	4.93	8.63E-12	3.41E-13	4.85	1.08E-11	3.96E-13
10.071	0.01	0.01	9.93	1.23E-10	5.87	8.33E-12	3.36E-13	4.85	1.10E-11	3.99E-13
10.110	0.01	0.01	9.89	1.23E-10	6.06	7.77E-12	3.28E-13	5.54	9.20E-12	3.75E-13
10.118	0.01	0.01	9.88	1.23E-10	6.22	8.46E-12	3.38E-13	5.87	1.44E-11	4.42E-13
10.099	0.01	0.01	9.90	1.23E-10	6.57	8.13E-12	3.34E-13	6.19	7.46E-12	3.51E-13
10.059	0.01	0.01	9.94	1.23E-10	6.71	7.56E-12	3.25E-13	6.32	7.70E-12	3.55E-13
10.083	0.01	0.01	9.92	1.23E-10	6.89	6.56E-12	3.10E-13	6.27	7.81E-12	3.56E-13
10.133	0.01	0.01	9.87	1.23E-10	7.05	7.83E-12	3.29E-13	6.37	7.99E-12	3.59E-13
10.108	0.01	0.01	9.89	1.23E-10	7.72	8.77E-12	3.43E-13	6.49	1.28E-11	4.21E-13
10.056	0.01	0.01	9.94	1.23E-10	7.87	9.34E-12	3.51E-13	6.77	1.14E-11	4.04E-13
9.949	0.01	0.01	10.05	1.25E-10	8.2	7.56E-12	3.25E-13	6.68	1.44E-11	4.42E-13
10.570	0.01	0.01	9.46	1.17E-10	8.37	7.44E-12	3.23E-13	6.8	1.48E-11	4.46E-13
9.939	0.01	0.01	10.06	1.25E-10	8.73	5.71E-12	2.97E-13	6.87	1.50E-11	4.49E-13
10.073	0.01	0.01	9.93	1.23E-10	9.3	3.81E-12	2.66E-13	7.1	7.72E-12	3.55E-13
10.077	0.01	0.01	9.92	1.23E-10	9.47	3.40E-12	2.59E-13	7.3	7.02E-12	3.46E-13
10.123	0.01	0.01	9.88	1.23E-10	9.97	3.35E-12	2.58E-13	7.83	1.72E-12	2.67E-13

* Measured aqueous phase concentration at sampling time determined via LSC.

Table C4: Pu(IV) Sorption to silica under CO_2(g)-free conditions. Note: Data at 62 days is shown but was not used in the report or modeling efforts due to CO_2(g) diffusion into the vial.

Total Sample Mass (g)	$[Na^+]$	$[Cl^-]$	$[SiO_2]$ (m^2 L^{-1})	$[Pu]_{Total}$	pH after 24 hours	$[Pu]_{aqu}$* after 24 hours	Error $[Pu]_{aqu}$* after 24 hours	pH after 60 days	$[Pu]_{aqu}$* after 60 days	Error $[Pu]_{aqu}$* after 60 days
10.112	0.01	0.01	9.89	1.23E-10	4.16	7.19E-11	8.89E-13	4.52	2.67E-11	4.67E-13
10.129	0.01	0.01	9.87	1.23E-10	4.47	6.71E-11	8.36E-13	4.50	1.82E-11	3.84E-13
10.124	0.01	0.01	9.88	1.23E-10	4.66	5.46E-11	7.13E-13	4.67	2.36E-11	4.37E-13
9.967	0.01	0.01	10.03	1.25E-10	5.07	2.56E-11	4.20E-13	5.06	7.76E-12	2.83E-13
10.146	0.01	0.01	9.86	1.22E-10	5.73	2.71E-11	4.36E-13	6.02	7.93E-12	2.85E-13
10.103	0.01	0.01	9.90	1.23E-10	6.10	3.33E-11	4.99E-13	5.83	1.29E-12	2.19E-13
9.210	0.01	0.01	10.86	1.35E-10	6.44	4.46E-11	6.13E-13	6.34	9.94E-13	2.16E-13
10.141	0.01	0.01	9.86	1.22E-10	6.72	4.04E-11	5.72E-13	6.42	5.45E-13	2.12E-13
10.095	0.01	0.01	9.91	1.23E-10	6.75	3.43E-11	5.09E-13	6.43	3.68E-13	2.10E-13
10.089	0.01	0.01	9.91	1.23E-10	6.98	3.40E-11	5.07E-13	6.53	5.93E-13	2.12E-13
10.079	0.01	0.01	9.92	1.23E-10	7.11	3.19E-11	4.86E-13	6.53	3.41E-13	2.10E-13
10.120	0.01	0.01	9.88	1.23E-10	7.44	2.20E-11	3.82E-13	6.68	4.22E-13	2.11E-13
10.101	0.01	0.01	9.90	1.23E-10	7.87	2.41E-11	4.05E-13	6.68	5.35E-13	2.12E-13
13.480	0.01	0.01	7.42	9.21E-11	7.96	2.52E-11	4.15E-13	6.91	3.61E-13	2.10E-13
9.974	0.01	0.01	10.03	1.24E-10	8.27	1.75E-11	3.34E-13	7.00	1.02E-12	2.17E-13
8.888	0.01	0.01	11.25	1.40E-10	8.58	1.95E-11	3.55E-13	7.03	3.49E-13	2.10E-13
10.129	0.01	0.01	9.87	1.23E-10	9.17	2.48E-11	4.12E-13	7.33	1.39E-12	2.20E-13
10.126	0.01	0.01	9.88	1.23E-10	9.22	2.36E-11	3.99E-13	7.43	1.76E-12	2.24E-13
10.122	0.01	0.01	9.88	1.23E-10	9.67	2.93E-11	4.58E-13	8.56	5.56E-12	2.61E-13

* Measured aqueous phase concentration at sampling time determined via LSC.

Table C5: Pu(V) sorption to gibbsite under CO_2(g) equilibrated conditions. Note: Reported HCO_3^-/CO_3^{2-} concentrations based on initial solution conditions. Some diffusion of CO_2(g) occurred over the course of the experiment.

Total Sample Mass (g)	$[Na^+]$	$[Cl^-]$	$[\alpha\text{-}Al(OH)_3]$ ($m^2\ L^{-1}$)	$[HCO_3^-]/[CO_3^{2-}]$	$[Pu]_{Total}$	pH after 24 hours	$[Pu]_{aqu}$* after 24 hours	Error $[Pu]_{aqu}$* after 24 hours	pH after 62 days	$[Pu]_{aqu}$* after 62 days	Error $[Pu]_{aqu}$* after 62 days	pH after 300 days	$[Pu]_{aqu}$* after 300 days	Error $[Pu]_{aqu}$* after 300 days
10.068	0.01	0.01	10.28	1.44E-7	1.18E-10	4.03	1.17E-10	1.67E-12	4.47	1.15E-10	1.15E-10	4.4	1.14E-10	8.16E-13
10.039	0.01	0.01	10.31	4.37E-7	1.18E-10	4.63	1.17E-10	1.67E-12	4.55	1.18E-10	1.18E-10	4.45	1.17E-10	8.35E-13
9.983	0.01	0.01	10.38	4.37E-7	1.19E-10	4.48	1.18E-10	1.68E-12	4.58	1.17E-10	1.17E-10	4.59	1.14E-10	8.15E-13
9.999	0.01	0.01	10.37	1.32E-6	1.19E-10	5.03	1.17E-10	1.66E-12	4.99	1.10E-10	1.10E-10	4.88	8.87E-11	6.67E-13
10.054	0.01	0.01	10.33	4.03E-6	1.18E-10	5.63	1.14E-10	1.64E-12	5.36	1.12E-10	1.12E-10	5.32	8.16E-11	6.25E-13
10.018	0.01	0.01	10.32	4.03E-6	1.19E-10	5.76	1.16E-10	1.66E-12	5.8	1.09E-10	1.09E-10	5.61	7.96E-11	6.13E-13
10.175	0.01	0.01	10.15	1.22E-5	1.16E-10	6.04	1.09E-10	1.58E-12	6.13	1.02E-10	1.02E-10	6.06	6.79E-11	5.44E-13
10.442	0.01	0.01	9.88	3.71E-5	1.14E-10	6.65	9.70E-11	1.43E-12	6.74	7.15E-11	7.15E-11	6.7	2.29E-11	2.62E-13
9.984	0.01	0.01	10.40	3.71E-5	1.19E-10	6.67	1.03E-10	1.50E-12	6.61	8.67E-11	8.67E-11	6.41	5.82E-11	4.85E-13
9.887	0.01	0.01	10.48	0.000112	1.21E-10	7.2	9.02E-11	1.35E-12	6.96	5.74E-11	5.74E-11			
10.215	0.01	0.01	10.12	0.000342	1.16E-10	7.51	7.37E-11	1.16E-12	7.25	1.00E-11	1.00E-11	7.23	3.01E-12	1.03E-13
9.934	0.01	0.01	10.41	0.000342	1.19E-10	7.57	6.67E-11	1.08E-12	7.47	1.21E-11	1.21E-11	7.38	5.12E-13	7.29E-14
9.965	0.01	0.01	10.39	0.00104	1.19E-10	7.99	3.96E-11	7.45E-13	7.8	1.28E-12	1.28E-12			
9.981	0.01	0.01	10.35	0.003157	1.19E-10	8.52	2.85E-11	6.05E-13	8.25	3.82E-13	3.82E-13	8.29	7.21E-13	7.59E-14
9.947	0.01	0.01	10.43	0.00315	1.19E-10	8.51	3.03E-11	6.29E-13	8.2	6.30E-13	6.30E-13	8.35	4.03E-13	7.14E-14
9.997	0.01	0.01	10.39	0.00720	1.19E-10	9.05	2.62E-11	5.76E-13	8.91	6.06E-13	6.06E-13	8.78	1.11E-12	8.17E-14
10.010	0.01	0.01	10.37	0.00845	1.19E-10	9.43	2.12E-11	5.08E-13	9.27	9.59E-13	9.59E-13	8.99	8.23E-13	7.77E-14
10.027	0.01	0.01	10.33	0.00848	1.19E-10	9.82	1.85E-11	4.70E-13	9.5	1.81E-12	1.81E-12	9.14	5.53E-13	7.40E-14
9.971	0.01	0.01	10.39	0.00973	1.19E-10	10.25	1.64E-11	4.41E-13	10.16	3.70E-12	3.70E-12			

* Measured aqueous phase concentration at sampling time determined via LSC.

Table C6: Pu(V) sorption to silica under CO_2(g) equilibrated conditions. Note: Reported HCO_3^-/CO_3^{2-} concentrations based on initial solution conditions. Some diffusion of CO_2(g) occurred over the course of the experiment.

Total Sample Mass (g)	$[Na^+]$	$[Cl^-]$	$[SiO_2]$ (m^2 L^{-1})	$[HCO_3^-]$ /$[CO_3^{2-}]$	$[Pu]_{Total}$	pH after 24 hours	$[Pu]_{aqu}$* after 24 hours	Error $[Pu]_{aqu}$* after 24 hours	pH after 62 days	$[Pu]_{aqu}$* after 62 days	Error $[Pu]_{aqu}$* after 62 days
10.163	0.01	0.01	10.40	1.44E-7	1.18E-10	3.98	9.16E-11	1.37E-12	4.03	4.60E-11	4.17E-13
9.992	0.01	0.01	10.54	4.38E-7	1.20E-10	4.63	8.26E-11	1.27E-12	4.44	4.11E-11	3.81E-13
10.013	0.01	0.01	10.53	4.37E-7	1.20E-10	4.46	8.76E-11	1.32E-12	4.87	7.64E-12	1.52E-13
10.143	0.01	0.01	10.40	1.33E-6	1.18E-10	5.12	6.07E-11	1.00E-12	5.03	3.47E-12	1.14E-13
10.350	0.01	0.01	10.10	4.03E-6	1.15E-10	5.34	5.93E-11	9.86E-13	5.17	3.65E-12	1.15E-13
9.972	0.01	0.01	10.57	4.04E-6	1.20E-10	5.85	3.85E-11	7.32E-13	5.5	1.07E-12	8.72E-14
10.053	0.01	0.01	10.56	1.22E-5	1.19E-10	6.2	3.27E-11	6.58E-13	6.2	9.64E-13	8.61E-14
10.019	0.01	0.01	10.51	3.72E-5	1.20E-10	6.46	2.30E-11	5.32E-13	6.4	4.35E-13	7.89E-14
10.008	0.01	0.01	10.53	3.72E-5	1.19E-10	6.72	2.16E-11	5.14E-13	6.44	5.60E-13	8.09E-14
10.067	0.01	0.01	10.64	1.13E-4	1.19E-10	7.25	1.26E-11	3.88E-13	6.75	6.80E-13	8.24E-14
9.993	0.01	0.01	10.52	3.43E-4	1.20E-10	7.48	5.41E-12	2.73E-13	7.35	5.61E-13	8.13E-14
10.021	0.01	0.01	10.52	3.42E-4	1.19E-10	7.47	4.88E-12	2.62E-13	7.45	5.43E-13	8.07E-14
10.019	0.01	0.01	10.51	1.04E-3	1.20E-10	8.06	5.95E-12	2.81E-13	7.87	1.04E-12	8.68E-14
9.993	0.01	0.01	10.55	3.16E-3	1.20E-10	8.42	1.89E-11	4.78E-13	8.32	1.61E-12	9.35E-14
10.001	0.01	0.01	10.59	3.16E-3	1.20E-10	8.51	2.18E-11	5.18E-13	8.32	2.38E-12	1.02E-13
10.017	0.01	0.01	10.57	7.20E-3	1.19E-10	8.96	6.64E-11	1.07E-12	8.82	2.91E-12	1.08E-13
10.030	0.01	0.01	10.46	8.46E-3	1.19E-10	9.38	8.17E-11	1.25E-12	9.12	3.68E-12	1.16E-13
10.015	0.01	0.01	10.59	8.46E-3	1.19E-10	9.54	8.47E-11	1.29E-12	9.35	3.98E-12	1.18E-13
10.002	0.01	0.01	10.50	9.74E-3	1.19E-10	10.05	8.23E-11	1.26E-12	9.86	6.09E-12	1.38E-13

* Measured aqueous phase concentration at sampling time determined via LSC.

Table C7: Pu(V) Sorption to gibbsite under CO_2(g)-free conditions. Note: Data at 62 days is shown but was not used in the report or modeling efforts due to CO_2(g) diffusion into the vial.

Total Sample Mass (g)	$[Na^+]$	$[Cl^-]$	$[\alpha\text{-}Al(OH)_3]$ (m^2 L^{-1})	$[Pu]_{Total}$	pH after 24 hours	$[Pu]_{aqu}$* after 24 hours	Error $[Pu]_{aqu}$* after 24 hours	pH after 62 days	$[Pu]_{aqu}$* after 62 days	Error $[Pu]_{aqu}$* after 62 days
10.036	0.01	0.01	9.96	1.32E-10	3.73	1.30E-10	1.82E-12	4.3	1.28E-10	1.79E-12
9.910	0.01	0.01	10.09	1.33E-10	4.17	1.31E-10	1.83E-12	4.44	1.32E-10	1.83E-12
10.033	0.01	0.01	9.97	1.32E-10	4.26	1.30E-10	1.81E-12	4.48	1.30E-10	1.81E-12
9.968	0.01	0.01	10.03	1.32E-10	4.88	1.29E-10	1.80E-12	5.01	1.26E-10	1.76E-12
10.187	0.01	0.01	9.82	1.30E-10	5.46	1.25E-10	1.75E-12	5.33	1.20E-10	1.70E-12
10.103	0.01	0.01	9.90	1.31E-10	5.59	1.27E-10	1.78E-12	5.28	1.21E-10	1.71E-12
10.151	0.01	0.01	9.85	1.30E-10	6.07	1.22E-10	1.72E-12	5.71	1.17E-10	1.66E-12
10.125	0.01	0.01	9.88	1.30E-10	6.26	1.21E-10	1.71E-12	5.88	1.20E-10	1.69E-12
10.026	0.01	0.01	9.97	1.32E-10	6.35	1.22E-10	1.72E-12	5.92	1.25E-10	1.75E-12
10.028	0.01	0.01	9.97	1.32E-10	6.46	1.20E-10	1.69E-12	6.04	1.15E-10	1.63E-12
10.091	0.01	0.01	9.91	1.31E-10	6.63	1.18E-10	1.67E-12	6.87	7.31E-11	1.15E-12
10.117	0.01	0.01	9.88	1.30E-10	6.79	1.13E-10	1.62E-12	6.44	9.21E-11	1.37E-12
10.115	0.01	0.01	9.89	1.31E-10	7.19	1.04E-10	1.52E-12	6.44	9.48E-11	1.40E-12
10.127	0.01	0.01	9.87	1.30E-10	7.32	9.53E-11	1.41E-12	6.6	6.58E-11	1.07E-12
10.067	0.01	0.01	9.93	1.31E-10	8.06	2.90E-11	6.23E-13	6.72	5.87E-11	9.81E-13
10.073	0.01	0.01	9.93	1.31E-10	8.45	1.24E-11	4.01E-13	7.11	4.31E-11	7.94E-13
10.121	0.01	0.01	9.88	1.30E-10	8.56	6.32E-12	3.09E-13	7.16	4.53E-11	8.21E-13
9.948	0.01	0.01	10.05	1.33E-10	9.57	3.11E-12	2.55E-13	7.3	3.73E-11	7.24E-13
9.131	0.01	0.01	10.95	1.45E-10	9.92	2.74E-12	2.48E-13	7.62	1.83E-11	4.82E-13

* Measured aqueous phase concentration at sampling time determined via LSC.

Table C8: Pu(V) Sorption to silica under CO_2(g)-free conditions. Note: Data at 62 days is shown but was not used in the report or modeling efforts due to CO_2(g) diffusion into the vial.

Total Sample Mass (g)	$[Na^+]$	$[Cl^-]$	$[SiO_2]$ (m^2 L^{-1})	$[Pu]_{Total}$	pH after 24 hours	$[Pu]_{aqu}$* after 24 hours	Error $[Pu]_{aqu}$* after 24 hours	pH after 48 hours	$[Pu]_{aqu}$* after 62 days	Error $[Pu]_{aqu}$* after 62 days
10.035	0.01	0.01	9.97	1.26E-10	4.08	9.06E-11	1.68E-12	3.92	8.50E-11	1.59E-12
9.937	0.01	0.01	10.06	1.27E-10	4.66	7.39E-11	1.39E-12	4.49	5.34E-11	1.08E-12
10.035	0.01	0.01	9.97	1.26E-10	5.09	5.93E-11	1.18E-12	5.04	5.02E-11	1.03E-12
9.948	0.01	0.01	10.05	1.27E-10	5.88	3.59E-11	7.91E-13	5.80	2.24E-11	5.63E-13
9.931	0.01	0.01	10.07	1.27E-10	6.30	2.60E-11	6.24E-13	6.20	1.42E-11	4.16E-13
9.879	0.01	0.01	10.12	1.28E-10	6.88	1.88E-11	4.99E-13	7.15	9.94E-12	3.34E-13
9.916	0.01	0.01	10.08	1.27E-10	7.14	1.07E-11	3.49E-13	7.39	4.48E-12	2.16E-13
9.935	0.01	0.01	10.07	1.27E-10	7.95	8.22E-12	3.00E-13	7.63	3.16E-12	1.83E-13
10.015	0.01	0.01	9.99	1.26E-10	7.85	2.48E-12	1.64E-13	7.72	1.27E-12	1.25E-13
9.893	0.01	0.01	10.11	1.28E-10	8.23	4.09E-12	2.07E-13	7.68	1.22E-12	1.23E-13
10.018	0.01	0.01	9.98	1.26E-10	8.65	1.84E-12	1.44E-13	8.29	1.22E-12	1.23E-13
9.947	0.01	0.01	10.05	1.27E-10	9.23	2.36E-12	1.61E-13	8.79	2.62E-12	1.68E-13
9.907	0.01	0.01	10.09	1.27E-10	9.67	6.67E-12	2.67E-13	9.51	7.52E-12	2.85E-13

* Measured aqueous phase concentration at sampling time determined via LSC.

Table C9: Pu(IV) sorption to montmorillonite under CO_2(g) equilibrated conditions. Note: Reported HCO_3^-/CO_3^{2-} concentrations based on initial solution conditions. Some diffusion of CO_2(g) occurred over the course of the experiment.

Total Sample Masss (g)	$[Na^+]$	$[Cl^-]$	[mont] (m^2 L^{-1})	$[HCO_3^-]$ /$[CO_3^{2-}]$	$[Pu]_{Total}$	pH after 24 hours	$[Pu]_{aqu}$* after 24 hours	Error $[Pu]_{aqu}$* after 24 hours	pH after 21 days	$[Pu]_{aqu}$* after 21 days	Error $[Pu]_{aqu}$* after 21 days	pH after 60 days	$[Pu]_{aqu}$* after 60 days	Error $[Pu]_{aqu}$* after 60 days
9.342	0.01	0.01	5.11	1.44E-07	1.13E-10	4.13	1.56E-11	5.10E-13	4.23	1.48E-11	4.94E-13	4.59	9.21E-12	3.58E-13
9.982	0.01	0.01	4.79	4.38E-07	1.08E-10	4.33	1.09E-11	4.12E-13	4.43	9.52E-12	3.87E-13	4.52	6.20E-12	2.92E-13
9.928	0.01	0.01	4.81	4.38E-07	1.12E-10	4.19	1.46E-11	4.80E-13	4.27	9.27E-12	3.80E-13	4.42	4.61E-12	2.58E-13
9.948	0.01	0.01	4.80	1.33E-06	1.07E-10	5.18	1.04E-11	4.05E-13	5.45	8.59E-12	3.71E-13	5.16	5.53E-12	2.79E-13
9.931	0.01	0.01	4.81	4.03E-06	1.13E-10	5.40	7.87E-12	3.52E-13	5.76	8.06E-12	3.57E-13	5.83	5.80E-12	2.82E-13
9.962	0.01	0.01	4.80	4.02E-06	1.12E-10	5.68	5.24E-12	3.04E-13	6.06	6.46E-12	3.28E-13	6.16	6.80E-12	3.03E-13
9.981	0.01	0.01	4.79	1.22E-05	1.11E-10	5.81	7.47E-12	3.45E-13	6.08	7.99E-12	3.56E-13	6.15	6.91E-12	3.06E-13
9.928	0.01	0.01	4.81	3.71E-05	1.12E-10	6.25	6.78E-12	3.32E-13	6.53	6.61E-12	3.31E-13	6.62	4.30E-12	2.51E-13
9.949	0.01	0.01	4.80	3.71E-05	1.12E-10	6.70	7.34E-12	3.43E-13	6.86	6.96E-12	3.37E-13	6.91	5.03E-12	2.67E-13
9.921	0.01	0.01	4.82	1.13E-04	1.13E-10	6.78	8.24E-12	3.59E-13	6.96	7.81E-12	3.52E-13	6.94	5.45E-12	2.75E-13
9.944	0.01	0.01	4.80	3.42E-04	1.11E-10	7.31	1.10E-11	4.14E-13	7.40	1.14E-11	4.22E-13	7.41	7.79E-12	3.24E-13
9.920	0.01	0.01	4.82	3.43E-04	1.10E-10	7.54	1.34E-11	4.59E-13	7.41	1.25E-11	4.44E-13	7.42	4.99E-12	2.66E-13
9.912	0.01	0.01	4.82	1.04E-03	1.13E-10	7.92	1.44E-11	4.74E-13	7.89	2.11E-11	6.02E-13	7.89	1.08E-11	3.85E-13
9.904	0.01	0.01	4.82	2.16E-03	1.12E-10	8.56	1.12E-11	4.15E-13	8.44	1.24E-11	4.40E-13	8.33	1.09E-11	3.89E-13
9.923	0.01	0.01	4.81	3.16E-03	1.11E-10	8.71	9.98E-12	3.93E-13	8.51	1.20E-11	4.33E-13	8.45	1.06E-11	3.82E-13
9.955	0.01	0.01	4.80	7.20E-03	1.10E-10	9.02	1.91E-11	5.68E-13	8.99	1.94E-11	5.75E-13	8.94	1.63E-11	4.98E-13
9.912	0.01	0.01	4.82	8.01E-03	1.11E-10	9.27	2.30E-11	6.42E-13	9.20	2.37E-11	6.56E-13	9.12	2.28E-11	6.24E-13
9.905	0.01	0.01	4.82	8.46E-03	1.12E-10	9.49	2.62E-11	7.01E-13	9.44	2.24E-11	6.29E-13	9.37	1.89E-11	5.45E-13
9.930	0.01	0.01	4.81	9.69E-03	1.12E-10	10.12	3.48E-11	8.68E-13	10.22	3.36E-11	8.47E-13	10.15	2.91E-11	7.48E-13

* Measured aqueous phase concentration at sampling time determined via LSC.

Table C10: Pu(V) sorption to montmorillonite under CO_2(g) equilibrated conditions. Note: Reported HCO_3^-/CO_3^{2-} concentrations based on initial solution conditions. Some diffusion of CO_2(g) occurred over the course of the experiment.

Total Sample Mass (g)	$[Na^+]$	$[Cl^-]$	[mont] (m^2 L^{-1})	$[HCO_3^-]$ /$[CO_3^{2-}]$	$[Pu]_{Total}$	pH after 24 hours	$[Pu]_{aqu}$* after 24 hours	Error $[Pu]_{aqu}$* after 24 hours	pH after 21 days	$[Pu]_{aqu}$* after 21 days	Error $[Pu]_{aqu}$* after 21 days	pH after 60 days	$[Pu]_{aqu}$* after 60 days	Error $[Pu]_{aqu}$* after 60 days	pH after 90 days	$[Pu]_{aqu}$* after 90 days	Error $[Pu]_{aqu}$* after 90 days
10.023	0.01	0.01	4.77	1.44E-07	1.49E-10	4.05	1.23E-10	1.15E-12	4.09	6.67E-11	8.05E-13	4.26	2.30E-12	2.48E-13	4.96	1.90E-12	2.02E-13
10.032	0.01	0.01	4.76	4.38E-07	1.49E-10	4.50	1.39E-10	1.25E-12	4.47	9.32E-11	9.73E-13	4.73	3.42E-11	5.72E-13	5.28	8.56E-12	2.59E-13
10.021	0.01	0.01	4.77	4.38E-07	1.49E-10	4.45	1.41E-10	1.26E-12	4.52	1.01E-10	1.02E-12						
10.021	0.01	0.01	4.77	1.33E-06	1.50E-10	4.90	1.42E-10	1.26E-12	5.08	1.04E-10	1.04E-12	5.50	5.02E-11	6.92E-13	5.94	3.30E-11	4.28E-13
10.051	0.01	0.01	4.75	4.03E-06	1.49E-10	5.58	1.42E-10	1.27E-12	5.82	1.03E-10	1.03E-12	5.98	5.81E-11	7.49E-13	6.03	4.67E-11	5.11E-13
10.017	0.01	0.01	4.77	4.03E-06	1.51E-10	5.68	1.43E-10	1.26E-12	6.10	1.03E-10	1.03E-12	6.22	6.72E-11	8.08E-13	6.35	4.09E-11	4.78E-13
10.075	0.01	0.01	4.74	1.22E-05	1.49E-10	5.74	1.43E-10	1.26E-12	6.29	9.58E-11	9.88E-13	6.33	4.67E-11	6.67E-13	6.68	2.57E-11	3.80E-13
9.987	0.01	0.01	4.78	3.72E-05	1.50E-10	6.74	1.41E-10	1.25E-12	6.66	9.16E-11	9.63E-13	6.65	4.20E-11	6.32E-13	6.68	2.99E-11	4.09E-13
10.003	0.01	0.01	4.78	3.72E-05	1.49E-10	6.86	1.42E-10	1.26E-12	6.72	9.36E-11	9.77E-13	6.71	4.63E-11	6.65E-13	7.01	2.01E-11	3.44E-13
10.026	0.01	0.01	4.76	1.13E-04	1.50E-10	7.14	1.38E-10	1.24E-12	6.98	7.59E-11	8.63E-13	6.98	3.03E-11	5.41E-13	7.45	2.91E-11	4.03E-13
10.032	0.01	0.01	4.76	3.43E-04	1.50E-10	7.68	1.34E-10	1.22E-12	7.41	7.80E-11	8.76E-13	7.45	3.94E-11	6.13E-13	7.48	2.61E-11	3.82E-13
10.006	0.01	0.01	4.77	3.43E-04	1.50E-10	7.56	1.36E-10	1.23E-12	7.41	7.46E-11	8.54E-13	7.45	3.58E-11	5.85E-13	7.98	1.74E-11	3.26E-13
10.016	0.01	0.01	4.77	1.04E-03	1.50E-10	7.21	1.35E-10	1.22E-12	7.87	3.78E-11	5.98E-13	7.86	1.89E-11	4.41E-13			
9.770	0.01	0.01	4.89	3.16E-03	1.53E-10	8.04	1.17E-10	1.11E-12	8.08	7.78E-11	8.76E-13	8.18	3.38E-11	5.68E-13	7.22	2.47E-11	3.7E-13
10.001	0.01	0.01	4.78	7.20E-03	1.49E-10	8.85	5.60E-11	7.31E-13	8.83	2.26E-11	4.73E-13	8.82	1.73E-11	4.33E-13	8.89	1.42E-11	3.01E-13
10.006	0.01	0.01	4.77	8.45E-03	1.50E-10	9.48	5.39E-11	7.16E-13	9.41	1.71E-11	4.22E-13	9.30	9.86E-12	3.45E-13	9.24	9.48E-12	2.72E-13
10.033	0.01	0.01	4.76	8.45E-03	1.49E-10	9.58	5.33E-11	7.11E-13	9.52	2.09E-11	4.58E-13	9.44	1.42E-11	3.96E-13	9.40	1.19E-11	2.84E-13
9.996	0.01	0.01	4.78	9.72E-03	1.50E-10	10.12	5.11E-11	6.96E-13	10.06	4.19E-11	6.31E-13	10.01	2.61E-11	5.03E-13	9.98	2.10E-11	3.52E-13

* Measured aqueous phase concentration at sampling time determined via LSC.

Table C11: Pu(IV) Sorption to montmorillonite under CO_2(g)-free conditions. Note: Data at 62 days is shown but was not used in the report or modeling efforts due to CO_2(g) diffusion into the vial.

Total Sample Mass (g)	$[Na^+]$	$[Cl^-]$	[Mont] (m^2 L^{-1})	$[Pu]_{Total}$	pH after 24 hours	$[Pu]_{aqu}$* after 24 hours	Error $[Pu]_{aqu}$* after 24 hours	pH after 62 days	$[Pu]_{aqu}$* after 62 days	Error $[Pu]_{aqu}$* after 62 days
10.071	0.01	0.01	4.74	2.20E-10	4.10	1.42E-11	3.83E-13	4.27	8.97E-12	3.32E-13
9.984	0.01	0.01	4.78	2.22E-10	4.38	1.40E-11	3.81E-13	4.63	6.83E-12	3.04E-13
10.366	0.01	0.01	4.61	2.14E-10	4.30	1.39E-11	3.80E-13	4.54	1.29E-11	3.79E-13
10.046	0.01	0.01	4.75	2.21E-10	5.10	1.55E-11	3.98E-13	5.31	1.15E-11	3.63E-13
9.989	0.01	0.01	4.78	2.22E-10	5.67	2.15E-11	4.64E-13	5.79	3.46E-11	6.01E-13
10.060	0.01	0.01	4.75	2.21E-10	5.81	1.52E-11	3.95E-13	6.50	1.70E-11	4.25E-13
10.011	0.01	0.01	4.77	2.22E-10	6.47	1.42E-11	3.83E-13	6.50	1.94E-11	4.51E-13
10.041	0.01	0.01	4.76	2.21E-10	6.80	1.32E-11	3.71E-13	6.50	2.22E-11	4.80E-13
10.010	0.01	0.01	4.77	2.22E-10	7.19	1.28E-11	3.66E-13	6.57	1.59E-11	4.13E-13
9.950	0.01	0.01	4.80	2.23E-10	7.25	1.23E-11	3.60E-13	6.62	2.31E-11	4.89E-13
10.043	0.01	0.01	4.76	2.21E-10	7.49	1.58E-11	4.01E-13	6.64	1.74E-11	4.29E-13
10.018	0.01	0.01	4.77	2.22E-10	7.56	1.45E-11	3.88E-13	6.80	2.15E-11	4.73E-13
10.007	0.01	0.01	4.77	2.22E-10	7.74	1.72E-11	4.17E-13	6.95	2.15E-11	4.74E-13
10.018	0.01	0.01	4.77	2.22E-10	7.95	2.18E-11	4.67E-13	6.95	2.43E-11	5.02E-13
9.974	0.01	0.01	4.79	2.23E-10	8.67	3.46E-11	5.94E-13	6.98	1.67E-11	4.22E-13
9.984	0.01	0.01	4.78	2.22E-10	9.07	4.75E-11	7.12E-13	7.15	3.34E-11	5.89E-13
9.971	0.01	0.01	4.79	2.23E-10	9.16	4.46E-11	6.86E-13	7.13	2.67E-11	5.26E-13
9.987	0.01	0.01	4.78	2.22E-10	9.80	6.58E-11	8.70E-13	7.27	2.77E-11	5.34E-13
9.964	0.01	0.01	4.79	2.23E-10	10.05	6.52E-11	8.65E-13	7.52	5.95E-11	8.20E-13

* Measured aqueous phase concentration at sampling time determined via LSC.

Table C12: Pu(V) Sorption to montmorillonite under CO_2(g)-free conditions. Note: Data at 62 days is shown but was not used in the report or modeling efforts due to CO_2(g) diffusion into the vial.

Total Sample Mass (g)	$[Na^+]$	$[Cl^-]$	[Mont] (m^2 L^{-1})	$[Pu]_{Total}$	pH after 24 hours	$[Pu]_{aqu}$* after 24 hours	Error $[Pu]_{aqu}$* after 24 hours	pH after 62 days	$[Pu]_{aqu}$* after 62 days	Error $[Pu]_{aqu}$* after 62 days
9.992	0.01	0.01	4.78	1.31E-10	4.19	1.25E-10	1.64E-12	4.33	3.54E-11	6.61E-13
9.942	0.01	0.01	4.80	1.32E-10	4.76	1.28E-10	1.66E-12	4.67	8.24E-11	1.18E-12
9.988	0.01	0.01	4.78	1.31E-10	4.79	1.29E-10	1.67E-12	4.70	3.47E-11	6.52E-13
9.979	0.01	0.01	4.79	1.31E-10	5.22	1.28E-10	1.66E-12	5.22	5.14E-11	8.4E-13
9.902	0.01	0.01	4.82	1.32E-10	5.95	1.25E-10	1.63E-12	5.73	7.2E-11	1.07E-12
9.878	0.01	0.01	4.84	1.32E-10	5.83	1.28E-10	1.66E-12	5.91	5.99E-11	9.33E-13
9.925	0.01	0.01	4.81	1.32E-10	6.32	1.28E-10	1.66E-12	5.91	7.06E-11	1.05E-12
9.923	0.01	0.01	4.81	1.32E-10	6.55	1.26E-10	1.65E-12	-	5.34E-11	8.62E-13
9.924	0.01	0.01	4.81	1.32E-10	6.73	1.26E-10	1.64E-12	6.17	4.96E-11	8.21E-13
9.929	0.01	0.01	4.81	1.32E-10	6.90	1.23E-10	1.61E-12	6.07	6.05E-11	9.41E-13
9.933	0.01	0.01	4.81	1.32E-10	7.06	1.16E-10	1.54E-12	6.41	4.13E-11	7.28E-13
9.901	0.01	0.01	4.82	1.32E-10	6.93	1.26E-10	1.64E-12	6.29	4.01E-11	7.16E-13
9.939	0.01	0.01	4.81	1.32E-10	7.25	1.18E-10	1.55E-12	6.41	3.49E-11	6.56E-13
9.964	0.01	0.01	4.79	1.31E-10	7.83	1.04E-10	1.40E-12	6.58	3.25E-11	6.27E-13
10.038	0.01	0.01	4.76	1.30E-10	8.08	9.84E-11	1.35E-12	6.44	2.36E-11	5.24E-13
9.987	0.01	0.01	4.78	1.31E-10	8.59	2.30E-11	5.09E-13	6.66	4.58E-11	7.78E-13
9.922	0.01	0.01	4.81	1.32E-10	9.03	8.36E-12	3.15E-13	6.75	5.65E-11	8.97E-13
9.678	0.01	0.01	4.94	1.35E-10	9.44	9.73E-12	3.35E-13	6.93	6.91E-11	1.03E-12

* Measured aqueous phase concentration at sampling time determined via LSC.